Elucidating the mode of action of bioactive small molecules on the basis of High Content Analysis

Von der Fakultät für Lebenswissenschaften

der Technischen Universität Carolo-Wilhelmina

zu Braunschweig

zur Erlangung des Grades einer

Doktorin der Naturwissenschaften

(Dr. rer. nat.)

genehmigte

D i s s e r t a t i o n

von Thadigiri Aruna Jyothi Raja
aus Lucknow, India

1. Referentin:	Prof. Dr. Ursula Bilitewski
2. Referent:	Prof. Dr. Ludger Beerhues
eingereicht am:	28.04.2014
mündliche Prüfung (Disputation) am:	16.07.2014

Druckjahr 2014

Vorveröffentlichungen der Dissertation

Teilergebnisse aus dieser Arbeit wurden mit Genehmigung der Fakultät für Lebenswissenschaften, vertreten durch die Mentorin der Arbeit, in folgenden Beiträgen vorab veröffentlicht

Publikationen

Frei, R., Staedler, D., Raja, A., Franke, R., Sasse, F., Gerber-Lemaire, S., Waser., J*. Total Synthesis and Biological Evaluation of Jerantinine E. Angew. Chem. Int. Ed. 2013, 52, 13373 –13376.

Lu, H-H., Raja, A., Franke, R., Landsberg, D., Sasse, F., Kalesse, M*. Synthesis and Biological Evaluation of Paleo-Soraphens. Angew. Chem. Int. Ed. 2013, 52, 13549 –13552.

Tagungsbeiträge

Raja A, Franke R. Sasse F. Biological profiling of small molecules using impedance measurement (Poster). Natural Products Conference, Lanzarote, Spain (2012).

Contents

Acknowledgements

I would like to thank my supervisor Dr. Florenz Sasse for allowing me to work in his lab and for his continuous guidance. I greatly admire his immense knowledge and years of experience in the field of chemical biology. Thank you for giving the liberty to try out new things, being patient with the outcome even when things didn't work out as expected which was more often the case and for critical inputs regarding the project.

I would like to thank my thesis committee members Prof. Dr. Susanne Häußler and Dr. Victor Wray for their critical but helpful suggestions and advices. I thank Prof. Dr. Ursula Bilitewski for being my mentor during the course of my study and for her valuable inputs. I also thank Prof. Dr. Ludger Beerhues and Prof. Dr. Stefan Schulz for being a part of the Examination Committee.

Thanks to our collaboration partners Prof. Dr. Jèrôme Waser (Lausanne, Switzerland), Prof. Dr. Markus Kalesse (Hannover, Germany), and Prof. Dr. Rolf Müller (Saarbrucken, Germany) for providing me with the compounds for this study. I also thank Prof. Dr. Sabine Laschat (Stuttgart, Germany) and Dr. Rainer Schobert (Bayreuth, Germany) for providing me with compounds to study though they could not be included in this project but formed a part of the publications.

I am immensely thankful to both Dr. Randi Diestel and Mr. Christian Holz for providing me with continuous support and being patient enough to guide me in using automated microscope for the presented study. I also thank Dr. Joachim Reichelt and Uthayakumar Muthukumarasamy for carrying out the docking studies for small molecule described in this study. I would also like to thank Dr. Raimo Franke for playing an important role as a Bioinformatician during the course of the project.

I would like to thank my colleagues not just from my department but also from others who helped me in various ways during the study. Thanks Bettina, Chriselle, Galina, Garima, Heike, Michelle, Surya, Wera, Yazh. I also thank my entire department of CBIO for all the help.

Thanks to Chriselle, Devesha, Garima, Ramya, Madhu, Sayantan, Surya, Uthay, and Yazh for making this place much closer to home. Special thanks to Yazh, if not for her I would not be here to start with.

I am grateful to my family for always being there and for their love and affection. Last but not the least I am also thankful to Joseph Kartik Iyappan, for giving me all the reasons to see it through till the end. I would like to dedicate this thesis to my father.

Abbreviations

ABTS	2,2'-Azino-bis(3-ethylbenzothiazoline-6-sulphonic acid)
Ac	Acetone
ATCC	American Type Culture Collection
ATP	Adenosine triphosphate
BCA	Bicinchoninic acid
BSA	Bovine serum albumin
CCD camera	Charge-coupled device camera
CDK	Cyclin dependent kinase
CREB	cAMP response element binding protein
DAPI	4', 6-Diamidino-2-phenylindole
DARTS	Drug affinity responsive target stability
DMEM	Dulbecco’s modified Eagle’s medium
DMSO	Dimethyl sulfoxide
DNA	Deoxyribonucleic acid
DSMZ	Deutsche Sammlung von Mikroorganismen und Zellkulturen
EBSS	Earle's balanced salt solution
ECIS	Electrical cell-substrate impedance sensing
ER	Endoplasmic reticulum
FBS	Foetal bovine serum
FITC	Fluorescein isothiocyanate
GAPDH	Glyceraldehyde 3-phosphate dehydrogenase
GRP94	Glucose regulated protein 94
HRP	Horseradish peroxidase
HCA	High content analysis
HCIA	High content image analysis
KCl	Potassium chloride
kD	Kilo Dalton

LOH	Loss of heterozygosity
MAPK	Mitogen-activated protein kinase
Mdm2	Mouse double minute 2
MeV	Million electron volts
mRNA	Messenger ribonucleic acid
MeOH	Methanol
min	Minute
MTP	Microtitre plate
NaCl	Sodium chloride
OD	Optical density
O.N	Overnight
PAGE	Polyacrylamide gel electrophoresis
PBS	Phosphate buffer solution
PI3 Kinase	Phosphoinositide 3-kinase
PTEN	*P*hosphatase and *ten*sin homologue deleted on chromosome 10
PDK1	Phosphoinositide-dependent kinase-1
PMA	Phorbol myristate acetate
POD	Peroxidase
rpm	Rotation per minute
RT-CES	Real-time cell electronic sensing
SC-35	Spliceosome component
SGK1	Serum-and glucocorticoid-induced kinase 1
siRNA	Small interfering ribonucleic acid
SDS	Sodium dodecyl sulphate
TBS	Tris-buffered saline
TBST	Tris-buffered saline-Tween
TGF-β	Transforming growth factor β
TRITC	Tetramethylrhodamine isothiocyanate

Abstract

Natural products are a prime source of “lead” compounds whose full potential still remains untapped. These lead compounds owe their biological diversity to a broad spectrum of mechanisms which are often difficult to elucidate. This study applied high content analysis methods as a first step to get hints towards the mode of action (MoA) of a set of compounds of interest. These methods included two cell-based approaches, one based on automated microscopy which provides information on the action of the compounds in the form of immunofluorescence images and the other based on the xCELLigence system providing impedance curves as a result of a real-time monitoring of cell perturbations. Profiles from individual approaches were compared with those of reference compounds whose mechanisms were known and well established.

Indications provided by HCA formed the basis for elucidating the MoA of few selected bioactive compounds, namely jerantinine E, paleo-soraphen A & B, and Dsz A_1 and Z. The cytotoxicity of these compounds varied from micro- to subnanomolar ranges in cancer cells. Their activities could be attributed to different mechanisms. Jerantinine E, an indole alkaloid, induced a depletion of the microtubular network of cells. It inhibited the tubulin polymerisation *in vitro* in low micromolar ranges. Paleo-soraphen A & B, genetic derivatives of soraphen A, were not only less active than their parent compound but also seem to have different mechanisms supporting the concept of evolutionary optimization. Paleo-soraphen A on one hand showed a mechanism similar to that of soraphen A whereas paleo-soraphen B seems to deviate. It showed effects that are similar to the topoisomerase I inhibitor camptothecin.

Most potent among all were disorazol (Dsz) A_1 and Z which have been known as tubulin polymerisation inhibitors. Detailed investigations presented here revealed additional targets that have been overlooked so far. These targets are addressed at even lower concentrations. Drug affinity responsive target stability (DARTS) approaches showed that Dsz A_1 binds to the phosphatase enzyme PTEN which antagonizes the PI3K/Akt pathway whereas Dsz Z targets the regulatory unit of PI3 kinase, p85. Western blot analysis provided the interesting revelation that Dsz A_1 and Z, though showing structural similarity have different targets and are affecting different pathways. Dsz A_1 on one hand affects the PI3K/Akt pathway whereas the effect of Dsz Z is independent of Akt. It stalls the PI3K/SGK pathway. Dsz Z induces a dephosphorylation of p85. Knockdown studies of the respective target proteins confirmed their involvement in the different pathways. Measuring mono- and oligonucleosome enrichment confirmed the decisive role of PTEN in apoptosis induction by Dsz A_1. Docking studies conducted on PTEN with Dsz A_1 showed an important interaction of the epoxide group with the amino acids $Arg^{172,\ 173}$ and Thr^{319}. Caspase activity measurements in knockdown cells provided evidence of the role played by p85 in apoptosis induction by Dsz Z.

Zusammenfassung

Naturstoffe sind eine vorzügliche Quelle für Leitstrukturen, deren Potential bei weitem noch nicht ausgeschöpft ist. Diese Leitstrukturen verdanken ihre biologische Vielfalt einem breiten Spektrum an Wirkmechanismen, die aber oft schwierig aufzuklären sind. Diese Studie benutzte „High-Content"-Analysemethoden als ersten Schritt, um Hinweise auf den Wirkmechanismus ausgewählter Verbindungen zu bekommen. Diese Methoden umfassten zwei zell-basierte Ansätze; einer basierend auf automatischer Mikroskopie liefert Informationen über die Wirkung von Verbindungen in Form von Immunfluoreszenz-Bildern und der andere basierend dem xCELLigence-System Impedanzkurven als Ergebnis eines Echtzeit-Monitoring von Zellstörungen. Die Profile der individuellen Ansätze wurden mit denen von Referenz-Verbindungen verglichen, deren Wirkmechanismus bekannt und gut untersucht ist.

Die Hinweise aus der High-Content-Analyse bildeten die Grundlage für die Aufklärung der Wirkmechanismen einiger ausgewählter bioaktiver Verbindungen: Jerantinine E, Paläo-Soraphen A und B und Disorazol A_1 und Z. Die Zytotoxizität dieser Verbindungen bei Krebszellen lag im mikro- bis subnanomolaren Bereich. Ihre Aktivitäten konnten auf verschiedene Wirkmechanismen zurückgeführt werden. Das Indolalkaloid Jerantinine E führte zu einem Abbau des mikrotubulären Netzes der Zelle. Es hemmte die Tubulinpolymerisation *in vitro* im unteren mikromolaren Bereich. Paläo-Soraphen A und B, „genetische" Derivate von Soraphen A, waren nicht nur weniger aktiv als die Mutterverbindung, sie scheinen auch verschiedene Wirkmechanismen zu haben, was das Konzept einer evolutionären Optimierung unterstützt. Während Paläo-Soraphen A einen Wirkmechanismus ähnlich dem von Soraphen A zeigte, scheint Paläo-Soraphen B davon abzuweichen. Es zeigte Effekte, die dem Topoisomerase-I-Hemmer Camptothecin ähnlich sind.

Am wirksamsten waren Disorazol (Dsz) A_1 und Z, die bislang als Hemmer der Tubulin-Polymerisation bekannt waren. Die hier vorgestellten detaillierten Untersuchungen haben zusätzliche Zielproteine aufgedeckt, die bislang übersehen wurden. Diese werden sogar bei noch niedrigeren Konzentrationen adressiert. DARTS-Ansätze (drug affinity responsive target stability) zeigten, dass Dsz A_1 an das Phosphatase-Enzym PTEN bindet, was zu einer Hemmung des PI3K/Akt-Signalwegs führt, während Dsz Z auf p85 abzielt, die regulatorische Einheit der PI3-Kinase. Western-Blot-Analysen lieferten den interessanten Befund, dass Dsz A_1 und Z, obwohl sie strukturelle Ähnlichkeiten zeigen, verschiedene Zielproteine haben und auf verschiedene Signalwege einwirken. Dsz A_1 beeinflusst den PI3K/Akt-Signalweg, während der Effekt von Dsz Z unabhängig von Akt ist. Es blockiert den PI3K/SGK-Signalweg. Dsz Z induziert eine Dephosphorylierung von p85. Knockdown-Studien mit den entsprechenden Zielproteinen bestätigten ihre Einbindung in die verschiedenen Signalwege. Eine Messung der Anreicherung von Mono- und Oligonuclesomen bestätigte die maßgebende Rolle von PTEN in der Apoptose-Induktion durch Dsz A_1. Docking-Studien mit PTEN und Dsz A_1 zeigten eine wichtige Interaktion der Epoxidgruppe mit den Aminosäuren $Arg^{172, 173}$ und Thr^{319}. Caspase-Aktivitätsmessungen in Knockdown-Zellen belegten die Rolle von p85 in der durch Dsz Z induzierten Apoptose.

1 Introduction

Natural products are naturally derived metabolites and products from microorganisms, plants and animals. These products have been exploited for human use for thousands of years. It was not until Pasteur discovered that fermentation is caused by living cells that ushered in the antibiotic era which started with discovery and development of penicillin from fungus *Penicillium notatum* (Strobel et al., 2004). From this point on microbes were investigated as a source of bioactive natural products.

Natural products are the most productive source of leads for drug development. Well over 80% of drug substances are derived from natural products or inspired from them (Newman et al., 2000). They cover a range of therapeutic indications like anti-cancer, anti-infectives, and anti-diabetics, among others (Harvey, 2008). Undoubtedly, the major producers of secondary metabolites are members of the *Actinomycetales*, especially from the genus *Streptomyces*, followed by *Bacillus* as well as *Pseudomona*s. However, over the last decades, myxobacteria have emerged as promising source of bioactive molecules. Natural products derived from myxobacteria exhibits many unique structural features as well as novel mode of actions making them attractive lead structures for drug development (Weissman and Muller, 2009).

1.1 Myxobacteria and their secondary metabolism

The work of the Höfle and Reichenbach research groups at HZI, Braunschweig, Germany resulted in the isolation of more than 7500 myxobacterial strains, all of which are currently housed in the institute's collection and at DSMZ (Deutsche Sammlung von Mikroorganismen und Zellkulturen) (Weissman and Muller, 2009).

Myxobacteria are Gram-negative δ-proteobacteria occupying habitats ranging from soil to bark of trees, decaying plant materials and marine environment (Wenzel and Muller, 2009). They secrete exo-enzymes which allow them to use a range of biological macromolecules like cellulose as food source which also includes whole microorganisms such as fungi and bacteria. During unfavourable growth conditions, cells aggregate to form a pseudoplasmodium-like slimy mass which ultimately transforms into a complex, multi-cellular fruiting body harbouring propagative spores (Weissman and Muller, 2010).

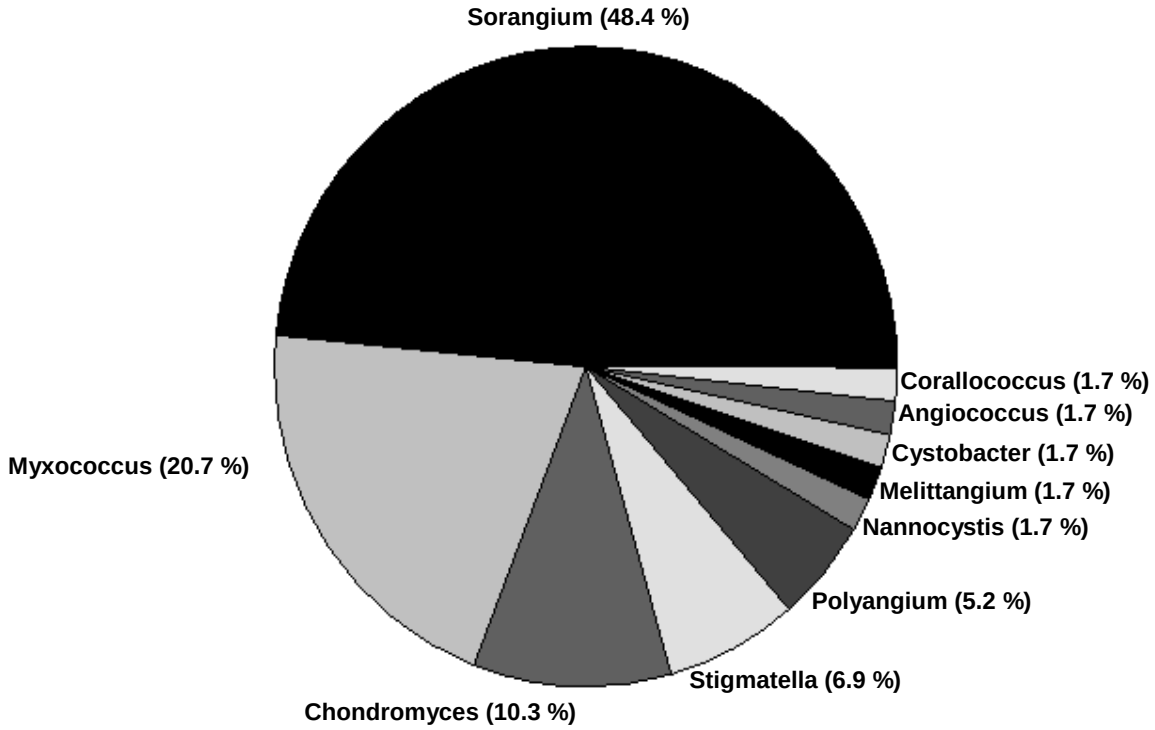

Figure 1.1: Myxobacterial producers of novel secondary metabolites (adapted from (Gerth et al., 2003)

Among myxobacteria (Figure 1.1), the genus Sorangium is particularly valuable, as 48.4% of the metabolites isolated from myxobacteria, including the potent anti-tumour compound epothilone, derive from this group. The majority of myxobacterial metabolites are polyketides, nonribosomal polypeptides or hybrids of the two structures, many of which are synthesized on huge molecular assembly lines composed of polyketide synthase (PKS) and nonribosomal polypeptide synthase (NRPS) multienzymes (Schneiker et al., 2007). Many of the myxobacterial metabolites not only belong to multiple structural classes but also have number of chemical variants. Furthermore, the genome of several strains has been sequenced and shown that the myxobacteria have greater secondary metabolite producing ability than suggested by its fermentation under standard laboratory conditions. *Sorangium cellulosum* So ce56 has by far the largest known sequenced genome from any bacterium (13 Mbp) which correlates to its ability of secondary metabolism (Weissman and Muller, 2010).

Sorangium strains exhibit physiological features of myxobacteria like movement by gliding, biofilm formation and fruiting body formation as depicted in Figure 1.2.

Natural products are the end products of complex multistep biosynthetic processes. As mentioned earlier two major multifunctional enzyme systems called polyketide synthases (PKS) and non-ribosomal peptide synthases (NRPS) assemble simple building blocks such as coenzyme-A-activated carboxylic acids and amino acids to form secondary metabolites. Mostly secondary metabolites are derived from modular PKS and NRPS megasynthases but many of them are frequently directed by a mixed PKS-NRPS system. Even when the myxobacteria adhere to a single megasynthase, they deviate from the norm and show

iterative use of modules, module skipping or unusual arrangement of core domains within the module (Wenzel and Muller, 2007).

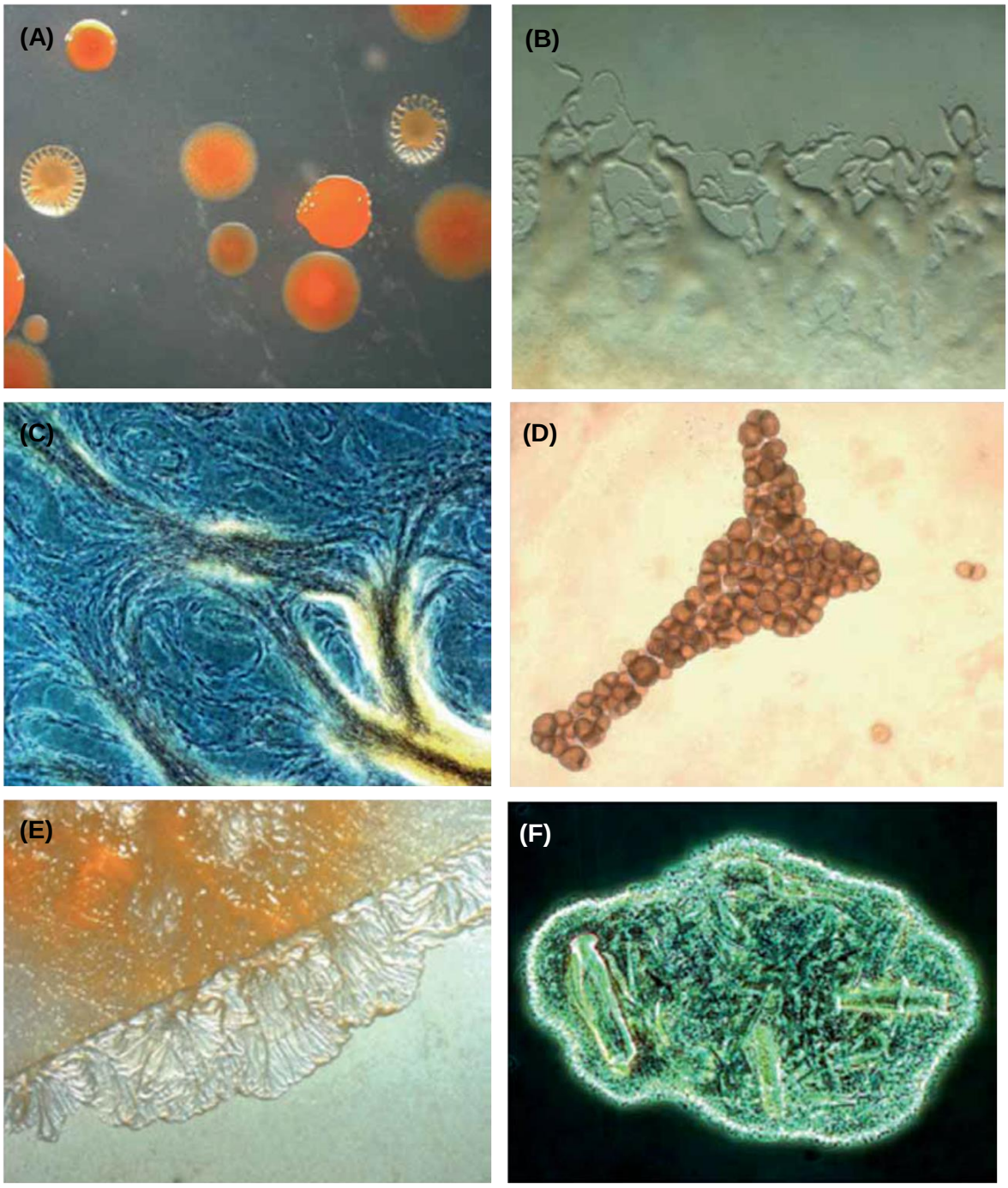

Figure 1.2: Physiological characteristics of S. cellulosum So ce56

(A). S. cellulosum colonies. (B, C) Swarming growth patterns. (D) Fruiting bodies. (E) Growth on cellulose as sole carbon source. (F) Adherence to crystalline cellulose (Schneiker et al., 2007)

The most commonly observed bioactivity among myxobacterial metabolites is anti-yeast/fungal at 54% followed by antibacterial activity at 29%. Other bioactivities like anti-malarial, immunosuppressive, insecticidal and herbicidal activities are rare but noteworthy. The most famous group of compound isolated from myxobacteria up to now are the epothilones that were discovered in *Sorangium cellulosum*. The epothilones interfere with

the dynamic of the tubulin/microtubule system in the cells. They induce a stabilization of microtubules and thereby show the mode of action similar to taxol, a compound originally isolated from the bark of the Pacific yew tree that was approved as an anti-cancer drug in the 1990s. A semi-synthetic analogue of epothilone B, ixabepilone, was also approved for clinical use in the US for treatment of aggressive breast cancer in 2007 as it is active not only against taxol-resistant tumours but also multi-resistant P-glycoprotein expressing tumours (Weissman and Muller, 2010; Zhao et al., 2013).

1.2 High Content Analysis

Early stages of the drug discovery process form a continuous pipeline of steps including target identification, target selection, primary screening and candidate optimization (Giuliano, 1997). Target identification involves selecting a target generally a gene or a protein, which is involved in pathophysiology of a disease. This target should be able to interact with and be affected by the drug. This is followed by target validation which is to confirm that the target is actually involved in the disease. These two steps are performed by scientists who deal with people at clinical level like physicians. Once the target is validated through experiments both *in vitro* and *in vivo* scientists now could look for suitable drug against these targets (www.innovation.org). They search for a molecule or “lead” compound that may act on the validated target to change the course of the disease for good. These lead compounds could come from any source ranging from nature to chemically synthesized compounds to genetically engineered biomolecules. As we have seen earlier nature provides us with plethora of options for lead compounds that could fight against many diseases. In order to scan through all the bioactive molecules one requires rapid screening and hit identification methods. High throughput screening (HTS) is one such tool which identifies natural products and synthetic molecules as potential drug leads using automated screening of large collections (libraries) of compounds for activity as inhibitors or activators of specific biological targets (Koehn and Carter, 2005). Once bioactive molecules have been screened and identified, these could be analysed further for their specificity and mechanism making use of high content analysis (HCA) methods (Bickle, 2010).

Cell-based assays proved to be a very useful tool to investigate the effect of compound treatment within cellular context overcoming the limitations of biochemical assays (Denner et al., 2008). These cell-based assays could be labelled for detecting various cellular functions. Typical detection methods available are based on radioisotopes, optical absorbance, fluorescence and luminescence which require labelling of ligand, enzyme or tracer molecules. Other detection technologies which are label-free are well emerging in the past several years, including acoustic field-based detection and electrical detection based on cell-substrate impedance measurement.

1.2.1 Automated Microscopy

Visual assays, in which a target of interest is labelled with a fluorophor and observed using a microscope, are notable among other types of assays in terms of the amount and the quality of information acquired from a single assay (Carpenter, 2007). Image-based assays provide us with information ranging from a general phenotype such as the cell's health to a very specific phenotype such as localization of phosphorylated form of a protein. Even a single label such as nuclear staining can not only allow counting the number of cells but also indicate cell cycle progression and apoptotic state based on measurement of its DNA content and morphology. Such rich information is collected from individual cells and hence the term "high content".

However, results of such approach have shown limited statistical validation due to low-throughput owing to restricted size of samples analysed, requiring laborious manual collection of images followed by visual inspection of thousands of images (Carpenter, 2007; Denner et al., 2008). To overcome these shortcomings, two major technologies, automated microscopes and cell image analysis software have gathered attention and made image-based assays adaptable to high throughput analysis of small-molecules. The resulting process has earned the name "high throughput high content analysis" (Carpenter, 2007).

An automated microscope is equipped with a digitally charged coupled device (CCD) camera allowing machine-readable measures of cell perturbation caused by compound treatment and employs a software environment for automated analysis of acquired images to quantify cellular processes (Denner et al., 2008; Perlman et al., 2004).

For the success of automated analysis of "hit" compounds, the scope of variability should be kept to minimum, starting with cells used for high content analysis which should be checked for their quality to provide high-quality and consistent cell preparations. Selected cells are harvested and dispensed into 384/1536-well microtitre plates (MTPs) with transparent bottom for microscopy. This particular step could either be manual or robotic however automated dispensers are preferred for fast generation of cell plates from constantly stirred cell suspensions using minimal sheering force.

Depending on the cell concentration and the rate of growth, cell plates are incubated under optimal conditions and then treated with small-molecule libraries which are dissolved in dimethylsulphoxide (DMSO). To reduce assay variance, multiple cell plates could be treated with the same library plate. All small molecules are either present at a single concentration or multiple concentrations in case of dose-response analysis. Drugs with known mode of action were selected to later compare the cell phenotype of the test compounds with that of known drugs. After optimal incubation of the cells with the compound, cells are fixed and labelled with one or more antibodies and a nuclear marker (Shariff et al., 2010).

Following sample preparation in which cellular targets are labelled with fluorophors, an automated microscope is used for acquiring the images. Software associated with such a microscope allows predefinition of microscope processes that makes unattended image acquisition possible (Figure 1.3).

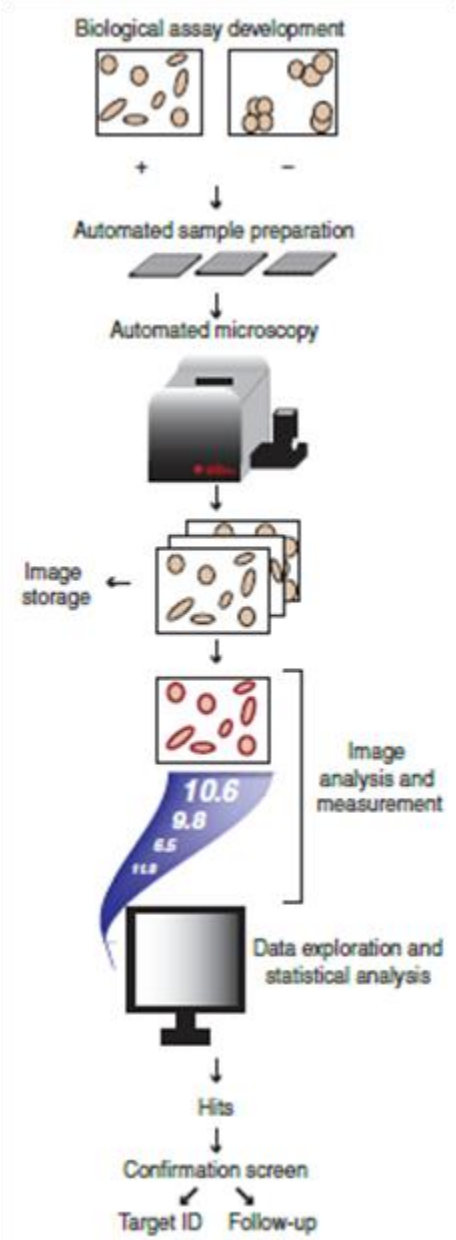

Automated image analysis helps to quantify and correlate multiple phenotypic responses. Fluorescent signals that serve as readout for a specific cellular phenotype has to be defined with the analysis software. Parameters such as intensity measurement, cell size and shape are considered. Background signals are separated by setting a threshold value for each fluorescence channel. The image algorithm scans through the images based on these defined specifications. This process provides us with numerical data obtained from images which are analysed later using different statistical methods to provide us with clusters of test compounds with reference compounds. Follow-up experiments are carried out later to confirm the findings of automated microscopy.

Figure 1.3: Major steps for high-throughput analysis using an automated microscope (Carpenter, 2007).

Although high content image analysis provides us with rich information, it is still limiting in terms of cost and time of labelling, loss of cells due to several cell-washing steps, interference with physiological condition by the labelling molecule and most importantly this assay is a single-point assay which can only provide us with a “snapshot” of the experiment (Atienza et al., 2006; Solly et al., 2004) and not a kinetic measurement. Therefore it becomes essential to lookout for assays which are non-invasive and provide us with kinetic data of biological and cellular processes. A detailed description of one such an approach adapted for this study is shown in the following section.

1.2.2 xCELLigence – Impedance measurement

Giaever et al. in 1984 first reported of electrical cell-substrate impedance sensing (ECIS) for real-time measurement of cellular processes. Several reports have since been shown to use this technology for monitoring cellular processes like macrophage adherence and their activation, change in cell morphology due to cytoskeletal rearrangement, cell migration etc.

Impedance-based real-time cell analysis (RTCA, also trademarked as xCELLigence) system is another variation of ECIS which helps in a number of biological assays including cell proliferation, cytotoxicity, cell growth inhibition and apoptosis assays. RTCA system (ACEA Biosciences Inc., San Diego, CA) consists of four components: the electronic microtitre plates (E-plate™), RTCA-SP (single plate), which is placed inside an incubator maintained at optimal temperature and CO_2 condition, an electronic sensor analyser, which sends and receives electronic signals and a computer which runs the RT-CES (Real time cell electronic

sensing) software and continuously acquires and displays the data (Atienza et al., 2006). This is a label free non-invasive cell-based assay which was used in this study.

Principle of RT-CES

The basic principle of RTCA is similar to that described by Giaever and co-workers for ECIS. The ionic environment present both at the electrode/solution interface and in the bulk solution determine the electronic impedance of an electrode. This ionic environment undergoes a change through field-directed movement and concentration gradient-driven diffusion under applied electrical field. Inside an electrolyte solution, total electrode impedance has two components: resistance of the solution itself whose contribution is so small that it is ignored and the impedance at the electrode/solution interface. Whereas in the presence of cells, the local ionic environment changes leading to addition of the third component: impedance of cells. The more the number of cells that attach to the electrodes, the larger would be the change in electrode impedance which is further increased upon the extent of cell's attachment as shown in Figure 1.4 (Solly et al., 2004).

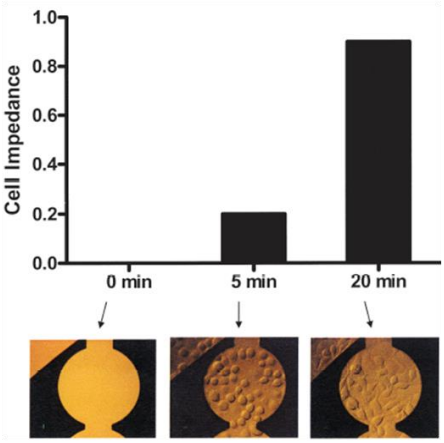

Figure 1.4: Electrode impedance plotted against time

With time, cells attach and spread on the electrode. As the time passes, with the same number of cells at the start point, impedance increases due to better cell attachment and its spread over the electrode (Solly et al., 2004).

In the RTCA system, an electronic analyser measures the electrode impedance. A voltage of 10 mV AC is applied to the electrode for ~0.1 s to pass electrical current through the circuit. This voltage does not disturb the cell function as it is much smaller than the resting potential of a typical mammalian cell which was proved in an experiment involving NIH 3T3 fibroblast cells. There was no notable change in their proliferation after application of 200 mV, 10 kHz voltage signals to the electrode for ~30 min (Solly et al., 2004).

A dimensionless parameter, Cell Index (CI) is derived as a relative change in measured electrical impedance to represent cell status. A CI of 0 will represent either the absence of cells or cells have not yet adhered to the well bottom. This value increases as the cells begin to adhere and also with change in cell status such as cell morphology, adhesion or viability. Figure 1.5 shows a diagrammatic representation of change in the cell index over a period of time before and after addition of the compound

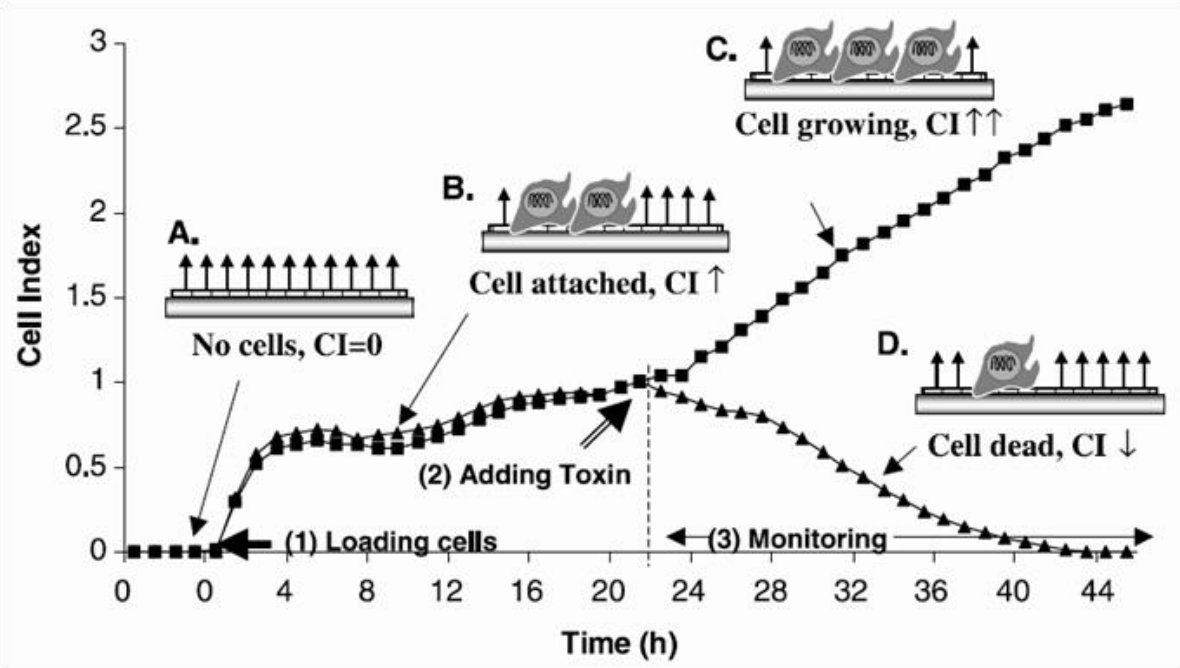

Figure 1.5: Compound mediated cytotoxicity and its effect on cell index (CI)

Cells are seeded in an E-plate™ and put in an RTCA SP station which is placed inside an incubator maintained at 37°C (10% CO_2). Background impedance measurement is taken in part A followed by addition of cell suspension (1) and allowing the cells to grow for 24 h as depicted by part B. The test compound is added after 24 h (2) and the change in impedance is measured for the next few days (3). Different compounds have different effects on the cell morphology and viability. Some compounds will have no effect or rather aid in cell proliferation (C) causing an increase in CI or they could either be cytostatic or cytotoxic leading to drop in CI as shown by part D (Xing_JZ et al., 2006).

The xCELLigence system provides us with a platform to monitor live cell behaviour in real time in a non-invasive way over the entire course of experiment, including cell attachment, spreading, proliferation and any treatment with compounds. Because of the real-time nature of the data acquisition, cellular manipulations and treatments can be performed. Due to kinetic nature of this method, both short-term and long-term cellular responses to a particular treatment can be monitored in order to rule out off-target effects. Hence, impedance readout for each treatment leads us to unique cellular response profiles, which can prove to be predictive in terms of mechanism of action (Atienza et al., 2006).

In our approach we have studied change in CI upon treatment of cells with small molecules over a period of time. The cells treated with reference compound (drugs with known mechanism) showed a particular impedance curve pattern characteristic of their mode of action. When compared to test compound impedance this pattern provided us with hints about their mechanism.

1.3 Elucidation of mode-of-action

To increase the likelihood of drug success and reducing the attrition rate, clear understanding of the drug's mechanism is crucial. According to the US food and drug administration (FDA), only 8% of the drugs entering the phase of clinical trial are eventually approved. An investigational drug against Alzheimer, dimebon entered phase 2 of clinical trial based on several studies showing different mechanism but none showed a clear picture as to how exactly the drug worked. However, later companies like Pfizer and Medivation announced that the drug did not develop cognitive ability in phase 3 trial, which was the basis on which it was selected at the first place for further trial (Editorial, 2010).

Understanding a drug's mechanism not only reduces later stage failure but also enables better dosing through monitoring a drug's effect on the target pathway and stratifying clinical trials to focus on those patients who are more likely to respond.

Even when the mechanism is known, it is often difficult to predict side effects. Nevertheless, in a long run, mechanistic knowledge of the drug is worthwhile to increase the chances of drug approval, saving money, time and most importantly, the lives of patients (Editorial, 2010).

1.3.1 PI3K pathway effectors

The phosphatidylinositol 3-kinase (PI3K) pathway has been conserved evolutionarily from yeasts to mammals (Chalhoub and Baker, 2009). This pathway became the prime focus in mid-1980s, when it became apparent that PI3K activity was physically and functionally associated with transforming activity of viral oncogenes, such as polyomavirus (Vivanco and Sawyers, 2002).

PI3Ks are a family of intracellular lipid kinases that phosphorylate the 3'-hydroxyl group of phosphatidylinositols (PI) and phosphoinositides (Chalhoub and Baker, 2009). PI3Ks are grouped into three classes (I-III) according to their substrate preference, sequence homology, structure and function. Due to relevance to the project only class I have been described here.

Class I PI3Ks: Class I PI3Ks are divided into two sub-families, depending on the receptors to which they couple. Class IA PI3Ks primarily phosphorylates inositol-containing lipids, known as phosphatidylinositols (PtdIns) at their 3' position (Figure 1.6). The primary *in vivo* substrate is PtdIns (4, 5) P_2 (hereafter called PIP_2), which is converted to PtdIns (3, 4, 5) P_3 (called PIP_3) (Vivanco and Sawyers, 2002). Members of Class IA are heterodimers of a regulatory subunit (with three isoforms: p85α, p85β and p55γ encoded by PI3KR1, PI3KR2 and PI3KR3 genes respectively) and a p110 catalytic subunit (also with three isoforms p110α, p110β and p110δ encoded by PI3KCA, PI3KCB and PI3KCD genes, respectively).

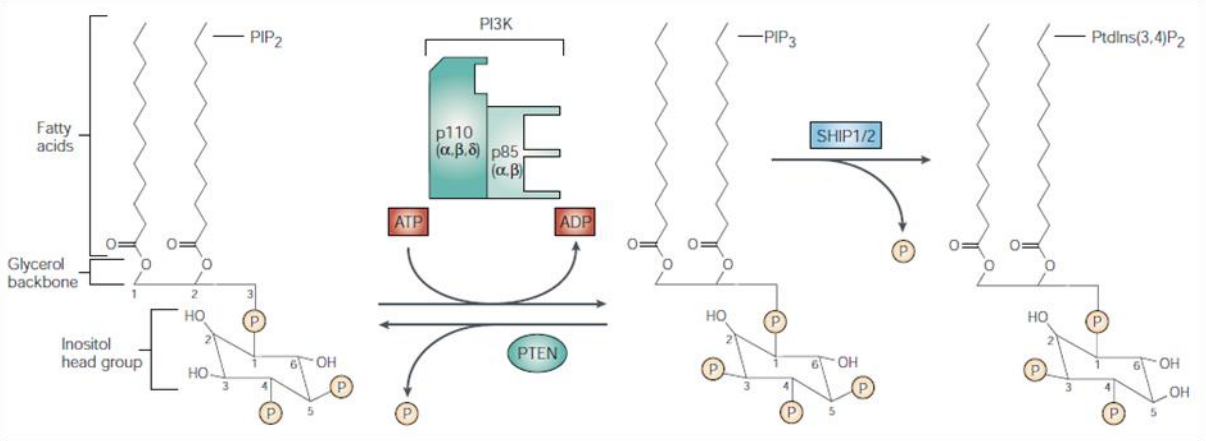

Figure 1.6: PtdIns (4, 5) P_2 to PtdIns (3, 4, 5 cycle

Phosphatidylinositol phosphates are composed of a membrane-associated phosphatidic acid group and a glycerol moiety which is linked to a cytosolic phosphorylated inositol head group. Phosphatidylinositol 3-kinase (PI3K) can phosphorylate PtdIns (4, 5) P_2 (PIP_2) at the D3 position to form a second messenger PtdIns (3, 4, and 5)P_3 (PIP_3). Dephosphorylation of PIP_3 to regenerate PIP_2 is accomplished by the 3'-phosphatase PTEN. Additionally, PIP_3 can also be dephosphorylated at the D5 position by SHIP1 or SHIP2 to generate PIP_2, another potential second messenger (Vivanco and Sawyers, 2002).

The class IA p85 regulatory isoforms have a common core structure consisting of a p110-binding domain (also called the inter-SH_2 domain) (Figure 1.7) flanked by two Src-homology 2 (SH2) domain. The longer isoforms, p85α and p85β, also have an extended N-terminal region (dashed outline) containing a Src-homology 3 (SH3) domain and a BCR homology (BH) domain flanked by two proline-rich (P) regions.

The p110 catalytic domain consists of an N-terminal p85 binding domain that interacts with the p85 regulatory subunit, a Ras-binding domain (RBD) that mediates activation of the small GTPase Ras, a C2 domain, a phosphatidylinositol kinase homology (PIK) domain and a C-terminal catalytic domain (Engelman et al., 2006; Jiang and Liu, 2009).

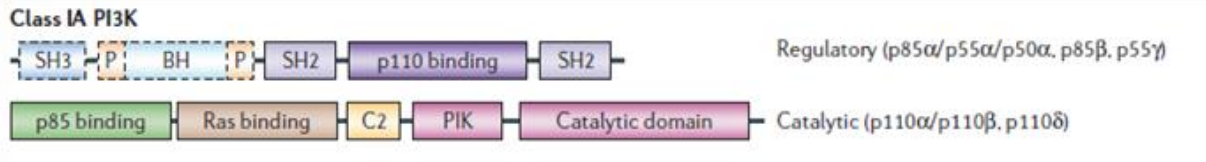

Figure 1.7: Classification of phosphatidylinositol 3-kinase (PI3K) family members (Engelman et al., 2006)

In terms of substrate specificity, *in vivo*, class I PI3Ks primarily generate PIP_3 from PIP_2, whereas class III PI3Ks generate phosphatidylinositol 3-phosphate (PI-3-P) from PI. Class II PI3Ks preferentially generate PI-3-P and phosphatidylinositol-3,4-bisphosphate (PI-3,4-P_2) *in vitro*, and might generate PI-3-P, PI-3,4 P_2 and possibly PIP_3 *in vivo* (Engelman et al., 2006).

1.3.1.1 Activation and regulation of PI3K

Extensive knowledge regarding PI3K activation and regulation has come from genetic studies in *Caenorhabditis elegans* and *Drosophila melanogaster*, both of which have a single class IA PI3K controlling growth and metabolism. Although this knowledge has increased our

understanding but PI3K activation and regulation is more complex in mammals due to multiple family members of the PI3K signalling pathway.

Relatively little is known about the specific functions of class II and III PI3Ks. Commonly used PI3K inhibitors, wortmannin and LY294002, inhibit class I and III PI3Ks and to a lesser extent class II PI3Ks. This lack of class specificity increases the importance of developing isoform-specific small molecule inhibitors which would also help in clarifying distinct cellular functions of different PI3Ks (Engelman et al., 2006).

Although signalling through all classes of PI3K is connected to key growth-regulatory processes, so far a key role in cancer has been demonstrated selectively for class IA PI3Ks (Chalhoub and Baker, 2009).

p85 is directly associated with many active tyrosine kinases (*e.g.*, PDGFR [platelet-derived growth factor receptors], EGFR [epidermal growth factor receptors] etc.) (Mellor et al., 2012) through physical interaction of its SH2 domain with phosphotyrosine residue in the context of a YXXM consensus sequence on the kinase (Figure 1.8). In some cases, the p85-RTK interaction is indirect and occurs through intermediate phosphoproteins, such as the insulin receptor substrates IRS1 and IRS2. In response to extracellular cues class IA PI3Ks catalyse the formation of PIP_3 from PIP_2. PIP_3 transduces activating signals by binding to proteins having pleckstrin homology (PH) domains like Akt (protein kinase B) and PDK1 (3-phosphoinositide-dependent kinase 1), thereby recruiting them to the membrane (Chalhoub and Baker, 2009).

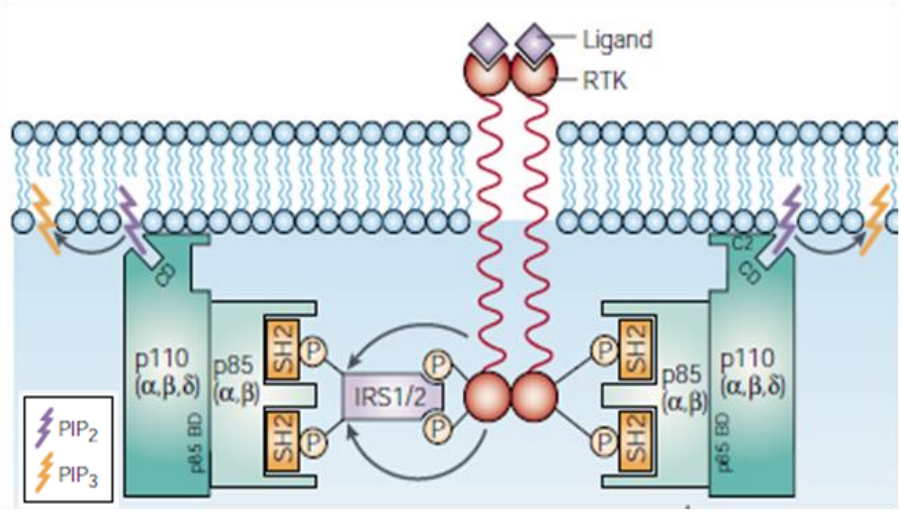

Figure 1.8: Model of PI3K activation

Autophosphorylation of ligand-activated receptor tyrosine kinases (RTKs) causes recruitment of the inactive heterodimeric class IA PI3Ks through interaction of phosphotyrosine residues on the receptor and SRC-homology 2 (SH2) domains on the PI3K p85 regulatory subunit, or the adaptor proteins IRS1 and IRS2. Phosphorylation of IRS1 and IRS2 generates docking site for SH2 domains of p85 inducing proper assembly of the signalling complex. These SH2-phosphotyrosine interactions bring PI3K in close proximity to its substrate PIP_2 at the plasma membrane to convert it to PIP_3 (Vivanco and Sawyers, 2002).

Once recruited to the plasma membrane PH-domain containing serine/threonine kinase named PDK1 phosphorylates Akt on Thr^{308}. Phosphorylation at Thr^{308} is necessary and sufficient for Akt activation; however, maximal activation requires additional phosphorylation

at Ser^{473} by PDK2, a kinase characterized biochemically but its molecular identity still remains undetermined. Akt is activated by a dual regulatory mechanism that requires both recruitment to plasma membrane and phosphorylation by PDKs at Thr^{308} and Ser^{473} (Vivanco and Sawyers, 2002).

Upon Akt activation, (Figure 1.9) biological consequences could be categorized into survival, proliferation and growth (Liang and Slingerland, 2003). Akt functions in an anti-apoptotic pathway by phosphorylating several components of the cell-death machinery, *e.g.*, BAD, a pro-apoptotic member of the BCL2 family of proteins, thereby inhibiting the catalytic activity of the pro-death protease, caspase-9. Akt can also influence cell survival by indirect effects on two central regulators of cell death – nuclear factor κB (NF-κB) and p53 (Vivanco and Sawyers, 2002). Upon phosphorylation of mouse double minute 2 (Mdm2) by Akt, it is translocated into the nucleus where it binds with p53. Mdm2 ligates ubiquitin to p53 which targets it for degradation by proteasome (Mayo and Donner, 2002). Akt can also affect proliferation through signalling cell cycle machinery components like cyclin D1 etc. Proliferation refers to cell division, which leads to an increase in cell number, whereas growth refers to the synthesis of macromolecules, which results in increased cell mass or size. Therapeutic targeting of the PI3K pathway is being developed at a rapid pace (Courtney et al., 2010). Pharmacological studies with the inhibitor rapamycin indicate that the Akt pathway regulates mTOR (Vivanco and Sawyers, 2002).

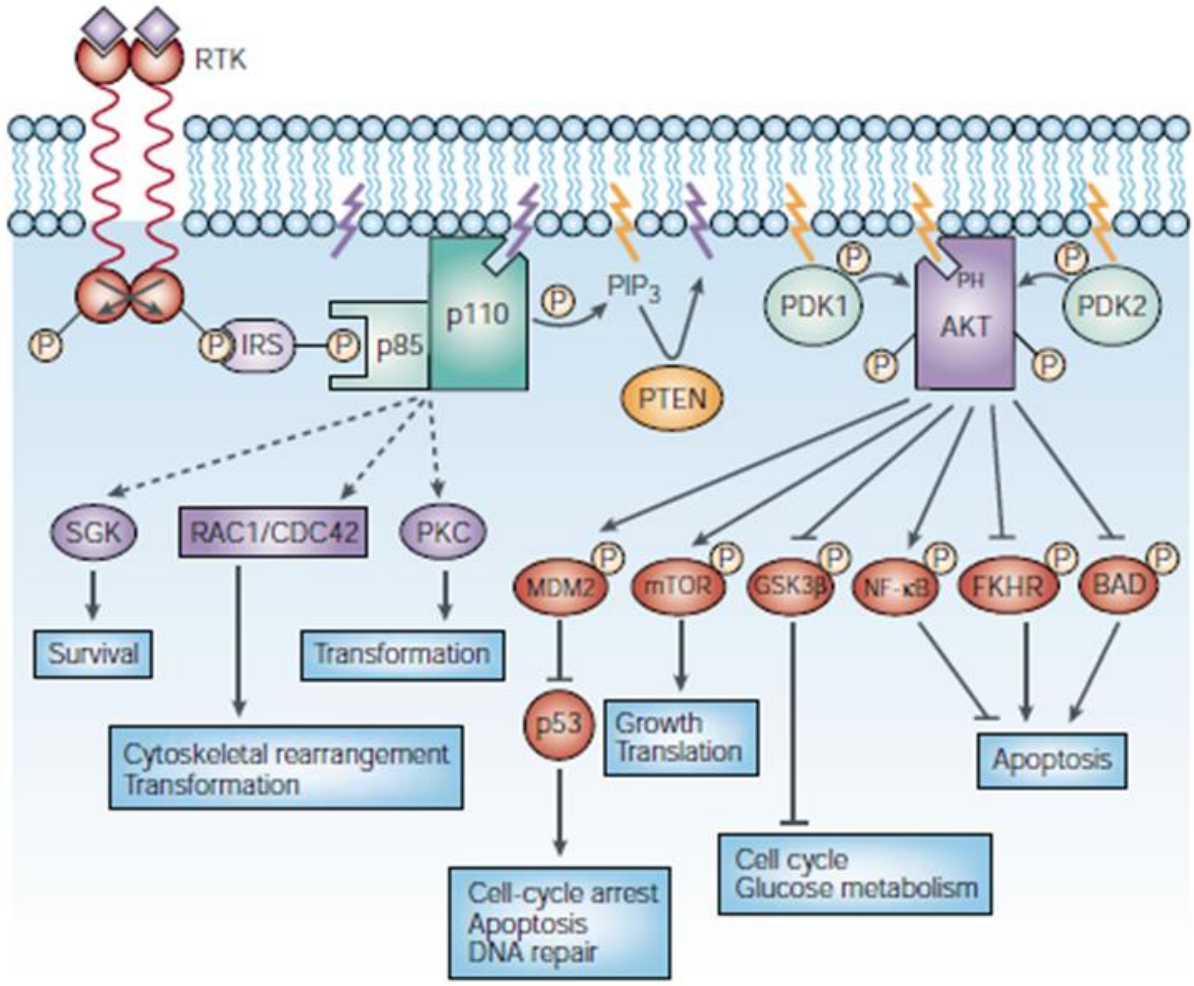

Figure 1.9: PI3K signalling and downstream activation of various proteins

Activation of class IA PI3K occurs through stimulation of RTKs leading to assembly of receptor-PI3K complex. This complex localizes at the membrane where PIP_2 is converted to PIP_3 by p110 catalytic unit of PI3K. PIP_3 serves as second messenger activating PH domain containing proteins like Akt and PDK1. Through Akt phosphorylation, activation and inhibition of several target takes places resulting in cellular growth, survival and proliferation. Additionally, PI3K has been shown to regulate the activity of other cellular targets like the serum and glucocorticoid-inducible kinase (SGK), the small GTP-binding proteins RAC1 and CDC42, and protein kinase C, in an Akt-independent manner through a poorly characterised mechanism. The activity of these target leads to survival, cytoskeletal rearrangement and transformation. GSK3β, glycogen synthase kinase-3β (Adapted from (Vivanco and Sawyers, 2002)).

The popular use of the phrase "PI3K-Akt pathway" in scientific literature shows that Akt is a crucial downstream target of PI3K. But Akt is not the only effector protein because PI3K and PIP_3 can activate a growing list of signalling pathway (Figure 1.9), many of which are consistent with oncogenesis, *e.g.*, activation of small GTP-binding proteins CDC42/RAC1 and activation of the serum and glucocorticoid-inducible kinase (SGK). CDC42 and RAC1 are best known for their role in regulating cytoskeletal movement and cell motility, and can function as oncogenes in fibroblasts when overexpressed.

The serum and glucocorticoid-inducible kinase (SGK) family has attracted recent attention because of their high homology to Akt and similar functional effects on survival pathways. The SGKs encode serine/threonine kinases that can be activated by IGF1 (Insulin growth factor-1) and other stimuli in a PI3K-dependent manner (Figure 1.9) (Vivanco and Sawyers,

2002). There are three isoforms of SGK, namely SGK1, SGK2 and SGK3 with similar substrate specificity to Akt (Bruhn et al., 2013). The amino acid sequences of the three isoforms are 80% identical with one another in the catalytic domain whereas the short C-terminal non-catalytic domain is less similar (44-68% identity). They also vary in their tissue distribution pattern and response to serum activation. SGK is activated by phosphorylation at Thr^{256} by PDK1 *in vitro* and phosphorylation is greatly enhanced by the mutation of Ser^{422} to Asp (Kobayashi and Cohen, 1999; Kobayashi et al., 1999; Park et al., 1999). Due to lack of literature information on other isoforms, only SGK1 will be discussed in section 1.3.1.4.

PI3K is tightly regulated in normal cells both at regulatory and catalytic activity levels. SH3 and BCR domains of p85 regulatory unit are postulated to have negative regulatory role towards p110 catalytic unit and these two domains are absent in the splice variants of p85α-p55α and p50α. (Figure 1.7) This is consistent with the observation that both p55α and p50α are efficient activators of p110 than p85α. A pre-formed, inactive p85-p110 complex is present in the cytoplasm of resting cells, waiting to be activated upon appropriate cues. PI3K becomes active when the p110 catalytic subunit is in close proximity to its lipid substrates in the plasma membrane and also by interaction between RTKs and p85 relieving the inhibitory effect of p85 on p110 kinase activity due to conformational change in the p85-p110 complex.

Regulation is not only carried out at the kinase level but also with the levels of PIP_3. PIP_3 is barely detectable in mammalian cells under unstimulated growth conditions. Several PIP_3 phosphatases (PTEN, SHIP1 and SHIP2) ensure optimum levels of PIP_3. PTEN, a 3' lipid phosphatase converts PIP_3 back to PIP_2. Its function and regulation will be discussed in detail in section 1.3.1.2. SHIP (SH2-domain containing inositol 5-phosphate) also acts on PIP_3 but removes phosphate from the 5' position rather than 3', forming PI (3, 4) P_2, another second messenger. PI (3, 4) P_2 also recruits Akt at the plasma membrane and reduces the levels of PIP_3. However PTEN, unlike SHIP1 gives a strong cancer phenotype in mice. In addition, SHIP1-knockout mice have shown to develop myeloproliferative syndromes, indicating that PI (3, 4)P_2 can activate certain mitogenic pathways (Sulis, 2003; Vivanco and Sawyers, 2002).

1.3.1.2 PTEN phosphatases

The PTEN (*p*hosphatase and *ten*sin homologue deleted on chromosome 10) lipid phosphatase is the most important negative regulator of PI3K signalling pathway (Cully et al., 2006). PTEN antagonizes the PI3K signalling pathway by dephosphorylating the 3' position of the inositol ring of PIP_3 (Leslie and Downes, 2002) and thus inactivating downstream signalling which ultimately stops cell proliferation. (Figure 1.10) PTEN is tumour suppressor (Hafsi et al., 2012) located at 10q23 (GenBank accession number AF067844) (Stambolic et al., 2001), also named as "mutated in multiple advanced cancers" (MMAC) and "TGF-β-regulated and epithelial cell-enriched phosphatase" (TEP-1) (Cantley and Neel, 1999). It was identified to be frequently mutated/deleted in various human cancers (Freeman et al., 2003). Non-phosphorylated form of PTEN is the active form which acts against the PI3K pathway (Rabinovsky et al., 2009).

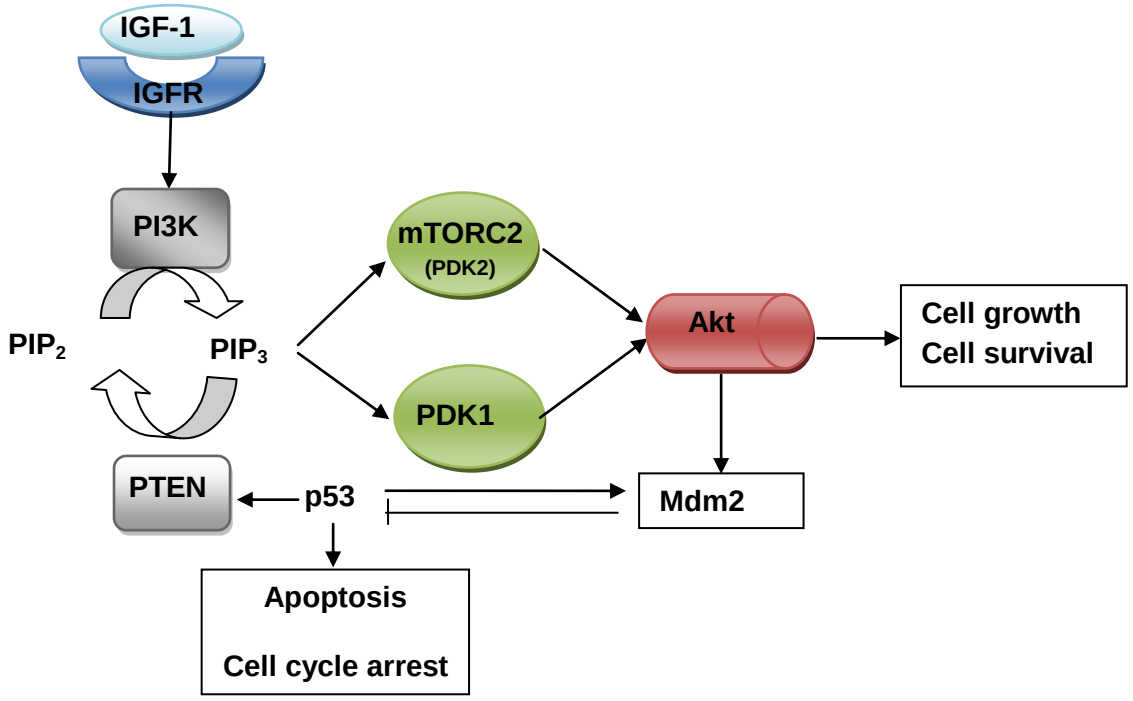

Figure 1.10: Interconnections between PI3K-Akt pathway and p53 involving PTEN

p53 negatively regulates Akt and mTOR pathway through upregulation of PTEN in response to stress. Akt-Mdm2-p53 forms a negative feedback loop to negatively regulate p53, whereas p53-PTEN-Akt-Mdm2 forms a loop to positively regulate p53. PI3K converts PIP_2 to PIP_3 which in turn recruits PH-domain containing proteins like Akt and PDK1 and 2 to plasma membrane to phosphorylate downstream protein which aid in cell growth and survival. On the other hand PTEN converts PIP_3 to PIP_2 thereby acting against PI3K pathway (Adapted from (Feng, 2010).

Structure: PTEN is a 403-amino-acid protein (Figure 1.11) and a member of the large PTP family (protein tyrosine phosphatase) (Leslie and Downes, 2004). It reveals a phosphatase domain similar to that of protein phosphatases but has an enlarged active site important for accommodation of PI. The PTEN C2 domain binds to the phospholipid membrane *in vitro*, and mutation of basic residues that could mediate membrane recruitment reduces PTEN's membrane affinity and its ability to suppress the growth of glioblastoma tumour cells.

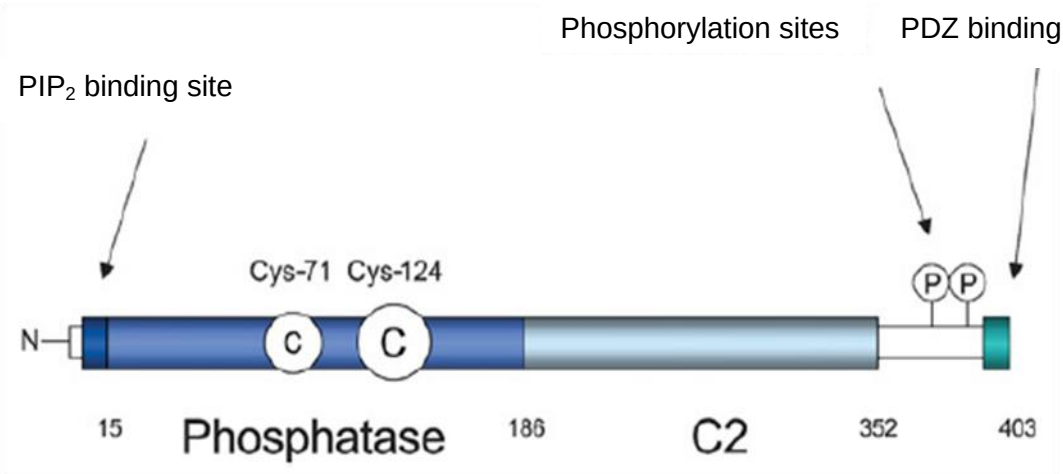

Figure 1.11: The PTEN protein

The PTEN protein consists of 403-amino-acid. The N-terminal phosphatase domain (amino acid 7-185) and the C2 domain (186-351) are both required for enzymatic activity. The catalytic cysteine residue (Cys-71 & 124) forms a disulphide bond when the enzyme is oxidized. It is still not clear whether in a cell PIP_2 motif responds to PIP_2 or to more acidic lipid such as phosphatidylserine. The PDZ binding domain at the C-terminal end is represented by a small region whose function is still not clear. The phosphorylation sites in the C-terminal tail are represented by a circled letter P (Lee et al., 1999).

PTEN can dephosphorylate tyrosine, serine and threonine-phosphorylated peptides. This activity requires highly acidic substrate which is fulfilled by PIP_3. Tumour-derived mutation spreads evenly to the two domains, and mutations in either reduces or eliminates PTEN's growth suppression activity (Das et al., 2003; Lee et al., 1999).

Regulation: Unlike several signalling enzymes, PTEN lacks a regulatory domain and appears to have relatively high constitutive phosphatase activity, both *in vitro* and in cells. Studies have shown that PTEN can be regulated by phosphorylation, membrane recruitment and oxidation (Tamguney and Stokoe, 2007). Phosphorylation of a cluster of serine and threonine residues (Ser^{370}, Ser^{380}, Thr^{382}, Thr^{383} and Ser^{385}) on PTEN induces a conformational switch whereas de-phosphorylation makes PTEN highly susceptible to proteolysis, increases its affinity for anionic lipids and enhances its localization to the plasma membrane (Leslie and Downes, 2004).

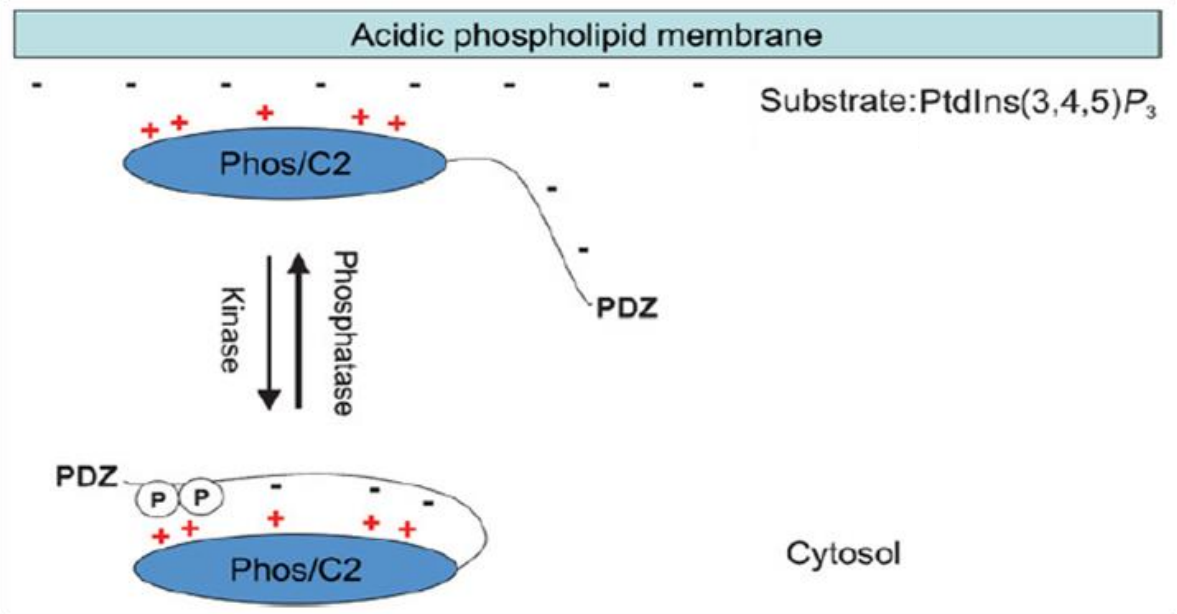

Figure 1.12: PTEN regulation by phosphorylation

Phosphorylated residues in the C-terminal tail of PTEN interact with the basic regions of the phosphatase (Phos) and C2 domain, causing masking of the basic membrane-binding surface of PTEN by C-terminal tail. This causes PTEN to remain in the cytosol and away from PIP_3. Dephosphorylation of these residues releases the C-terminal tail, allowing the electrostatic interaction of both the domains with acidic membranes (Leslie and Downes, 2004).

PTEN is highly sensitive to oxidation, with a disulphide bond being formed between the active-site cysteine Cys^{124} and Cys^{71}. Oxidation could be both due to experimental oxidative stress and by endogenous production of reactive oxygen species which could lead to PTEN's inactivation (Leslie and Downes, 2004).

1.3.1.3 PTEN inactivation in tumours

Mutations in various kinds of sporadic tumours and tumour cell lines first showcased the involvement of the PTEN gene. The classical view has been that tumour suppressor genes are recessive, such that both the allele should be lost for a tumour to develop but in case of PTEN partial loss or haplo-insufficiency gives a selective advantage to the tumour cells (Leslie and Downes, 2004). Knock-out mice lacking PTEN are embryonic lethal, whereas mice with one copy of PTEN have diminished Fas-mediated apoptosis and a high incidence of cancer. (Campbell et al., 2003). PTEN mutation is most prominently found in advanced glial tumours (at least 30% of primary tumours and 50-60% of cell lines) but also prostate, endometrial, renal and small-cell lung carcinoma. Germ-line mutations in PTEN cause rare autosomal dominant inherited cancer syndromes namely Cowden disease, Lhermitte–Duclos disease and Bannayan–Zonana syndrome (Cantley and Neel, 1999; Sansal and Sellers, 2004). Several mechanisms have come to light with regards to the PTEN inactivation which includes mutation in the coding sequence of PTEN, loss of heterozygosity (LOH) and loss of expression of PTEN protein (Leslie and Downes, 2004).

Mutations within the coding sequence mostly inactivate the phosphatase activity of the encoded enzyme. The majority of PTEN mutations in sporadic tumours and possibly all mutations in PTEN-associated inherited conditions fall in this category of loss of enzyme activity. However, there are other forms of tumour, too which have a strong phosphatase

activity but are still not able to suppress the tumour development indicating that the tumour suppressive activity is not entirely dependent on phosphatase activity. Mutation in the C-terminal tail mostly does not affect the enzymatic activity but affects the protein stability.

Breast and lung tumours show another mechanism of loss of heterozygosity. Immunohistochemical analysis suggests that in many tumours, one PTEN allele is deleted, and although these tumours retain one copy of PTEN with no detectable defect, expression of PTEN is lost (Leslie and Downes, 2004).

All the above description provides us with evidence of PTEN to be a potent anticancer target in tumours in which for some reason PTEN becomes inactive or not produced in adequate amounts.

1.3.1.4 Serum and glucocorticoid-inducible kinase 1 (SGK1)

SGK1 was originally cloned as a gene transcriptionally stimulated by serum and glucocorticoids in rat mammary tumour cells. The human SGK1 was discovered as a cell volume regulated gene upregulated by cell shrinkage. SGK1 is ubiquitously expressed. The gene encoding human SGK1 is localized to chromosome 6q23. SGK1 participates in the regulation of transport, hormone release, neuroexcitability, inflammation, cell proliferation and apoptosis by activating a variety of ion channels, regulation of enzymes like GSK3 and transcription factors.

Proliferative signals help in shuttling of SGK1 into the nucleus thereby activating it (Firestone et al., 2003). PI3K pathway converts PIP_2 to PIP_3 which causes phosphorylation and activation of SGK1 by PDK1 at Thr^{256} within the activation loop of SGK1 and Ser^{422} in C-terminal domain, presumably by PDK1-like enzyme (Firestone et al., 2003) (Figure 1.9). In terms of structure, SGK has a catalytic domain homologous to Akt (54% identity), but lacks the PH domain unlike Akt (Lang and Cohen, 2001; Sakoda et al., 2003). SGK1 modifies cell survival by phosphorylating Mdm2 thus enhancing Mdm2-dependent p53 ubiquitylation with subsequent proteosomal p53 degradation. Like in case of Akt, SGK1 also has an Mdm2-p53 autoregulatory loop.

SGK1 is upregulated in several tumours. It mediates the glucocorticoids induced resistance of breast cancer cells to chemotherapy (Lang et al., 2009; Lang et al., 2006). Stimulation of amino acid, peptide, creatine and glucose transport by SGK1 meets the excessive demand of rapidly growing tumour cells.

Downregulation of SGK1 is seen in case of prostate cancer, ovarian tumour and hepatocellular carcinoma; presumably SGK1-dependent functions are taken up by other SGK isoform and Akt.

Taken together the available evidence indicating the role of SGK1 contribution towards tumour development and progression, it forms a potential target for tumour therapy (Lang et al., 2010).

1.4 Bioactive small molecules

As described earlier nature provides us with range of bioactive molecules which not only are important for the survival of the producer but can also be used by other organisms to fight against various invasions like bacterial or fungal infection. Knowing a small molecule is biologically active is as important as knowing its mechanism to utilize its full potential. Therefore, selected compounds were investigated in this study, in terms of their bioactivity towards their mode of action.

1.4.1 Jerantinine E

Indole alkaloids with fascinating structural features have not only attracted synthetic chemist but also biologist because of their remarkable bioactivity. Best representation for this particular group of compound is vinblastine. But due to difficulty in *de novo* synthesis of novel vinblastine analogues, much simpler anti-cancer agents were looked for, *e.g.*, new Aspidosperma alkaloids which were originally isolated from *Aspidosperma* trees. Seven new Aspidosperma indole alkaloids, jerantinine A–G were reported by Kam and co-workers in 2008. These were isolated from leaf extracts of Malayan plant *Tabernaemontana corymbosa* (Figure 1.13) which has a widespread distribution in pantropical regions (Frei et al., 2013; Lim et al., 2008).

One of these jerantinine E (Figure 1.13) displayed significant cytotoxic activity against human cervix carcinoma cells (KB-3-1) which is rare among Aspidosperma alkaloids

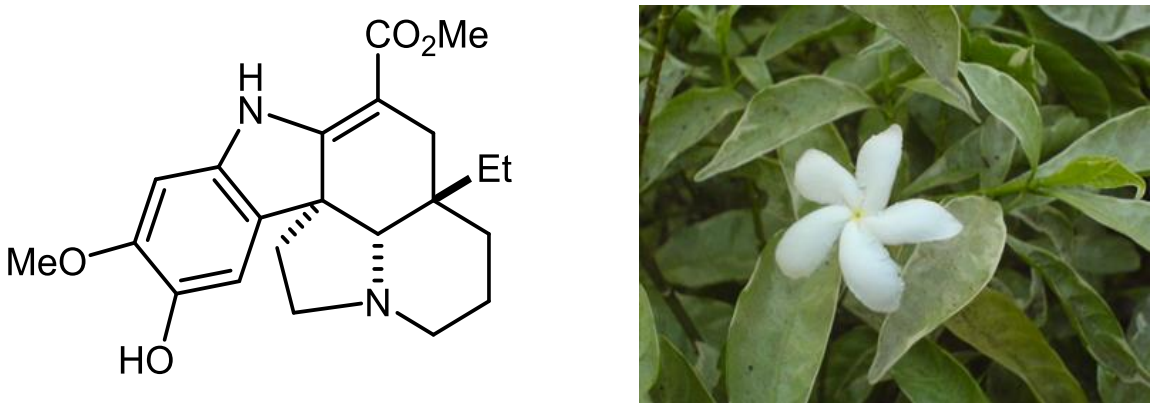

Figure 1.13: Structure of jerantinine E and its source, Tabernaemontana corymbosa

Jerantinine E showed cytotoxicity against vincristine-sensitive (IC_{50}=2.55 µM) and vincristine-resistant (IC_{50}=2.03 µM) epidermoid carcinoma cell lines compared to 0.0054 µM and 1.2 µM by vincristine respectively (Lim et al., 2008). The mode of action for the cytotoxicity was not known. The availability of a significant amount of synthesised jerantinine E allowed us to investigate in this direction.

1.4.2 Paleo-soraphen A and B

Polyketides derived from fungi and bacteria have been in focus of both chemical and biological investigations. The biosynthesis of polyketides follows a modular linear assembly of various enzymes whose genetic analysis can not only be used to rationalize its biosynthesis but also to predict the stereochemical outcome. However deviating from the norms of modular synthesis, most of the polyketide synthases show at least one enzymatic step to be non-productive. Whether this is a consequence of an evolutionary process or the chemical consequence of the substrate is still unknown (Lu et al., 2013).

Soraphens were discovered in the myxobacterium *Sorangium cellulosum* in 1994 (Gerth et al., 1994) and found to be strong inhibitors of the eukaryotic acetyl-coenzyme A carboxylase (ACC). Investigation on the biosynthetic origin identified two positions of the isolated natural product that differed from the genetically expected outcome (Schupp et al., 1995; Wenzel et al., 2006). The compounds that would be expected were prepared synthetically. These compounds were called paleo-soraphen A & B, which are derivatives of soraphen obtained from following the complete intact modular assembly of its polyketide synthases. These were studied to see if and how their biological behaviour is changed. Structurally, a double bond is expected between the C2 and C3 position established by module 8 but is missing in soraphen A due to the inactivity of the dehydratase activity within that domain. (Figure 1.14) There is still a double bond between C9 and C10 which is absent in case of paleo-soraphen B and is proposed to be due to postketide transformations and not a direct consequence of PKS (Lu et al., 2013).

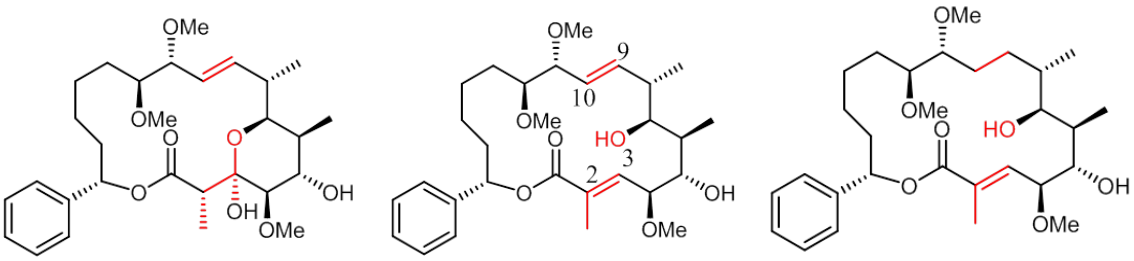

soraphen A **paleo-soraphen A** **paleo-soraphen B**

Figure 1.14: Structure of soraphen A and synthetic polyketides derived from genetic analysis (Lu et al., 2013)

Soraphen A showed antifungal activity, therefore we wanted to study if this activity is still maintained in its derivatives or has acquired a totally different target.

1.4.3 Disorazols

Disorazols, forming a new class of microtubule disrupting macrodiolides, were isolated from the fermentation broth of the myxobacterium *Sorangium cellulosum* strain So ce12 (Hopkins and Wipf, 2009). They comprise a family of 29 variants first isolated in 1994, exhibiting some of the highest cytotoxicities towards animal cells (IC_{50} for disorazol A_1 = 1.6 pM against KB-3-1 cervical carcinoma cells)

1.4.3.1 Disorazol A_1

Disorazol A_1 (Dsz A_1) was identified as the major component, comprising 70% of the relative mass amount compared to the remaining 28 disorazols (Hopkins and Wipf, 2009) isolated from *Sorangium cellulosum* So ce12. Its structure was found to be a macrocyclic ring with two oxazole rings and an epoxide group (Figure 1.15) (Irschik et al., 1995). Dsz A_1 shows exceptional subnanomolar activity against a panel of cancer cell lines.

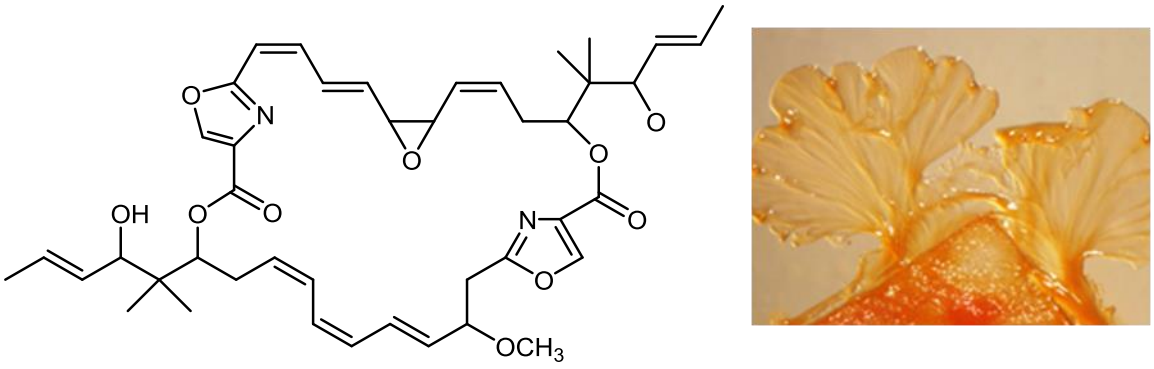

Figure 1.15: Structure of disorazol A_1 (Dsz A_1) and its myxobacterial source

Dsz A_1 is active against many filamentous fungi but not against yeast and bacteria (Irschik et al., 1995). To date Dsz A_1 remains the most extensively studied member of the disorazol family due to its biological activity and mode of action. (Elnakady et al., 2004) demonstrated that the antimitotic effect of Dsz A_1 originates from its tubulin polymerization inhibitory activity. They provided evidence that Dsz A_1 acts in a concentration-dependent manner and independent of microtubule-associated proteins (MAPs), directly exerting its effect on tubulin during polymerization. Immunofluorescence staining showed that at lower concentrations (13 pM) interphase microtubules were not impaired but a nuclear fragmentation was detectable whereas at higher concentration (>100 pM) the microtubular network was completely disrupted. Mitotic cells showed an abnormal spindle formation (Elnakady et al., 2004). Treatment with Dsz A_1 causes a cell cycle arrest at G_2/M checkpoint triggering apoptotic cell death cascade (Hopkins and Wipf, 2009). Dsz A_1 has a high inhibitory effect even against the multi-drug resistant cell line KB-V1 expressing high Pgp levels. Enhanced Pgp levels causes enhanced drug efflux and reduce drug accumulation which is a leading cause for resistance shown towards paclitaxel or Vinca alkaloids.

Immunofluorescence staining showed a nuclear localization of the tumour suppressor protein p53 (Elnakady et al., 2004) at lower concentrations of Dsz A_1. Though the microtubular network was not altered much at low concentration, its dynamics could be suppressed enhancing the trafficking of p53 towards the nucleus. Paclitaxel and vincristine have also shown similar effect of p53 nuclear trafficking at a concentration lower than what is required for effecting tubulin polymerization (Chumakov, 2000; Giannakakou et al., 2002). To investigate the role of p53 translocation upon Dsz A_1 treatment, its mode of action was studied in more detail.

1.4.3.2 Disorazol Z

Disorazol Z (Dsz Z, Figure 1.16) is produced by fermentation of the myxobacterium *Sorangium cellulosum* So ce1875. It shows potent inhibition of tumour cell lines (IC_{50} = 1.3 nM in KB/HeLa cells) (Guenther et al., 2013).

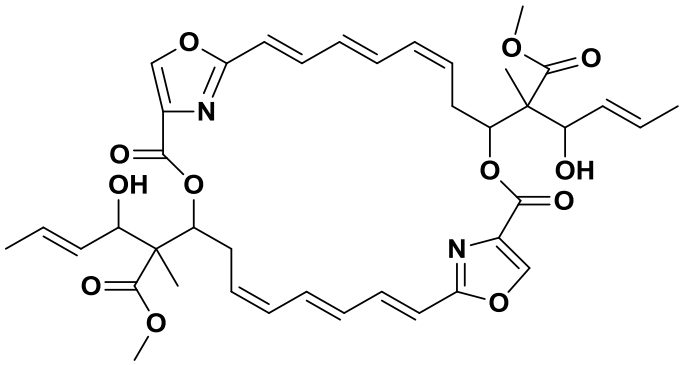

Figure 1.16: Structure of disorazol Z (Dsz Z)

With human Gonadotropin releasing hormone (GnRH receptor [hGnRH-R]) positive cells, a dose-dependent inhibition of cell proliferation in presence of Dsz Z was observed unlike in case of hGnRH-R negative cells. This effect was not only receptor-mediated but its anti-proliferative efficacy was heightened by administering a conjugate of Dsz Z with [D-Lys^{6}]-LHRH (luteinizing hormone-releasing hormone). On the other hand only a moderate suppression of tumour growth was observed by using unconjugated Dsz Z (Guenther et al., 2013). A variety of tumours, including breast, ovarian and prostate express receptors for LHRH (also regarded as GnRH) which can increase the chances of targeting such tumours by directing these cytotoxic agents by covalently binding them to an LHRH agonist peptide. This conjugate when internalized into the cell will release the cytotoxic agent upon hydrolysis (Weissman and Muller, 2010). The bioactivity and detailed mode of action was also investigated during this study.

1.5 Aim of the project

Historically nature has been an important source of compounds, with knowledge of its toxic or medicinal properties often long predating knowledge of its precise target or mechanism (Schenone et al., 2013). High content methods can be used for both screening and profiling bioactive compounds to obtain hints about their mode of action by comparing them with compounds of known mechanism.

The study presented made use of high content analysis profiling to investigate the mode of action of selected compounds. Automated microscopy, a labelled cell-based profiling method formed the basis for further studies of their mechanisms along with a label-free non-invasive detection method – xCELLigence, which is based on impedance profiling. Our aim was to gain insights into the mode of action or at least to know the affected pathway for jerantinine E, an alkaloid, polyketides like paleo-soraphen A & B and two members of the disorazol family. The approaches utilized helped narrowing down the target search and follow-up studies have corroborated the hypothesis and elucidated their details.

2 Materials and methods

2.1 Materials

2.1.1 Equipment

Automated microscope	ImageXpress® Micro (Molecular Devices)
Cell counter	Cedex XS (Innovatis)
Cell culture incubator	CO_2-Auto-Zero (Heraeus)
Centrifuges	Biofuge (Heraeus)
	5810R (Eppendorf)
	5418R (Eppendorf)
Fluorescence microscope	Axioplan with Axiocam camera (Zeiss)
Gel electrophoresis system	Mini PROTEAN system (Bio-Rad)
Laminar airflow	Maxisafe 2020 (Thermo Fisher Scientific)
Microplate washer	405 Select TS (Biotek)
Plate reader	Infinite M200 pro (Tecan)
Robot pipette with pintool	Biomek FXP Laboratory Automation Workstation (Beckman Coulter)
Semi-dry transfer system	Trans-Blot® SD (Bio-Rad)
Shaker	Titramax 1000 (Heidolph)
xCELLigence incubator	MIDI 40, CO_2 incubator (Thermo Fisher Scientific)
xCELLigence RTCA system	RTCA SP (Acea Biosciences)
X-ray processor	Optimax (ClassicXray)

2.1.2 Software

AcuityXpress™ 2.1.0.2, Autodock 4.0, AxioVision 4.8, Cedex XS software, ChemDraw Std 12.0, GelQuantNET 1.8.2, i-Control™, ImageJ, MetaXpress 2.0.0.13, Microsoft Office 2010, R, RTCA software 1.2, SigmaPlot 12.3.

2.1.3 Consumables

All consumables were purchased from Becton Dickinson, Eppendorf, Greiner, Macherey-Nagel, Nunc, Thermo Fisher Scientific, TPP or Roth, unless otherwise stated. For high

content analysis, microtitre plates were obtained from Corning (384 well) and E-plate (96 well) for xCELLigence from Roche/Acea Biosciences.

2.1.4 Chemicals

All chemicals were obtained from Alexis Biochemicals, Bayer, Becton Dickinson, Fluka, Gibco, Invitrogen, JT Baker, Merck, Roche Diagnostics, Serva, Thermo Fisher Scientific, Roth or Sigma.

2.1.5 Antibodies/ Dyes

Anti-akt antibody (rabbit)	Cell Signaling
Anti-anillin (rabbit)	Bethyl Laboratories
Anti-calmodulin (mouse)	Invitrogen
Monoclonal anti-Pan Cytokeratin, Clone C-11 (mouse)	Sigma
Anti-c-Fos (rabbit)	Sigma
DAPI dihydrochloride	Sigma
Monoclonal GAPDH (HRP conjugate) (rabbit)	Cell Signaling
Anti-GRP94 (rat)	Sigma
Monoclonal anti-p53, Clone BP53-12 (mouse)	Sigma
Polyclonal anti-PI3 Kinase p110 (rabbit)	Cell Signaling
Polyclonal anti-PI3 Kinase p85 (rabbit)	Cell Signaling
Monoclonal anti-PTEN (D4.3) XP™ (rabbit)	Cell Signaling
Anti-PDK1	Cell Signaling
Monoclonal anti-Splicing Factor SC-35, Clone SC-35 (mouse)	Sigma
Trypan blue solution	Roche
Monoclonal anti-α-Tubulin, Clone B-5-1-2 (HCA),DM1A (mouse)	Sigma
Phospho-Akt (Ser473) (rabbit)	Cell Signaling
Phospho-CREB (rabbit)	Sigma

Phospho-p53 (Ser15) (rabbit)	Cell Signaling
Phospho-PDK1 (Ser241)(C49H2) (rabbit)	Cell Signaling
Phospho-p38 MAPK (Thr180/Tyr182) (rabbit)	New England Biolabs
Phospho-p44/42 MAPK (Thr202/Tyr204) (mouse)	New England Biolabs
Phospho-PI3K p85 (Tyr458)/p55 (Tyr199) (rabbit)	Cell Signaling
Phospho-p53 (Ser315) (rabbit)	Santa Cruz
Phospho-SGK (Ser 422) (rabbit)	Santa Cruz
SignalSilence® Control siRNA (Fluorescein conjugate)	Cell Signaling
SignalSilence® PI3 Kinase p85α siRNA I (mouse)	Cell Signaling
SignalSilence® PTEN siRNA II	Cell Signaling
Alexa Fluor 488 Phalloidin	Molecular Probes
Alexa Fluor 488 anti-rabbit (goat)	Molecular Probes
Alexa Fluor 549 anti-rabbit (goat)	Molecular Probes
Alexa Fluor 594 anti-mouse (goat)	Molecular Probes
Alexa Fluor 488 streptavidin	Molecular Probes
Alexa Fluor 488 anti-rat (rabbit)	Invitrogen
Anti-mouse (rabbit)	Dianova
Anti-rabbit (HRP-linked)	Cell Signaling

2.1.6 Culture media

The mammalian cell culture media used are listed in Table 2.1

Table 2.1: Media used for different cell lines

Cell line	Medium	Manufacturer	Supplements
A-549, L-929	MEM	Gibco	10% FBS (Lonza)
KB-3-1, A-431	DMEM	Lonza	10% FBS (Gibco)
PtK2	MEM	Gibco	1X Non-essential amino acids (Gibco) 1X GlutaMAX (Gibco) 10% FBS (Lonza)
PC-3	F-12 K	Gibco	10% FBS (Gibco)
MCF-7	DMEM	Gibco	1X Non-essential amino acids (Gibco) 1.5% Insulin (Gibco) 10% FBS (Lonza)
HUVEC	EMB®-2	Lonza	EMB®-2 bullet kit

2.1.7 Buffers

1. 10X SDS running buffer: 288 g glycine
   60.4 g Tris Base
   20 g SDS
   2 L distilled water

The buffer was diluted to 1X with distilled water to make working SDS running buffer.

2. 10X TBS buffer for western blotting (pH: 7.0): 160 g NaCl
   4 g KCl
   12.2 g Tris Base
   2 L distilled water

The working TBS solution was prepared by diluting the 10X buffer to 1X with distilled water.

TBST buffer was made by adding 1 mL Tween-20 to 1000 mL of 1X TBS buffer.

3. 10X blotting buffer: 25 mM Tris HCl
   192 mM Glycine

The working blotting buffer was prepared by diluting 10X buffer to 1X with distilled water.

2.1.8 Kits

BCA protein assay kit	Thermo Fisher Scientific
Caspase-Glo® 3/7 assay kit	Promega

Cell death detection ELISA ^{PLUS} kit	Roche
MycoAlert ® Mycoplasma Detection Kit	Lonza
SuperSignal® West Pico Luminol solution	Thermo Fisher Scientific
SuperSignal® West Femto Luminol solution	Thermo Fisher Scientific

2.1.9 Cell cultures

Table 2.2: Mammalian cell lines

Cell line	Source	Species	Origin	Morphology
A-549	DSMZ ACC 107	Human	Lung cancer	Epithelium-like
A-431	DSMZ ACC 91	Human	Epidermal cancer	Epithelium-like
KB-3-1	DSMZ ACC 158	Human	Cervical cancer	Epithelium-like
L-929	DSMZ ACC 2	Mouse	Connective tissue	Fibroblasts
MCF-7	DSMZ ACC 115	Human	Breast cancer	Epithelium-like
PtK2	ATCC CCL-56	Potoroo	Kidney	Epithelium-like
PC-3	DSMZ ACC 465	Human	Prostate cancer	Epithelium-like
HUVEC	Lonza C2519	Human	Umbilical vascular endothelium	Cobblestone-like

2.2 Methods

2.2.1 Working with mammalian cell cultures

2.2.1.1 Cultivation

Work with mammalian cell cultures was performed under sterile condition of laminar hood. The required media were warmed at 37°C before using. The cells were kept in cell culture flasks at 37°C and 10% CO_2. The media volume depended on the size of the cell culture flasks viz. 10 mL for 25 cm^2 (T25), and 30 mL for 75 cm^2 (T75) flasks. Adherent cells like L-929 and KB-3-1 were harvested and passaged when they were semi-confluent (~ 80-90% confluency). The cell layer was scraped with a cell scraper from the bottom of the vessel and the cells were suspended by repeatedly pipetting up and down with a sterile disposable plastic pipette. Other cell lines like PtK2, A-549, A-431, PC-3, MCF-7 were trypsinised for passaging. To trypsinise the cells, the culture media was removed and the cell surface was rinsed once with EBSS. Cells were later incubated at room temperature under clean bench for one min or two with 1 mL of pre-warmed trypsin. Pre-warmed trypsin was discarded and the flask was incubated at 37°C for 5-13 minutes. The trypsinisation was stopped by adding fresh culture medium. The serum in the culture medium inactivates trypsin. Subsequently, an aliquot with different dilutions depending on the requirement was transferred to a new cell culture flask with fresh medium. The primary HUVECs were trypsinised for 2 min, and the reaction stopped by incubation with a trypsin stop solution at 37°C for 5 min. Fresh media was added to make cell suspension which was centrifuged at 1500 rpm for 5 min. The supernatant was discarded to ensure complete removal of trypsin and trypsin stop solution. Fresh media was added again to prepare a cell suspension.

All cell lines were maintained up to 1 year in culture except for HUVEC which is best to use within 5-6 passages. They were then discarded and a new culture from cryo-preserve was restarted. All cell cultures were semi-annually tested for mycoplasma using MycoAlert® detection kit according to the manufacturer's protocol.

2.2.1.2 Storage of cells

For long term storage, the cells were harvested as for sub-culturing. They were then harvested by centrifugation (3000 rpm, 3 min), pelleted and re-suspended in 1 mL of freezing medium. They were transferred to cryo-tubes which were put into a freezing container (Nunc Cryo™ tube vials) at -70°C for at least 24 hours. After that the cells were maintained in a liquid nitrogen storage container at -196 ° C.

To reactivate the cryo-preserved cells, the cells were quickly thawed at 37°C and seeded in 10 mL of fresh medium in a T25 flask. After a day, the cell culture medium was changed to remove the freezing medium completely.

2.2.2 MTT assay

Anti-proliferative activity was measured in 96-well transparent plates. 60 µL of serially diluted compounds were added to 120 µL of suspended cells (50,000 cells/mL; duplicates). The end concentrations tested ranged from 37 µg/mL to 0.1 ng/mL. After five days of incubation with the compounds, the metabolic activity in each well was determined using an MTT (3-(4, 5-dimethylthiazol-2-yl)-2, 5-diphenyltetrazolium bromide) reagent. 20 µL MTT in PBS were added to give a final concentration of 0.56 mg/mL and incubated for two hours. MTT is reduced by dehydrogenase of the cell to form purple formazan crystals. The precipitate was washed with 100 µL PBS and dissolved in 100 µL isopropanol containing 0.4 % hydrochloric acid. The resulting colour was measured at 595 nm using a plate reader.

2.2.3 xCELLigence – High Content Analysis (HCA)

2.2.3.1 Equipment/Software

RTCA SP (Real Time Cell Analyser Single plate) instrument consisting of

RTCA analyser

RTCA SP station

E-plate 96 and

RTCA control unit

RTCA software 1.2.1

Software R version 2.12.2

2.2.3.2 Impedance measurement

Changes in impedance readings were measured over a period of five days. 60 µL of the cell media was added to both an E-plate and a normal micro titre plate (MTP) and left for half an hour under clean laminar hood to stabilise. Meanwhile cell suspension was prepared from L-

929 cells at a dilution of 1, 00,000 cells/mL. After half an hour background measurement was taken by placing the E-plate on the RTCA SP station which is placed inside an incubator at 37°C and 10% CO_2. Later 120 µL of cell suspension was added to each well and left under the clean laminar hood for half an hour for homogenous distribution of cells. Later the plate was placed for impedance measurement for 24 h by clamping the plate in the station. The following day the E-plate was taken out of the incubator and 1 µL of test compounds at a concentration of IC_{90} or highest available concentrations were added under the clean laminar hood. Table 2.3 shows the reference compounds included used for the analysis. These reference compounds were added in triplicates and change in impedance was recorded.

Table 2.3: Library of reference compounds

S. No.	Name	Mode of action	Concentration in library (μM)	S.No.	Name	Mode of action	Concentration in library (μM)
1.	A23187	ion-carrier (e.g. calcium)	110	**33.**	MG132	proteasome inhibitor	400
2.	Actinomycin D	transcription inhibitor	4.4	**34.**	Myriaporone	inhibits protein synthesis	70
3.	Alsterpaullone	CDK inhibitor	200	**35.**	Myxothiazol A	inhibits respiratory chain	12
4.	Amanitin	blocks mRNA synthesis	1000	**36.**	Neopeltolide	inhibits respiratory chain	100
5.	Anisomycin	inhibits protein synthesis	45	**37.**	Nocodazole	promotes microtubule depolymerisation	12
6.	Aphidicolin	inhibits DNA-polymerase	1000	**38.**	Okadaic acid	inhibits Ser/Thr phosphatases	10
7.	Apicidin	histone-deacetylase (HDAC) inhibitor	100	**39.**	Oligomycin	F-ATPase inhibitor	70
8.	Apicularen	V-ATPase inhibitor	31	**40.**	Oxamflatin	histone-deacetylase (HDAC) inhibitor	1200
9.	Archazolid B	V-ATPase inhibitor	3	**41.**	PD169316	p38-MAP-Kinase inhibitor	10,000
10.	Argyrin A	proteasome inhibitor	1000	**42.**	PMA	activates protein kinase C	3500
11.	Brefeldin A	vesicle trafficking	50	**43.**	Podophyllotoxin	promotes microtubule polymerisation	2.5
12.	Camptothecin	topoisomerase I inhibitor	450	**44.**	Puromycin	inhibits protein synthesis	500
13.	Chelerythrine	protein kinase C inhibitor	1000	**45.**	Purvalanol A	CDK inhibitor	2000
14.	Chivosazole A	actin polymerisation inhibitor	1.3	**46.**	Rapamycin	PI3-Kinase inhibitor	11
15.	Chondramid C	stabilises actin filaments	10	**47.**	Ratjadon C	blocks nuclear receptor	3.5
16.	Colchicine	inhibits microtubules	10	**48.**	Rhizopodin A	inhibits actin polymerisation	10
17.	Cruentaren A	F-ATPase inhibitor	14	**49.**	Saframycin Mx1	inhibits DNA synthesis	40
18.	Cycloheximide	inhibits protein synthesis	450	**50.**	SB202190	p38-MAP-Kinase inhibitor	10,000
19.	Cyclosporin A	affects calcium regulation	5500	**51.**	SB203580	p38-MAP-Kinase inhibitor	10,000
20.	Cytochalasin D	promotes actin depolymerisation	100	**52.**	Scriptaid	histone-deacetylase (HDAC) inhibitor	4000
21.	Dexamethasone	immunosuppressive effect	4500	**53.**	Simvastatin	inhibits cholesterol biosynthesis	800
22.	Doxorubicin	topoisomerase II inhibitor	340	**54.**	Soraphen A	inhibits lipid synthesis	400
23.	Emetine	inhibits protein synthesis	41	**55.**	Staurosporine	inhibits protein kinase	3
24.	Epothilone B	stabilises microtubules	0.55	**56.**	Taxol	microtubule stabiliser	25
25.	Etoposide	topoisomerase inhibitor	2300	**57.**	Trichostatin	histone-deacetylase (HDAC) inhibitor	310
26.	Gephyronic acid A	inhibits protein translation	60	**58.**	Tubulysin B	inhibits microtubule polymerisation	0.4
27.	Griseofulvin	inhibits spindle apparatus	10,000	**59.**	Tunicamycin	glycoprotein synthesis	700
28.	H89	protein kinase A inhibitor	10,000	**60.**	Velcade	proteasome inhibitor	11
29.	Indirubin-3'-monoxime	CDK inhibitor	8000	**61..**	Vinblastin	inhibits microtubule polymerisation	0.5
30.	LY294002	PI3-Kinase inhibitor	10,000	**62.**	Vioprolid A	PI3 Kinase inhibitor	7
31.	Methotrexate	inhibits DNA synthesis	50	**63.**	Wortmannin	PI3-Kinase inhibitor	10,000
32.	Mevastatin	inhibits cholesterol biosynthesis	1200				

The E-plate also had wells with DMSO or methanol added to it as a solvent control and it was ensured that its concentration did not exceed 0.1% DMSO or methanol. The same set of test compounds were added to the normal MTP and returned to the incubator at 37°C. The test compounds were done in triplicates and randomly distributed all over the E-plate to avoid batch affects. The E-plate was returned to the incubator and the impedance read over the span of four days. The comparative MTP was used for microscopic evaluation.

2.2.3.3 Analysis

The time-dependent cellular response profiles (TCRP) were recorded by Roche RTCA software. Data processing and mining workflow was implemented in the statistical programming language R, Version 2.12.2 (R Development Core Team, 2011). The analysis starts with importing the raw impedance data provided by RTCA software as cell index (CI) followed by its normalization as suggested by Abassi and colleagues (Abassi et al., 2009) by dividing the cell indices for each time point after the compound was added by the cell index at the reference point. The last measurement taken before compound addition was considered as the reference point. For subsequent analysis, only the readings after compound addition were considered. Median polish procedure was implemented to detect and remove the outliers. To retain the complexity of the data while reducing the dimensionality of the data set, cubic smoothing splines were used to approximate the TCRPs. Spline basis coefficients were used as descriptors to construct the distance matrix which was used for hierarchical cluster analysis. A heat map was generated which displays the Z-transformed values of the 22 descriptors which equals to basis spline coefficients. Hierarchical cluster analysis of the reference compounds together with the test compounds was carried out. Clustering of test compounds with reference compounds with known activity was used to predict the mode of action of test compound.

2.2.4 Automated microscopy – High content image analysis

2.2.4.1 Equipment/Software

Automated microscope consisting of the following

ImageXpress® Micro (IXM)

High-speed laser autofocus

Digital CCD-camera

300 Watt Xenon lamp

Filter sets:	DAPI
	FITC
	TRITC
	Texas Red
Nikon Objective:	4X Plan Apo, NA (Numerical Aperture) 0.20
	10X S Fluor, NA 0 50

20X S Fluor, NA 0.75

40X Plan Apo, NA 0.95

60X Plan Fluor, NA 0.85

Biomek

MetaXpress® 2.0.013

AcuityXpress™ 2.1.0.2

2.2.4.2 Preparation of HCA plates

Six MTP's (384 well) were prepared with KB-3-1 cells. Semi-confluent KB-3-1 cells were trypsinised and counted. 2500 cells/well were seeded (60 µL) leaving out all the edge wells due to technical difficulties of obtaining images using the automated microscope. Seeded plates were incubated at room temperature in a clean bench for one hour followed by incubation at 37°C for three hours. Meanwhile the 96-well stock plate containing the reference compounds, the HCA library, and the test compound dissolved in DMSO were placed at room temperature. The compounds included in the HCA library are similar to the one used in the xCELLigence system as shown in the previous section (Table 2.3).

After incubation, the plates were treated with the reference and test compounds using a liquid handling robot with pintool device. Each pin of the pintool adds approximately 70-80 nL of the compound to each well with one dip. Plates were then incubated at 37°C for overnight. Following day the plates were fixed and permeabilised either with ice-cold methanol:acetone (1:1) or 3.7% formalin/Triton X-100 depending on the antibody set used for a plate. Then the plates were washed with 50 µL/well of PBS. In all the liquid discarding steps a microplate washer (Biotek) was used. Plates were blocked for an hour with 10% FBS made in PBS. Blocking solution was discarded followed by addition of 20 µL/well of primary antibody as shown in Table 2.4. Plates were centrifuged for one minute at 1000 rpm followed by incubation at 37°C for one hour or at 4°C for overnight with sides sealed with parafilm to avoid evaporation and covered in aluminium foil. All the phospho antibodies were by default incubated for overnight (O.N.) at 4°C as longer incubation provided with better image results. Plates were washed with PBS and incubated with the secondary antibody (20 µL/well) for one hour at room temperature. Then the plates were washed and incubated with 2 µg/mL of DAPI (20 µL) for ten minutes. Plates were washed once and stored with 50 µL/well of PBS for microscopic viewing.

Table 2.4: Antibody sets

Set	Target	Source (reagent)	Fixation	Dilution	Incubation time
I	Actin	(Phalloidin)	Formalin	1:400	1 h
	α-tubulin	Mouse	Formalin	1:6000	1 h
II	ER	Rat	MeOH/Acetone	1:4000	1 h
	Cytokeratin	Mouse	MeOH/Acetone	1:2000	1 h
III	Anillin	Rabbit	Formalin	1:1000	1 h
	SC-35	Mouse	Formalin	1:4000	1 h
IV	Phospho-p38	Rabbit	Formalin	1:400	O.N.
	Phospho-p44/42	Mouse	Formalin	1:400	O.N.
V	c-Fos	Rabbit	Formalin	1:3000	1 h
	p53	Mouse	Formalin	1:1600	1 h
VI	Phospho-CREB	Rabbit	Formalin	1:1000	O.N.
	Calmodulin	Mouse	Formalin	1:400	O.N.

2.2.4.3 Acquisition

Images were acquired using MetaXpress with the settings described below.

Magnification: A 10X lens was used for both counting the cells as well as for high content image analysis (HCIA).

Camera binning: The ratio between the signal (intensity of the object of interest, S) and the noise (background, N) determines how hard it will be for the software to distinguish important features in an image. If the ratio is small it is more difficult for the software to distinguish between the object of interest and background. One way to increase the S/N ratio is to bin pixels, i.e., to combine adjacent pixels to create an effect of a single larger pixel. This is of course at the cost of image resolution. A camera binning of 2, i.e., combining 2*2 pixels to form one big pixel was found to be adequate maintaining acceptable levels of S/N ratio and good image resolution.

Camera gain: Specifies to the amplification to be applied to the camera output. Camera gain of 1 was found to give good image quality.

Plate: Settings had to be changed for different plates based on plate dimensions like height, length, width, diameter and thickness of the well bottom. One particular plate setting was optimized for Corning plate (catalogue #: 3683) and the same was used for all HCIA.

Well selection: Wells apart from the peripheral ones were selected to acquire images due to technical difficulties and also to get rid of edge effect encountered with KB-3-1 cells. The wells, in which neither the reference nor test compounds were added, were also excluded from image acquisition.

Site selection: The more number of sites per well are chosen the more data will be acquired but this makes the process slow and takes up huge memory space. To count the number of cells more sites were considered but for HCIA four sites/well were optimal.

Time lapse: Since HCIA is not a kinetic measurement, only one time point was considered.

Filters: Three filter sets were used:

DAPI: excitation: 358 nm and emission: 461 nm – used to count the number of cells

FITC: excitation: 494 nm and emission: 518 nm

Texas Red: excitation: 577 nm and emission: 620 nm

Autofocus option: There are two kind of autofocus option – laser and image based. Image based focusing selects the best focused image from multiple images which makes the operation slower whereas the laser based focusing sets the focus according to reflecting well bottom and then a manually set offset is utilized. This is faster but comes handy only if the object of interest is found in same distance from the well bottom. For HCIA always laser-based focusing was taken into consideration over image-based.

Wavelength settings: For each wavelength, exposure time and Z-position had to be adjusted manually. Initially the exposure time and Z-position was set based on negative control with DMSO only.

2.2.4.4 Image analysis - software and application modules

Acquired images were analysed using different application modules provided by MetaXpress. There are two different ways in which data can be analysed.

Cell and image-based analysis: Cell-based analysis takes into consideration individual cell whereas image-based analysis takes an average of all the sites in a well. In HCIA both kind of analysis were used and provided with almost similar results. Each of these analyses can make use of different application modules based on the requirement. About 18 different application modules are provided by MetaXpress® out of which few are mentioned in Table 2.5 which are quite useful for HCIA though mostly two were used, i.e., Multi Wavelength Cell Scoring (MWCS).and Transfluor.

Table 2.5: Different modules in MetaXpress

S. No.	Application modules	Purpose
1	Angiogenesis tube formation	Tube/vessel formation/inhibition in angiogenesis or development
2	Mutli Wavelength Cell Scoring (MWCS)	Cell Viability, Membrane potential, Cytotoxicity, Apoptosis
3	Transfluor	Studying intracellular structures
4	Translocation	Cell signalling by translocation
5	Count nuclei	Counting cells

Multi Wavelength Cell Scoring (MWCS): This module can be used when more than one type of staining has been carried out. Parameters such as size of the object (minimum and maximum width) and stain intensities are taken into consideration for each wavelength. The settings were manually altered for each wavelength. In our study we used three different wavelength i.e. W1: DAPI, W2: FITC and W3: Texas Red. Descriptors provided by MWCS which are used later for analysis are mentioned in Table 2.6.

Table 2.6: MWCS descriptors

Image-based analysis
Total cells: Total number of cells based on DAPI.
(%) Positive W2/W3: Number of cells stained for each wavelength (both absolute and relative)
Scoring profile 1--/12-/1-3/123: absolute number of cells which are stained for different wavelength, For example: 1-3 shows the number of cells stained only for 1(W1) and 3 (W3) but not 2 (W2) and so on.
Cell-based analysis
Total area: Nuclear surface
Stained area W1/W2/W3: Coloured surface of respective staining
Positive W2/W3: absolute number of cells stained for each wavelength
Average/integrated intensity W1/W2/W3: average/integrated intensity of each stain

Transfluor: This module was exclusively used for counting objects like pits and vesicles which were shown in case of SC-35 staining. Parameters such as the nucleus size, vesicle and pit count were taken into consideration. Descriptors provided by Transfluor are mentioned in Table 2.7.

Table 2.7: Transfluor descriptors

Image-based analysis
Pit count per cell: Total number of pits per cell
Pit average intensity: average intensity of all the pits in each well
Vesicle count per cell: absolute number of vesicles per cell
Vesicle average/integrated intensity: average or integrated intensity of all the vesicles in each well
Nuclear count: Total number of cells based on W1 wavelength
Nuclear average intensity: average intensity of all the cells in a well

All the descriptors for cell based analysis were the same as for image-based analysis except that each cell is taken into consideration unlike image-based analysis. Also, all the cell based descriptors have a prefix cell, *e.g.*, Cell:Total cell.

2.2.4.5 Data analysis – software and methodology

Huge amount of data obtained from application modules are analysed using AcuityXpress™. Workflow adopted to analyse these data is mentioned below.

Annotation: All the plates were first annotated before any analysis could be performed. Excel sheets containing names of all compounds and their concentration including negative control could be imported into AcuityXpress™ in *csv* format

Normalization: The data was normalized against the negative control since for this HCIA we didn't have positive control for all the test compounds. Each of the six plates was normalized separately based on cell or image based analysis. We used min-max scaling due to lack of positive control. All cell based parameters have a prefix of cell unlike image based parameter which has no prefix, *e.g.*, Total cells, Average intensity etc.

Creation of dataset: All the six plates used for one set of HCIA experiment were combined into one dataset. Two kinds of dataset can be created – cell-based and image-based. For each kind of dataset their respective descriptors should be used.

Centre and scaling the data: Data were transformed by scaling, i.e., subtracting mean from each data point and centring i.e. dividing each data point by variance (average of squared difference from the mean). This gave Z-values and helped in good interpretation of the data.

Different analysis method: After all the data transformation described above was carried out, data could be analysed using different analysis methods with AcuityXpress™ which provides both hierarchical and non-hierarchical clustering methods.

Hierarchical clustering is good for finding the relationship of each row or column in the dataset to every other row or column and also when one does not have prior knowledge of how the data will be clustered, as hierarchical clustering does not set the number of clusters to form before the analysis. In case of HCIA, hierarchical analysis was found to be more useful as we wanted to know how each compound clusters with every other compound included in the dataset. Hierarchical clustering produces tree structure called dendrogram which presents the distance of similarity between the clustered rows or columns. Figure 2.1 shows a typical row hierarchical cluster.

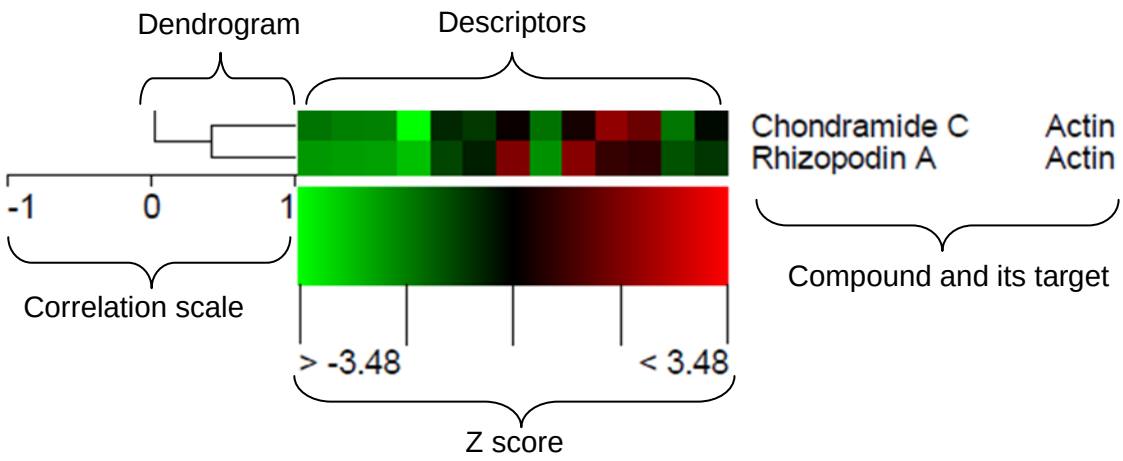

Figure 2.1: Typical example of hierarchical cluster analysis through heat map

Graphical representation of data where the Z-values for each measured parameter is represented by colours. In Figure 2.1 each coloured column indicates a descriptor and the colour gradations are based upon the Z-score. Z score is standard deviation from mean. For example a Z score of 0 has the same value as the mean whereas a Z score of 1 is exactly one standard deviation above the mean. Similarly a Z score of -1 is one standard deviation below the mean. Compounds with similar mode of action cluster together.

Non-hierarchical clustering method is used when one is more interested in separating rows (cells, compounds) into distinct classes than in the relationships between the classes. It forces the data into user-defined number of clusters. In this case the user has prior knowledge about the number of clusters they want to form. In our case, we performed gap statistics to identify the number of main clusters in the whole dataset and then used non-hierarchical clustering method to find that many clusters. This kind of clustering method includes Principal Component Analysis (PCA) and Self-Organizing Map (SOM).

SOM is used to group the rows together with similar pattern over the columns. The clusters are arranged in a two-dimensional grid. The benefit provided by this is a simple representation of similarity between the clusters. Clusters showing similar profile across rows occupy nearby slots on the grid whereas dissimilar ones will occupy distant slots. PCA on the other hand is used to produce a low dimensional summary of the data. When a large dataset like HCIA is being analysed, it's worthwhile to analyse the correlations among the parameters to ensure that measurements that should be correlated, are actually correlated. This can be done using PCA.

2.2.5 Immunofluorescence

Cell seeding: For immunofluorescence staining, cells were cultured on sterile coverslips with a diameter of 13 mm placed into the wells of a four well plate. PtK2 or A-549 cells were harvested by trypsinising a semi-confluent culture and diluted with their respective medium at 1:3 ratio. 750 µL of the diluted cell suspension was added to each well and incubated overnight to ensure complete adherence. Compounds were added the following day. Care was taken that the concentration of the vehicle solvent MeOH/DMSO did not exceed 0.5%/0.1% respectively. The cells were incubated with the compounds at 37°C for overnight.

Fixation: After compound incubation, the cells were either fixed with 750 µL of 3.7% formalin or methanol:acetone (MeOH:Ac; 1:1) for 10 minutes. The cells were washed once with sterile PBS and then treated for 5 min with 0.1% Triton X-100 in case of formalin fixation After Triton X-100 treatment, the cells were again washed once with sterile PBS.

Staining: Appropriate antibodies were used for staining. The primary antibody dilution varied with the antibody in use. Usually it was in the range of 1:100 to 1:500. The dilutions were prepared in sterile PBS containing 10% FBS. The cells were incubated for one hour with 240 µL of the primary antibody in each well at 37°C and then washed with PBS twice. Then the cells were incubated with 240 µL of a secondary antibody tagged by a fluorochrome for one hour (Alexa Fluor 488 or 594). The secondary antibody was diluted to 1:500 with sterile PBS containing 10 % FBS. The cells were washed twice with PBS. The coverslips were then removed from the wells, excess liquid removed by soft tissue paper and embedded (with the cells facing down) onto a microscope slide with a drop of embedding medium which either excluded or included DAPI depending on the requirement to stain the nucleus (ProLong Antifade).

Documentation: Images were taken with the CCD camera Axiocam mounted on the fluorescence microscope Axioplan (both from Zeiss). Neofluor objectives with magnifications of 63X and 100X were used for viewing. All the images were taken at 63X magnification.

2.2.6 SDS-PAGE

Sodium dodecyl sulphate polyacrylamide gel electrophoresis (SDS PAGE) was performed using commercially available gels from Bio Rad (4-20% Tris HCl gradient gel). Semi-confluent KB-3-1 cells were lysed using MPER® cell lysis buffer from Thermo Fisher Scientific and supplemented with HALT® protease/phosphatase inhibitor from Roche (1X). Protein was quantified using the Bradford method in BCA protein assay kit from Thermo Fisher Scientific.

20 µg of protein from the lysate was mixed with 5 µL of 4X SDS loading dye (Roth) and heated at 96°C for 12 minutes. Samples were left at room temperature for one min and short centrifuged to bring down any liquid which had evaporated to the Eppendorf's cap. The sample was then loaded to the individual wells of the SDS gel placed in a vertical electrophoresis tank with 1X SDS running buffer. A protein marker (10-250kDa range) was also loaded to one well. Electrophoresis was carried out at 120 V for 1.5 hours or till the loading front reached the end of the gel. Now this gel can either be stained with Coomassie Brilliant Blue or subjected to Western blot.

2.2.7 Western blot

Transfer: The protein bands from the SDS PAGE gel were transferred onto nitrocellulose membranes by a semi dry transfer method. The nitrocellulose membrane and extra thick Whatman filter paper was cut into 6 x 9 cm dimension. The membrane, 2 extra thick Whatman filter papers and the gel with protein bands were then soaked in 1X blotting buffer with 20% methanol for 30 minutes with gentle stirring to equilibrate the gel and remove SDS. Then the membrane was placed onto extra thick Whatman filter paper. The gel was layered over the membrane and another extra thick Whatman paper was placed. A roller was gently

rolled over this stack of paper and gel to remove any possible air bubbles lodged which might interfere with efficient transfer of protein bands. The transfer was allowed to proceed at constant voltage of 15V and 500 mA for 30 minutes.

Blocking and antibody incubation: The nitrocellulose membrane was then removed from the transfer cassette and washed in TSBT buffer for 5 minutes before blocking it with 5 % BSA prepared in TBST buffer at room temperature for two hours or at 4°C for overnight to block unspecific binding sites. The membrane was then shortly washed once with TBST. 10 µL of the stock antibody was added to 10 mL of TBST solution containing 1% BSA. This antibody mix was added to the blot and incubated at room temperature for 2 hours or at 4°C overnight. The primary antibody solution was removed, and blotted membrane washed 5 times (for 5 min each) with TBST. The blot was then incubated with 10 mL TBST containing 1% BSA and 5 µL of the secondary antibody conjugated to HRP. After incubation the membrane was washed thrice for 5 min each with TBST and prepared for detection.

Detection: Supersignal West Pico® or Supersignal West Femto® chemiluminescence detection kit (Thermo Fisher Scientific) was used for detection. The membrane was incubated with a mix of Enhancer and Stable Peroxide Buffer in equal parts for 5 minutes. The membrane was then transferred to an X-ray cassette. In the dark room an X-ray film was placed in the cassette and exposed for 0.5 to 5 minutes. The film was developed using an Optimax developing machine.

2.2.8 Coomassie Blue staining

Coomassie staining was carried out using Coomassie Brilliant Blue G-250 powder from Thermo Fisher Scientific. 1 g of powder was dissolved in 400 mL methanol and 100 mL acetic acid. The volume was made up to 1000 mL with distilled water. The SDS gel was removed from the electrophoresis cassette and washed once for 5 min in filtered Millipore water to remove the salts of the running buffer. Then the gel was immersed in Coomassie Blue solution and incubated at room temperature for a minimum of 1 h or overnight with gentle stirring. After staining the gel, the Coomassie Blue stain was removed and the gel destained with a solution made up with 30% methanol and 10% acetic acid. Balls made with Kim wipes were placed at the corner of the plate to speed up destaining as it removes any precipitate left by the staining solution. The gel was left in the destaining solution for a minimum of 2 h or till the bands were visible. Once the bands were clearly visible, destaining solution was replaced by distilled water.

2.2.9 DARTS

Preparation of cell lysate: KB-3-1 cells were cultured to 70-80% confluency in a 75 cm^2 (T75) cell culture flask. The cells were scraped and centrifuged at 3000 rpm for 5 min. The cell pellet was washed once with PBS and centrifuged again to remove any left out media. The pellet was resuspended in 800-1000 µL of MPER® lysis buffer (Pierce) based on the size of the pellet in a 1.5-mL Eppendorf tube and subjected to cell lysis on ice for 15-20 min. After cell lysis, the tubes were centrifuged at 4°C for ten minutes at maximum speed. The supernatant was collected and the protein content was measured using Bradford's assay.

Digestion with pronase®: 100 µg of the protein lysate was incubated with the compound at varying concentration and methanol (negative control) for two hours on ice. The mixture was digested with 0.03 µg of Pronase® (Roche) at 37°C for 30 min. The digestion was stopped by heating with 5 µL 4X loading dye (Roth).

Detection: The sample was separated by SDS-PAGE (4-20% Tris-HCl gels) and either subjected to Coomassie Blue staining or transferred onto a nitrocellulose membrane. The membrane was then subjected to western blotting with the required antibodies and made visible by chemiluminescence.

2.2.10 siRNA knockdown

Transfection: Confluent cells (KB-3-1 or L-929) were trypsinised and counted using cell counter. In a 6-well plate $2*10^5$ cells/well (2 mL) were seeded and incubated at 37°C until they were 60-80% confluent which usually is 18-24 h. After 24 h, cells were provided with 2 mL of fresh complete media and incubated at 37°C for one hour prior to transfection. During this one hour, a transfection mix was prepared from solution A and B for each well. Solution A consisted of 100 nM of siRNA in 150 µL of media without FBS. Solution B consisted of 9 µL of Lipofectamine® RNAiMAX reagent and 150 µL media without FBS. FBS or any kind of serum is excluded from the transfection mix preparation as it interferes with good transfection efficiency. Solution A was gently mixed with B and allowed to incubate at room temperature for 10 min. At the end of one hour incubation of cells with fresh complete media, the 6-well plate was removed from the incubator and 1.8 mL of the medium in each well was aspirated out. 300 µL of the transfection mix was added to each well and incubated at 37°C for one hour to allow an efficient uptake of siRNA by the cells. Later 1.5 mL of complete growth media was added to each well and the plates incubated at 37°C. After 48 h the media was discarded and replaced with fresh complete media. Test compounds and vehicle control were added to these transfected cells and incubated at 37°C for overnight.

Preparation of cell lysate: After incubation with test compound and vehicle control the media was discarded. The plate was placed on ice, 200 µL of MPER® lysis buffer added to each well and incubated for 10 min with gentle shaking to lyse the transfected cells. The well contents were placed in an Eppendorf tube and centrifuged at 4°C for ten minutes at maximum speed. Supernatant was collected and protein estimation was carried out using Bradford's assay.

Detection: The sample was separated by SDS-PAGE (4-20% Tris-HCl gels) and the protein bands transferred onto a nitrocellulose membrane. The membrane was then subjected to Western blotting with the required antibodies and made visible by chemiluminescence.

2.2.11 Apoptosis assay with cell death detection ELISA ^{PLUS}

The levels of apoptosis in the knockdown cells were measured using the cell death detection ELISA ^{PLUS} kit provided by Roche. The assay is based on a quantitative sandwich-enzyme-immunoassay principle using mouse monoclonal antibodies directed against DNA and histones. It's a photometric determination of mono- and oligonucleosomes in cell lysates produced in case of induced cell death. 20 µL of knockdown cell lysate was placed in a streptavidin-coated microplate (MP) and 80 µL of the Immunoreagent was added.

Immunoreagent was prepared by mixing 1/20 volume Anti-DNA-POD and 1/20 volume Anti-histone-biotin with 18/20 volume incubation buffer. Anti-DNA-POD and Anti-histone-biotin are monoclonal antibodies from mouse and bind to DNA and histone component of nucleosomes respectively. Anti-DNA-POD also gives a colour reaction whereas anti-histone-biotin captures the immunocomplex via biotin to the coated MP. MP with the lysate and the immunoreagent was incubated at room temperature for two hours with gentle shaking (300 rpm) after covering with adhesive foil. Solution was thoroughly removed by suction and rinsed thrice with 300 µL of ready to use incubation buffer provided in the kit. After solution was carefully removed, 100 µL of ABTS solution (provided in kit) was pipetted to each well and the plates incubated on a plate shaker at 250 rpm until colour developed. Colour development was stopped by adding 100 µL of ABTS stop solution and colour intensity was measured at 405 nm with reference wavelength of 490 nm using a plate reader.

2.2.12 Caspase-Glo® 3/7 assay

Caspase-Glo® 3/7 assay is a luminescent assay which measures the activities of caspase-3 and -7 which plays an effector role in apoptosis. Addition of Caspase-Glo® 3/7 reagent leads to cell lysis and caspase cleavage of the luminogenic substrate which contains the tetrapeptide sequence DEVD (Asp-Glu-Val-Asp) and a glow-type luminescent signal by luciferase. Luminescence is proportional to the amount of caspase activity. Caspase-Glo® 3/7 reagent was prepared before starting the experiment by combining the substrate with the buffer provided in the kit. 100 µL of the lysate was taken in a white bottom 96-well plate. Equal volume of the caspase-Glo® 3/7 reagent was added and incubated at room temperature for two hours. Luminescence was measured using a plate reader.

3 Results

3.1 Bioprofiling using advanced HCA methods

In order to judge the biological behaviour of a compound, its mode of action becomes paramount. As there is no easy and clear cut way how to proceed in that aspect, one task of this study was to evaluate modern approaches of high content analysis in getting hints about the mode of action of a compound. Treatment of cells with biologically active compounds brings about a change in their cellular status, inner structure and general morphology which can either be analysed by impedance monitoring of cell cultures or by comparing images of the cells showing phenotypic changes. The general idea is to compare new compounds of unknown mode of action with reference compounds whose mode of action is already known. For the reference library 63 compounds were selected which are commercially available. The compounds were dissolved in DMSO in their optimum concentration as given in Table 2.3.

3.1.1 Image analysis

The first profiling method investigated was high content image analysis (HCIA) using automated microscopy. In this approach KB-3-1 cells were treated overnight with the set of reference compounds and stained with 12 different antibodies which bind to a broad range of proteins, and are then made visible by fluorescence. Fluorescence images of cells were acquired then by automated microscopy. Data obtained from these images are transformed and used to define descriptors (Table 2.6 & Table 2.7) which form profiles for the compounds of interest that can then be compared using different statistical methods like hierarchical clustering, SOM and PCA.

Cluster analysis of profiles (Figure 3.1) of all the reference compounds based on the effect of the compounds on KB-3-1 cells provided us with different clusters. Few of the clusters are highlighted to show the reliability of the method, its strengths and weakness. Box 1 shows a clustering of two compounds which affect protein synthesis at a Euclidean distance of 0.57. Both cycloheximide (McKeehan and Hardesty, 1969) and myriaporone (Muthukumar et al., 2013) have been found to affect translational machinery at different levels. Box 2 shows a clustering of 6 compounds, out of which 4 affect microtubular dynamics at various Euclidean distances ranging from 0.54 to 0.72. But argyrin A and cruentaren A were found in the same group though they do not affect microtubule. This has been observed rather often, also in case of impedance measurement. This is probably due to some off-target which needs further investigation. Box 3 shows a clustering of the histone deacetylase (HDAC) affecting compounds, trichostatin (Furumai et al., 2001) and oxamflatin (Kim et al., 1999) at Euclidean distance of 0.56. PMA (phorbol-12-myristate-13-acetate) was also found in that group probably also due to some off-target. Box 4 shows a clustering of the V-ATPase inhibitors apicularen and archazolid B (Huss et al., 2005) at a Euclidean distance of 0.8. Box 5 shows a clustering of kinase inhibitors (0.7 to 0.85) together with the actin interfering compound chivosazol A. The next box (6) highlights a rather heterogeneous group that will be discussed later. Box 7 shows a clustering of compounds all of which affect the protein synthesis at different levels. Finally box 8 clusters together compounds affecting actin at a Euclidean distance of 0.42.

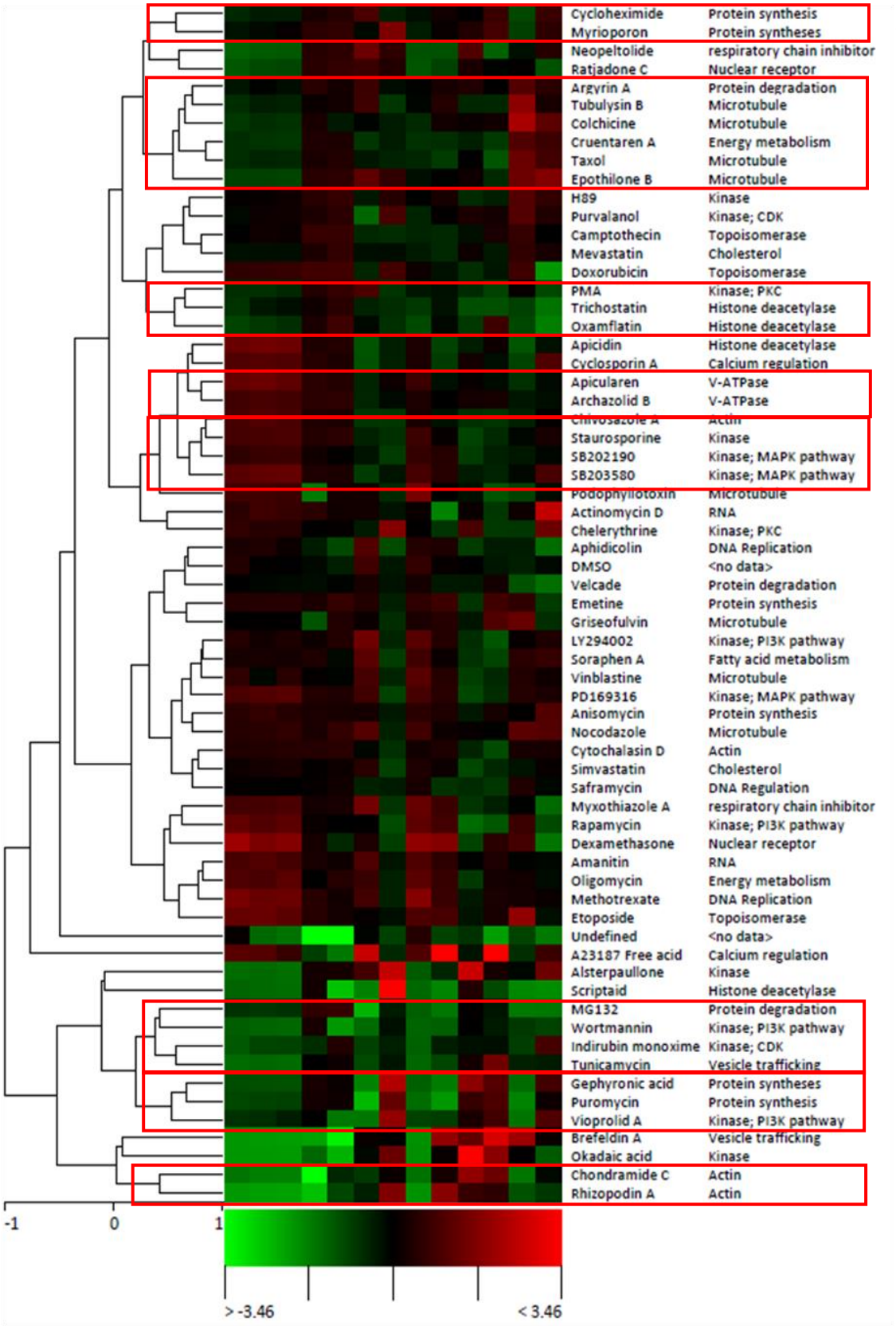

Figure 3.1: Hierarchical cluster analysis of 13-descriptor profiles of reference compounds generated by automated microscopy and image analysis

KB-3-1 cells were treated with reference compounds overnight. Descriptors considered: Total number of cells, total number of positive cells for FITC and Texas Red, % positive W2 and W3, pit count per

cell, pit average intensity, pit total area, vesicle count per cell, vesicle average intensity, vesicle area per cell, nuclear area per cell and nuclear average intensity.

SOM analysis performed on reference compound profiles is shown in Figure 3.2. This grid depicts 3*3 clusters which contain the coloured profiles of all the compounds in the cluster. The graph within each cluster shows the average trace of all the descriptors. The title bar shown above each cluster indicates the number of compounds included. Gray shade of the title bar represents the relative number of compounds in each cluster. A white bar indicates cluster with highest number of compounds, and black one the cluster with the least number. SOM analysis also arranges the clusters according to their similarity to each other. Similar clusters are placed close together while dissimilar ones are separated. Clusters diagonally opposite on the grid are essentially anti-correlated. The cluster with the pink border shows microtubule affecting compound along with others. This cluster includes 12 compounds. Clusters at the extremes tend to have the most variance, while clusters in the centre have least variance. Grouping shown by hierarchical clustering and SOM do not necessarily have to be similar.

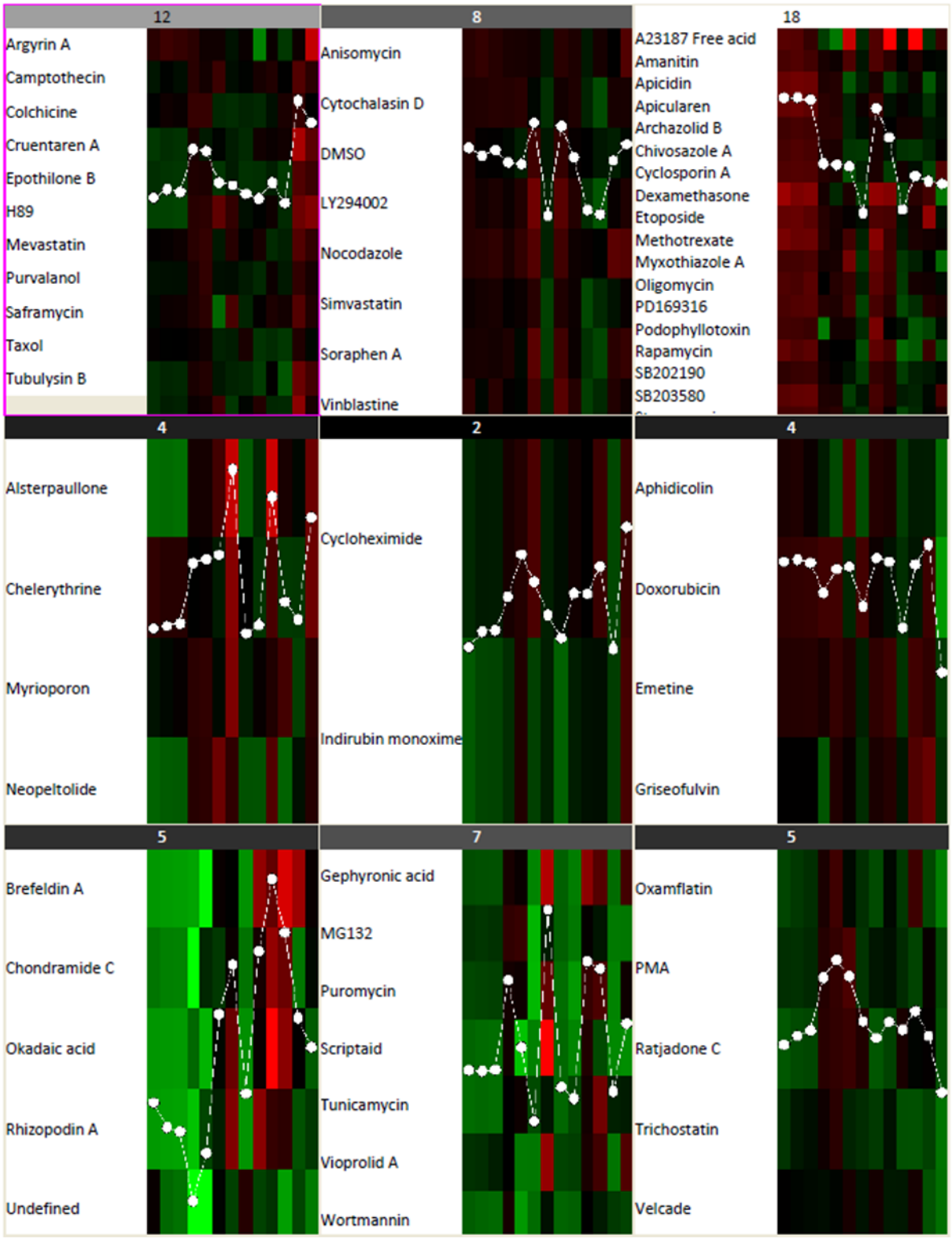

Figure 3.2: Self-organising maps (SOM) of descriptor profiles of reference compounds generated from image data gained by automated microscopy

KB-3-1 cells were incubated with the compounds overnight. The chosen descriptors were the same as used for hierarchical clustering (Figure 3.1).

PCA places all the compounds according to their descriptors profiles in a 3 dimensional space without premature categorization of the data. Figure 3.3 shows spread of all the 63 compounds in the form of dots. A few of these dots have been marked red; these dots represent those compounds which had clustered together in the cluster of SOM, which was highlighted in pink in Figure 3.2.

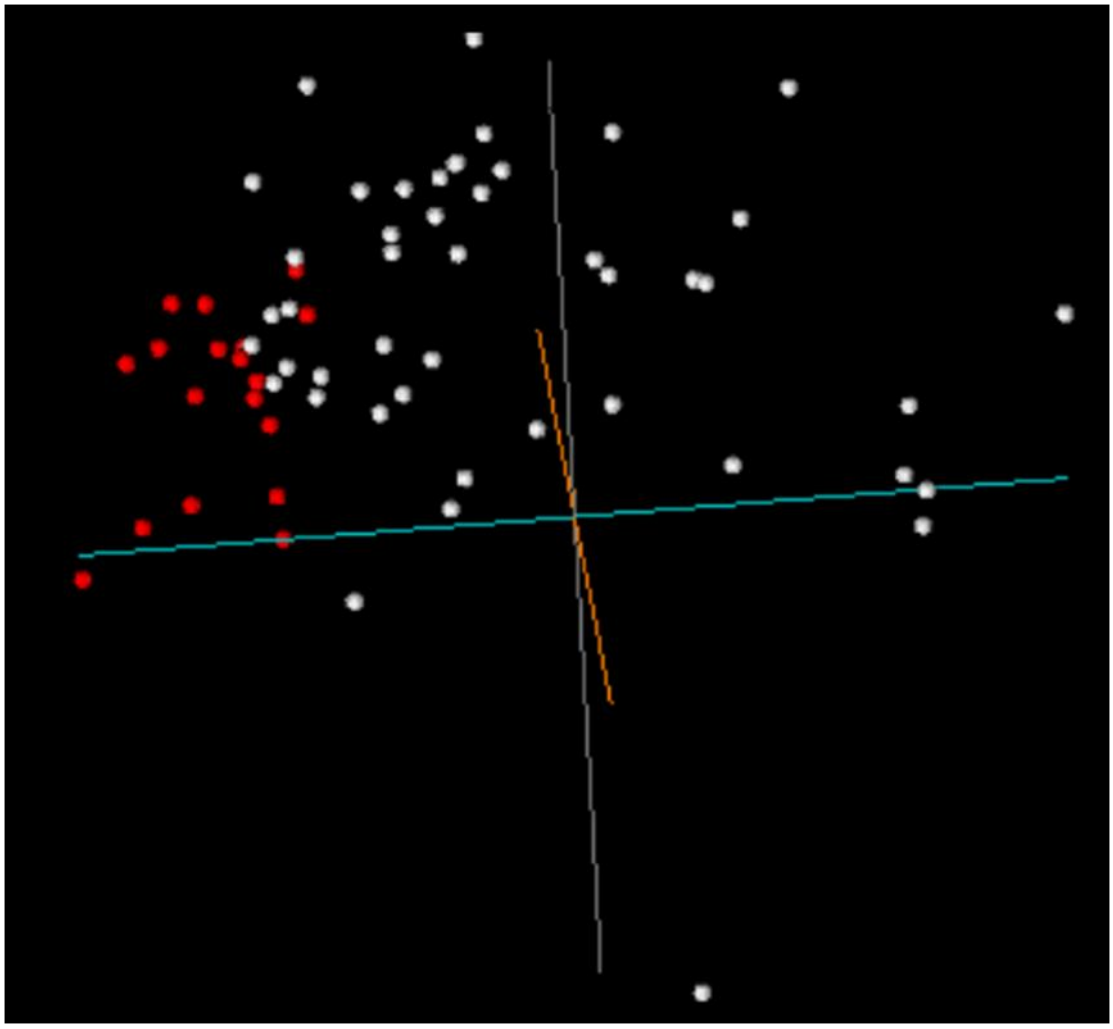

Figure 3.3: Principal Component Analysis (PCA) of the reference compounds according to descriptor profiles that were generated from image data by automated microscopy.

KB-3-1 cells were incubated with the compounds overnight. The descriptors chosen were the same as in hierarchical cluster analysis and SOM. The highlighted (red) dots show the compounds that were grouped in the upper left cluster by SOM analysis (Figure 3.2).

3.1.2 Impedance profiling

The second method of High Content Analysis that was investigated is based on impedance monitoring of cell cultures incubated with the compounds of interest. Impedance was monitored in a culture of L-929 cells which were seeded in wells of an E-plate which has got gold electrodes integrated in its well bottoms. Treatment of the cells with the compound brings about a change in their morphology and these changes are reflected in the change in

impedance and were measured over a period of 4 days. A dimensionless parameter, the Cell Index (CI) was derived as a relative change in measured electrical impedance to represent the cell status. The CI value increases as the cells start to adhere and alters with change in cell status such as cell morphology, adhesion or viability. Every compound gives a characteristic impedance curve which is depending on its mode of action. When compared with that of the reference compounds for which the MoA is already known, it should provide possible hints of the pathway targeted.

After incubation, the raw data were analysed using an R script for normalisation and Z-score calculation. The Z scores were the basis for the creation of compound profiles, depicted as heat maps, which were used for hierarchical cluster analysis with reference compounds as shown in Figure 3.4. For this analysis Euclidean distance was used to establish a similarity matrix.

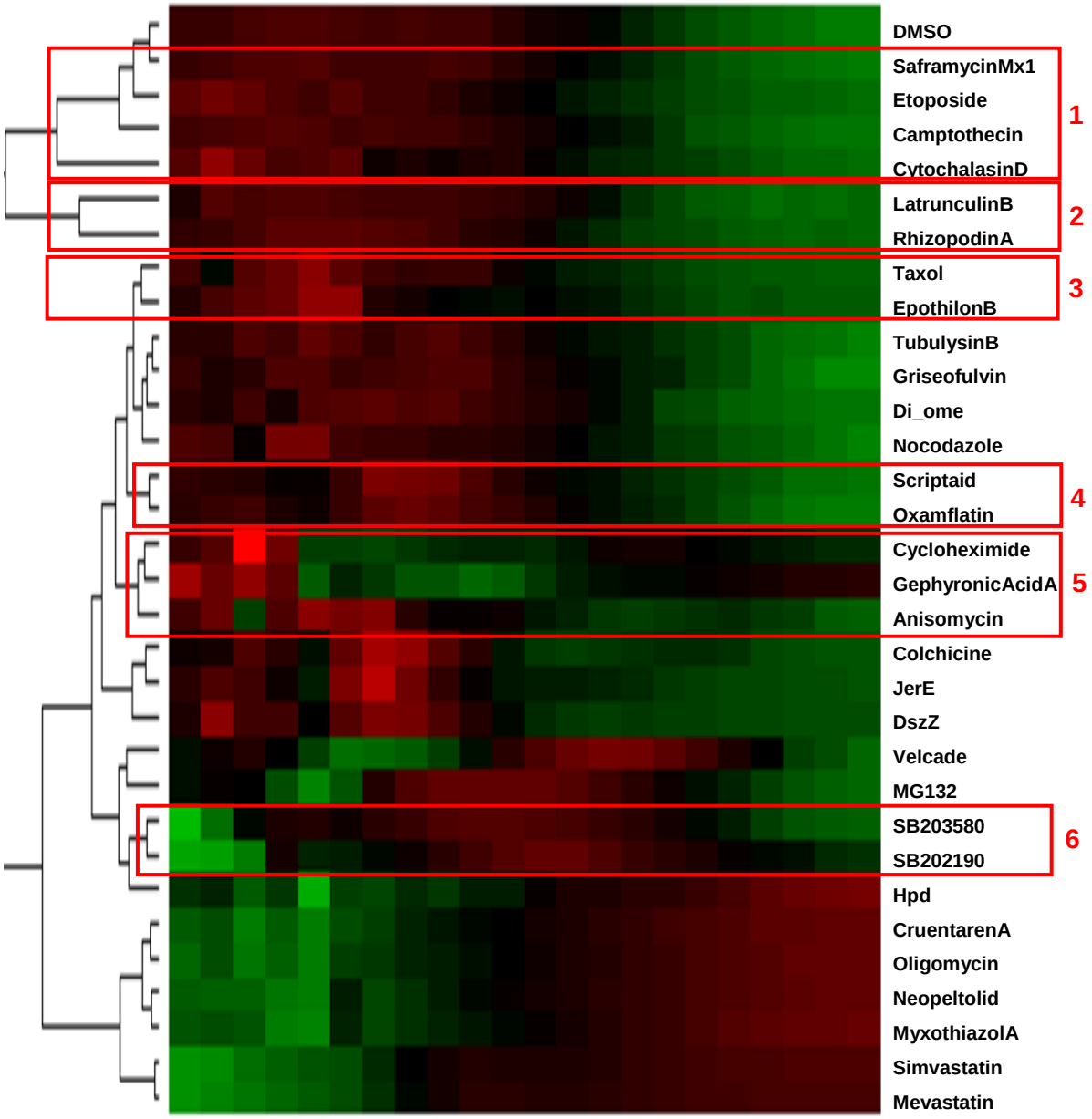

Figure 3.4: Hierarchical cluster analysis of reference compounds using an xCELLigence system

L-929 mouse fibroblasts were incubated with the compounds for 4 d. The resulting changes in impedance were used to form a profile for each compound. The basis are coefficients of spline approximation curves. Each of the 22 coloured columns represents a short time period. The gradation in the colour code signifies their Z-score i.e. distance from mean divided by the standard deviation. The results of a hierarchical cluster analysis show compounds with similar modes of action in close proximity.

The cluster analysis (Figure 3.4) showed grouping of compounds based on their impedance profile. Box 1 show a clustering of compounds inhibiting transcription, *e.g.*, both camptothecin (Desai et al., 2001) and etoposide (van Maanen et al., 1988) are topoisomerase I inhibitor whereas saframycin Mx1 also inhibits transcription but via a different mechanism (Irschik et al., 1988). Cytochalasin D also clusters with this group at varying range of Euclidean distances (2.48 to 3.39) though it acts on actin by inhibiting its polymerisation (MacLean-Fletcher and Pollard, 1980). Box 2 shows a clustering of actin

polymerisation inhibiting compounds at a Euclidean distance of 2.8. Box 3 shows a clustering of Taxol® and epothilone, both being microtubule stabilizers (Bollag et al., 1995; Horwitz, 1994). Scriptaid (Su et al., 2000) and Oxamflatin (Kim et al., 1999), inhibiting HDAC clustered together as shown in box 4. Compounds inhibiting translation at various levels are clustered in box 5. Box 6 shows a clustering of kinase inhibitors at a Euclidean distance of 0.4.

3.2 Cytotoxicity profiling of selected compounds with mammalian cell lines

Once both the profiling methods were established they should be applied to elucidate the mode of action of selected compounds, *i.e.*, jerantinine E, two paleo-soraphens, and two disorazols.

Different mammalian cell lines were used to test the toxicity of the selected compounds. These were human cancer cell lines including KB-3-1, PC-3, A-549, A-431 and MCF-7, transformed cell lines from mouse and potoroo – L-929 and PtK2, and primary HUVECs. Cells were incubated in 96-well micro-titre plates with serially diluted compounds for a period of 5 days. The influence of the compounds on the viability of the cells was measured by an MTT assay. Table 3.1 shows that Dsz A_1 and Z inhibited the cell viability in nanomolar ranges irrespective of cancer or primary cell line whereas the others were much less active.

Table 3.1: Cytotoxicity of alkaloids and polyketides in mammalian cells

The values represent the IC_{50} of the each compound measured by an MTT assay

Cell lines	Jerantinine E (µM)	Genetic soraphen A (µM)	Genetic soraphen B (µM)	Dsz A_1 (nM)	Dsz Z (nM)
L-929	3.9	>76	>76	0.05	1.14
KB-3-1	1.9	>76	30.2	0.0016	0.24
A-431	n.d	n.d	n.d	0.26	0.04
A-549	n.d	n.d	n.d	1.2	0.4
PC-3	n.d	n.d	n.d	0.1	0.23
PtK2	3.6	n.d	n.d	0.4	0.8
MCF-7	n.d	n.d	n.d	0.4	0.17
HUVEC	n.d	n.d	n.d	0.05	0.0005

Jerantinine E was also tested by others against breast and lung cancer cell lines (Frei et al., 2013). The moderately invasive breast cancer cell line MCF-7 and the highly invasive cell line MDA-MB-231 were incubated with jerantinine E and showed IC_{50} values between 4.4 µM and 6.0 µM after 24 and 72 h, respectively. Similar assays were carried out with lung cancer cell line A-549 and adenosquamous carcinoma cell line HT-178 which showed IC_{50} values between 1.0 µM to 8.8 µM after 24 and 72 h.

3.3 The mode of action of jerantinine E

For time dependent cell response impedance profiling L-929 cells were treated with jerantinine E at a concentration of 14 µM. After compound addition, cell response was measured for the next four days.

3.3.1 Impedance profiling with jerantinine E

After compound incubation, the raw data were analysed using an R script for normalisation and Z-score calculation. The Z scores were the basis for the creation of compound profiles, depicted as heat maps, which were used for hierarchical cluster analysis with reference compounds as shown in Figure 3.5. For this analysis the Euclidean distance was used to form a similarity matrix. The cluster analysis showed jerantinine E in closest neighbourhood to the microtubule affecting compounds colchicine with a Euclidean distance of 0.45.

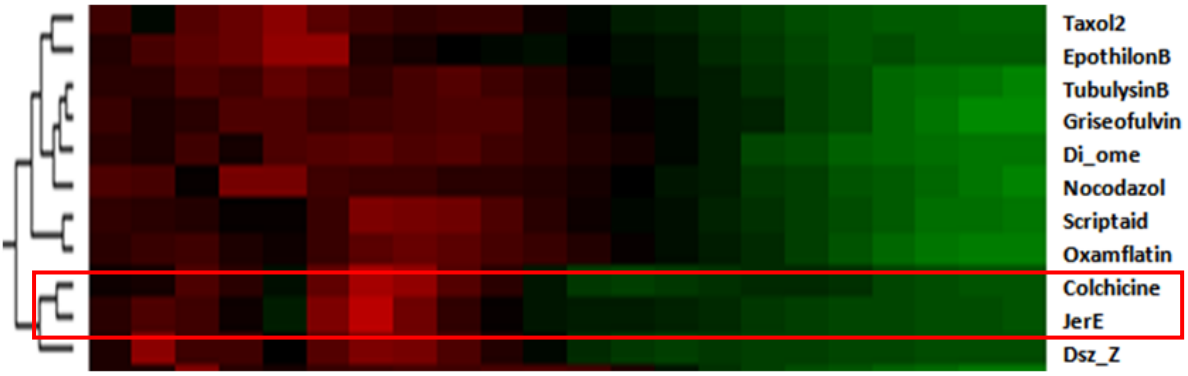

Figure 3.5: Hierarchical cluster analysis for jerantinine E using xCELLigence system

L-929 mouse fibroblasts were incubated with jerantinine E for 4 d. The resulting changes in impedance were compared with those of reference compounds. Basis coefficients of spline approximation curves are used for hierarchical cluster analysis. The results show compounds with similar modes of action in close proximity. Each of the 22 coloured columns represents a short time period. The gradation in the colour code signifies their Z-score i.e. distance from mean divided by the standard deviation. Red boxed area shows the clustering of jerantinine E with colchicine, a known microtubule destabilizer.

3.3.2 Effect of jerantinine E on the microtubular network in the cell

Based on impedance profiling jerantinine E was found to cluster with microtubule affecting compound like colchicine and disorazol, a possible effect on cellular microtubules and tubulin polymerisation *in vitro* was investigated.

PtK2 cells were incubated with jerantinine E at varying concentrations. Methanol treated cells were taken as negative control. After overnight incubation at 37°C, cells were fixed and stained with an anti α-tubulin antibody followed by an Alexa Fluor 488 tagged secondary antibody. DAPI was used to stain the nucleus. An effect on the nucleus was evident at a concentration of 5.5 µM (Figure 3.6 B), microtubular network started to disrupt from 16 µM (Figure 3.6 C) and was almost completely destroyed at 26 µM (Figure 3.6 D).

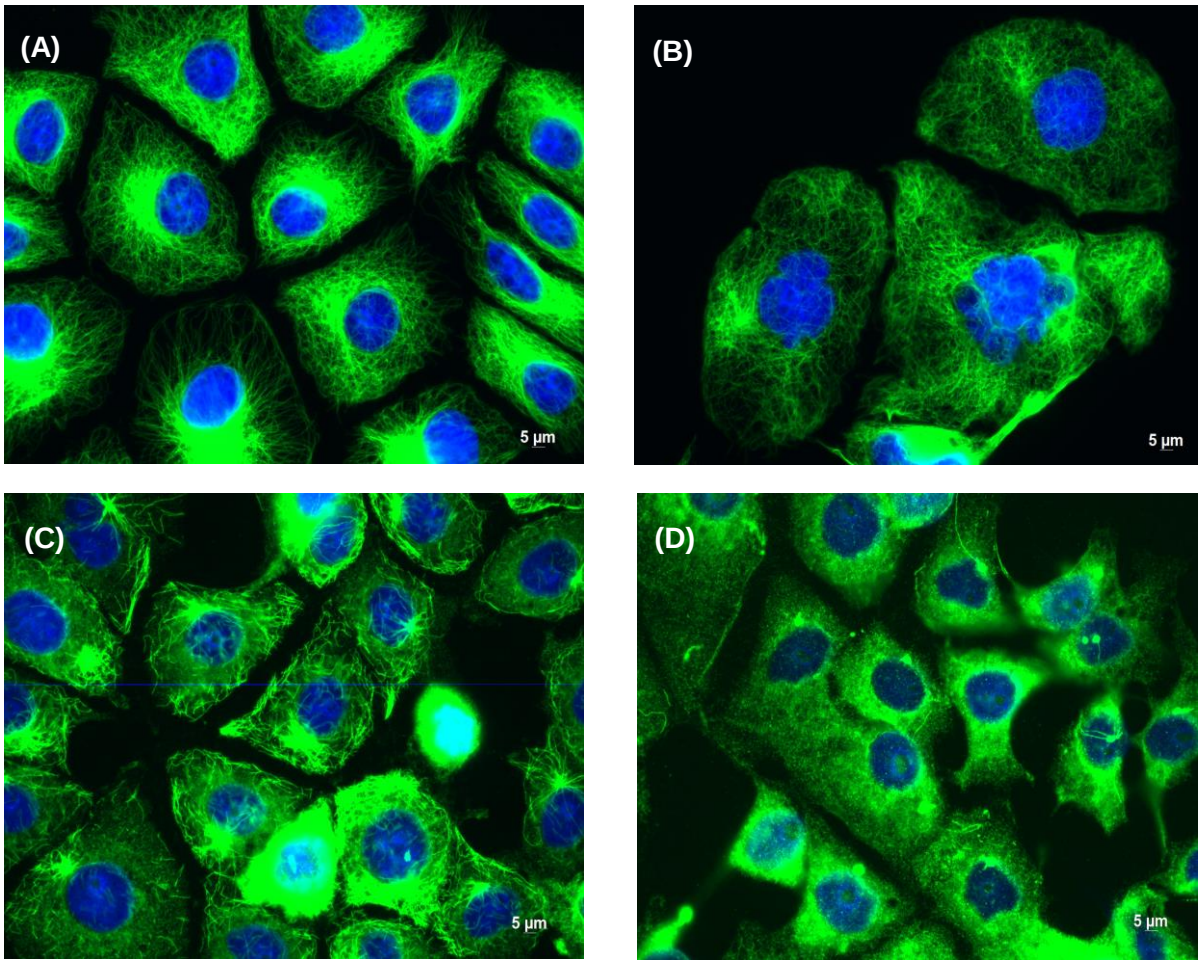

Figure 3.6: Effect of jerantinine E on cellular microtubules

Immunofluroscence staining of PtK2 cells which have been incubated with methanol (A) and jerantinine E at varying concentrations for overnight. Multinucleated cells are formed at 2 µg/mL (5.5 µM, B). At 6 µg/mL (16 µM, C) microtubules started to disintegrate and were almost completely disrupted at 10 µg/mL (26 µM, D). α-tubulin was probed using anti-α-tubulin antibody (green) and the nucleus (blue) was stained by DAPI.

3.4 The mode of action of paleo-soraphens

3.4.1 Impedance profiling with paleo-soraphen A and B

To characterize the action of the two paleo-soraphens, impedance profiling was carried out with L-929 cells at a concentration of 16 µM.

The data obtained from the resulting curves were used for hierarchical analysis together with the standard set of reference compounds. As can be seen from Figure 3.7, paleo-soraphen A (A) clusters with soraphen A at a Euclidean distance of 0.91, which makes it likely that it has the same mode of action. But paleo-soraphen B (B) did not cluster with its parent compound and found in close neighbourhood with camptothecin, a topoisomerase I inhibitor (Euclidean distance = 1.2).

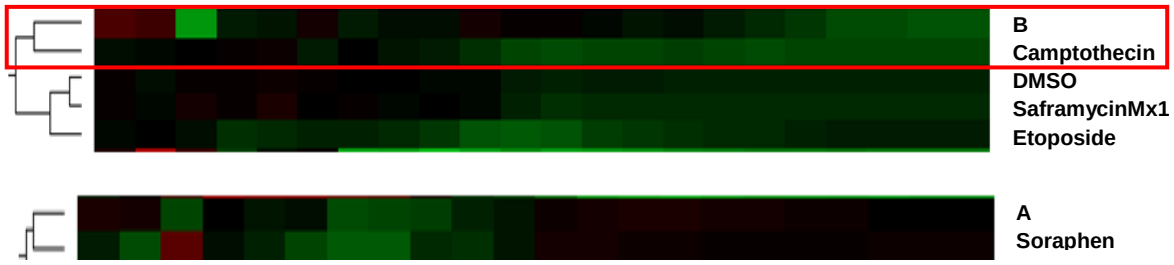

Figure 3.7: Hierarchical clustering for paleo-soraphen using xCELLigence system

L-929 mouse fibroblasts were incubated with paleo-soraphen A & B for 4 d. The resulting change in impedance was compared with those of reference compounds. Basis coefficients of spline approximation curves are used for hierarchical cluster analysis. The results show compounds with similar modes of action in close proximity. Each of the 22 coloured columns represents a short time period. The gradation in the colour code signifies their Z-score i.e. distance from mean divided by standard deviation. The red boxed areas show a clustering of paleo-soraphen A (A) with soraphen A whereas paleo-soraphen B (B) clusters with camptothecin.

3.4.2 Effect of paleo-soraphen on speckle size

Impedance profiling provided the indication that both paleo-soraphens have different targets. Paleo-soraphen A clustered with soraphen A but paleo-soraphen B showed a totally different and unexpected cluster behaviour. To investigate whether it has an effect similar to camptothecin, an immunofluorescence staining was carried out with PtK2 cells. Large volume of nuclear space is occupied by so called speckles were mRNA is transcribed and processed further for protein synthesis. These speckles can be detected using an anti-splicing factor SC-35 antibody. In mammalian cell nucleus, the splicing factors are concentrated in about 20-50 speckles, depending on the transcriptional activity. Topoisomerase I is a protein kinase directed towards the mRNA splicing factor SC-35. When treated with camptothecin (Figure 3.8 D), a known topoisomerase I inhibitor, the speckle structure within the nucleus changed from intermingled loops and dots to much smaller speckles with loss of loops (Elias et al., 2003). The same morphological changes were seen in cells treated with paleo-soraphen B (Figure 3.8 C). In contrast to that, paleo-soraphen A (Figure 3.8 A), which clustered with soraphen A in impedance profiling, showed speckle morphology similar to soraphen A treated cells (Figure 3.8 B).

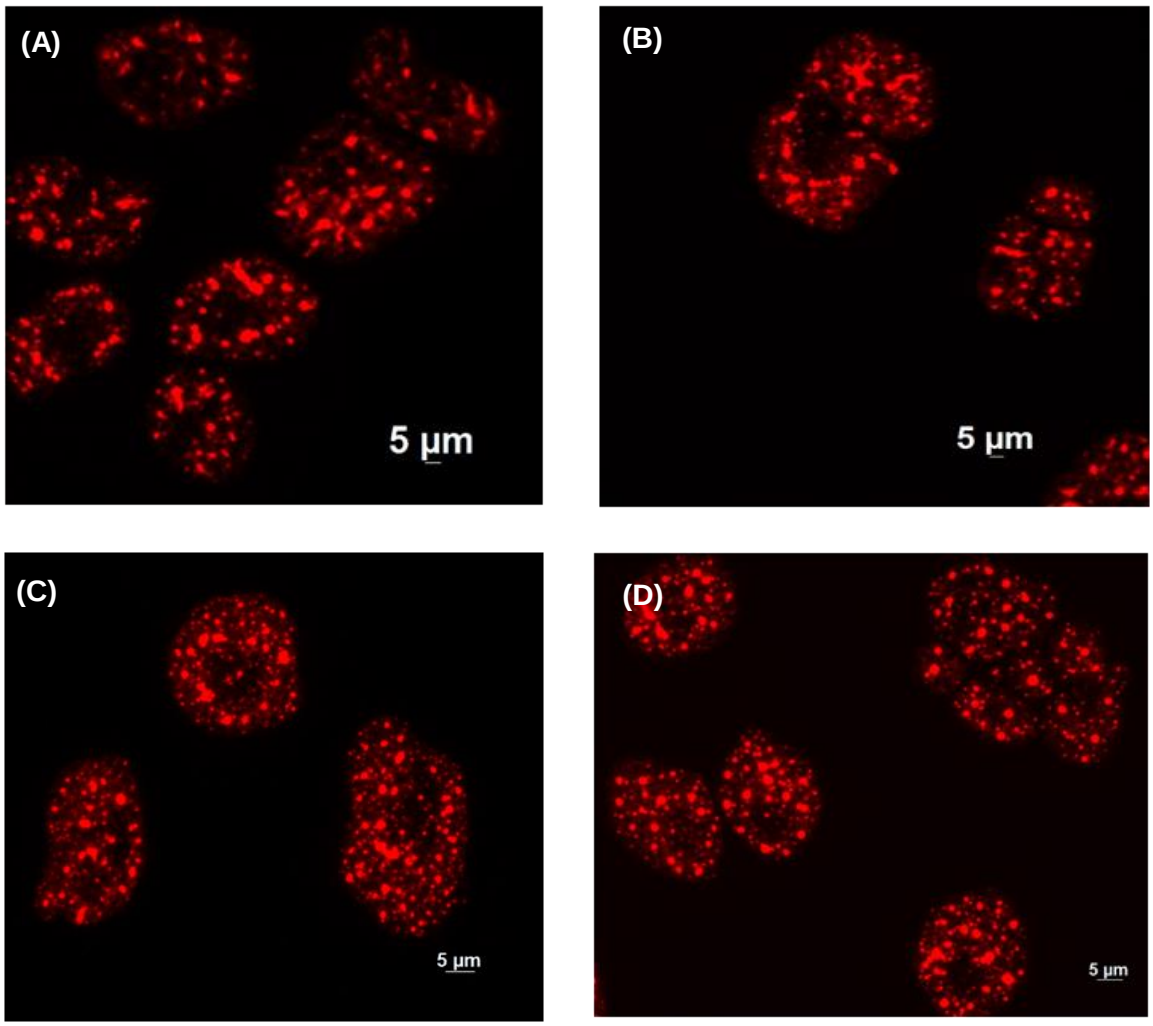

Figure 3.8: Paleo-soraphen affects the SC-35 speckle size

PtK2 cells were incubated with paleo-soraphen A (A, 30 µg/mL) and soraphen A (B, 30 ng/mL) for overnight and probed for the effect on speckle size by using anti SC-35 antibody (red) in the nucleus. Speckles in A and B are in form of intermingled loops whereas the speckles are much smaller and evenly distributed in case of PtK2 cells treated with paleo-soraphen B (C, 30 µg/mL) and resembles that of camptothecin (D) which was taken as the positive control.

The speckle sizes were quantified and are shown in Figure 3.9. The graph shows clear difference between cells treated with paleo-soraphen B and camptothecin on one side and paleo-soraphen A and soraphen A on the other side.

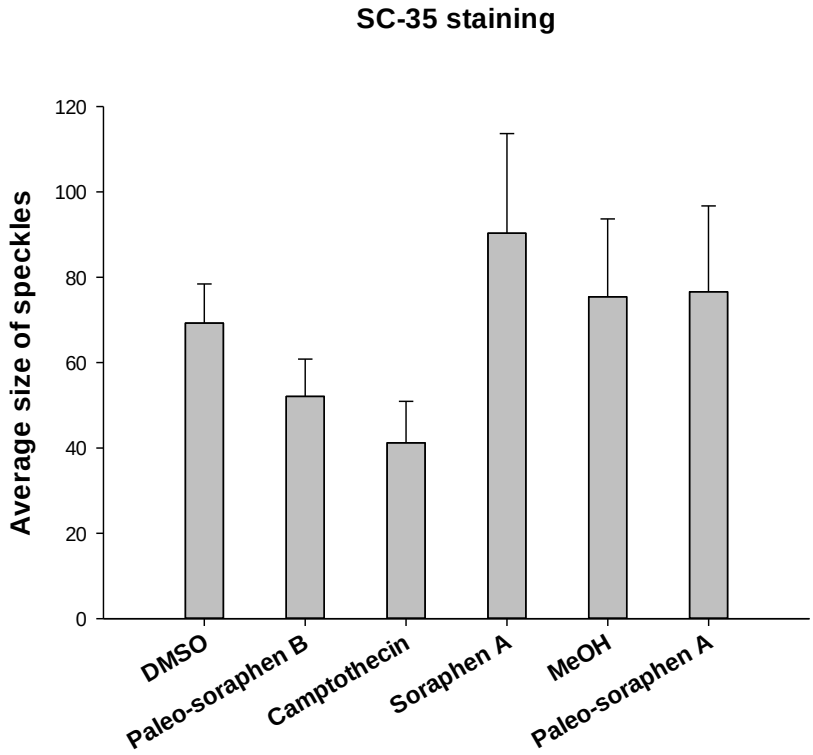

Figure 3.9: Effect on SC-35 speckle size by genetic paleo-soraphens

PtK2 cells were immunostained for SC-35 speckles using anti-SC-35 antibody after treating them with paleo-soraphens. The speckle size is reduced when incubated with camptothecin and paleo-soraphen B.

3.5 Profiling of disorazols

3.5.1 Impedance profiling

3.5.1.1 Disorazol A_1

For impedance readout usually the IC_{90} for L-929 cells are applied but in case of Dsz A_1 the reduction in cell viability did not reach the stage of IC_{90} even with highest concentration showing that probably Dsz A_1 is not cytotoxic but cytostatic in nature. However a concentration of 0.6 nM was used. Also a lower concentration of 1.3 pM was used to see any difference in the output but in this case it always clustered with vehicle control.

L-929 cells were treated with Dsz A_1 for a period of 4 days and the results obtained from impedance monitoring were used to create a distance map that was used for hierarchical cluster analysis with reference compounds as shown in Figure 3.10. For this analysis Euclidean distance was used as similarity matrix. The closest neighbour of Dsz A_1 was the microtubule affecting compound Taxol® at a Euclidean distance of 0.52. Other microtubule affecting compounds like tubulysin B, griseofulvin, nocodazole and epothilone B had distance of 0.58, 0.66, 0.69 and 0.73, respectively.

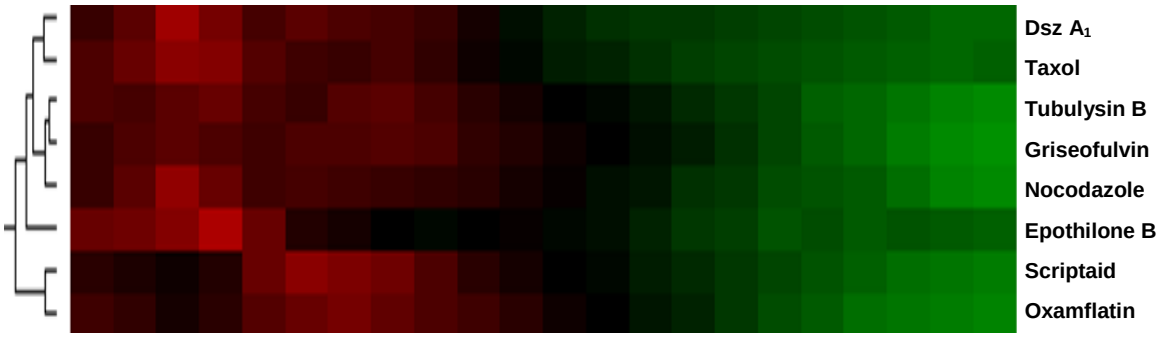

Figure 3.10: Hierarchical cluster analysis of impedance profiling data for Dsz A_1

L-929 mouse fibroblasts were incubated with Dsz A_1 for 4 d. The resulting changes in impedance were compared with those of reference compounds. Basis coefficients of spline approximation curves are used for hierarchical cluster analysis. The results show compounds with similar modes of action in close proximity. Each of the 22 coloured columns represents a short time period. The gradation in the colour code signifies their Z-scores i.e. distance from mean divided by standard deviation. The snapshot shows the clustering of Dsz A_1 with microtubule affecting compounds.

3.5.1.2 Disorazol Z

L-929 cells treated with Dsz Z did not reach IC_{90} as it is also cytostatic in nature like Dsz A_1. A concentration of 7.4 nM was used to treat and incubate the cells for a period of 4 days for impedance profiling.

As described in the previous section, characteristic impedance curves were obtained and analysed. Figure 3.11 show a clustering of Dsz Z with the microtubule affecting compound-colchicine with a Euclidean distance of 0.92. It has lower distance (0.78) with jerantinine E (Jer E).

Figure 3.11: Hierarchical cluster analysis of Dsz Z using xCELLigence system

L-929 mouse fibroblasts were incubated with Dsz Z for 4 d. The resulting changes in impedance were compared with those of reference compounds. Basis coefficients of spline approximation curves are used for hierarchical cluster analysis. The results show compounds with similar modes of action in close proximity. Each of the 22 coloured columns represent a short time period, the gradation in the colour code signifies their Z-score i.e. distance from the mean divided by standard deviation. The snapshot shows the clustering of Dsz Z with colchicine and jerantinine E.

3.5.2 Image profiling

3.5.2.1 Disorazol A_1 & Z

Image data were obtained from KB-3-1 cells treated overnight with Dsz A_1 and Z. Incubated cells were stained later with 6 pairs of antibodies as described earlier and prepared for automated microscopy. The images acquired were analysed in the same manner as the reference compounds.

Hierarchical clustering analysis of Dsz A_1 and Z with reference compounds is shown in Figure 3.12, Dsz A_1 clustered with the MAP kinase affecting compound SB202190 and

rapamycin at a Euclidean distance of 0.917 and 0.883, respectively. This differed from cluster analysis obtained with impedance data. Dsz Z clustered at a Euclidean distance of 0.961 with argyrin A and with the kinase inhibitor – indirubin monoxime at 0.889

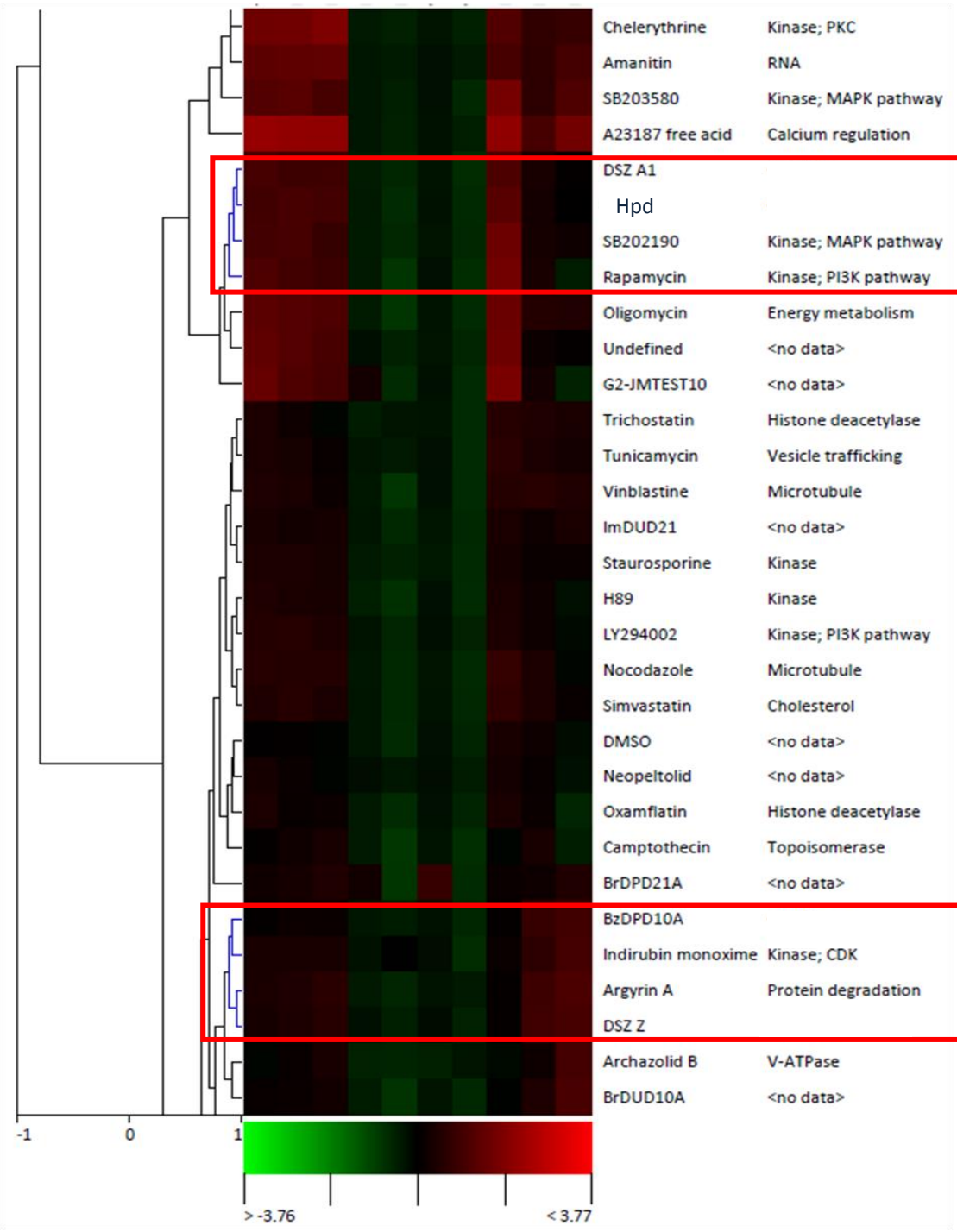

Figure 3.12: Hierarchical cluster analysis of descriptor profiles of Dsz A_1 and Z and reference compounds using automated microscopy

Images of KB-3-1 cells treated with Dsz A_1 and Dsz Z along with reference compounds were prepared as per the HCIA protocol. The images were captured using an automated microscope., Descriptors considered: Total number of cells, total number of positive cells for FITC and Texas Red, pit count per cell, pit average intensity, vesicle count per cell, vesicle average intensity, nuclear count, nuclear area per cell and nuclear average intensity.

3*3 clusters were formed out of which only two clusters in which Dsz A_1 and Z appeared are shown in Figure 3.13. Dsz A_1 grouped with not just compounds like kinase inhibitors PD169316 and rapamycin but also with other compounds, *e.g.*, etoposide which is a topoisomerase inhibitor. The similar was the case with Dsz Z which grouped with compounds affecting different targets like chivosazol affecting actin and griseofulvin that affects microtubules.

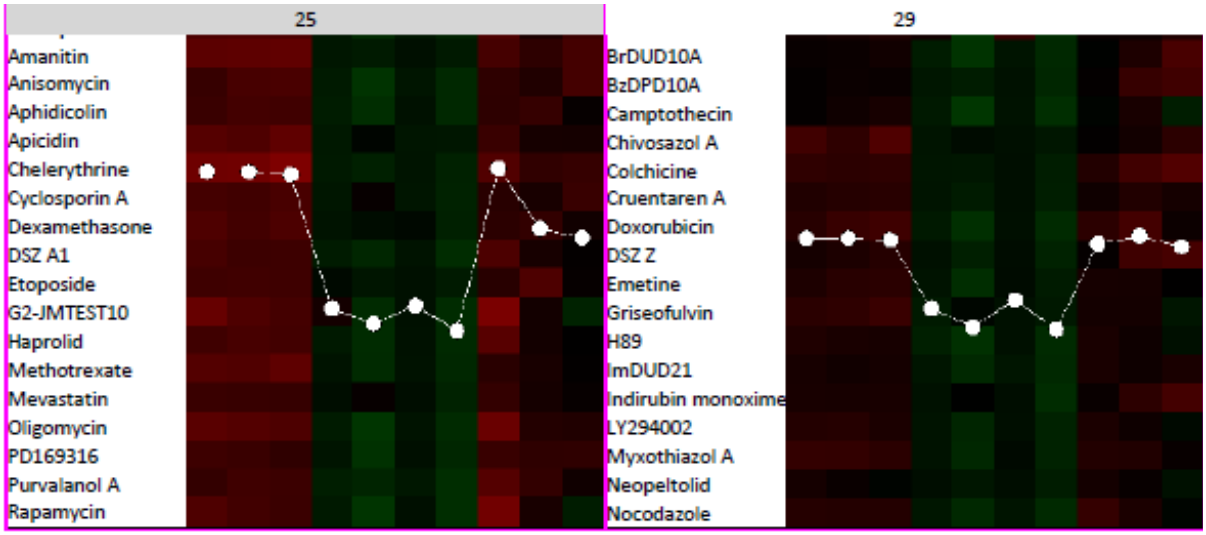

Figure 3.13: Self-Organizing Map (SOM) analysis of profiles of Dsz A_1 and Z and reference compounds by automated microscopy

*KB-3-1 cells were incubated overnight. SOM analysis was applied on profiles gained from the raw data of images acquired by automated microscopy. Only the relevant clusters of a 3*3 grouping are shown. Descriptors considered: Total number of cells, total number of positive cells for FITC and Texas Red, pit count per cell, pit average intensity, vesicle count per cell, vesicle average intensity, nuclear count, nuclear area per cell and nuclear average intensity.*

PCA was carried out and depicted in Figure 3.14. It shows proximity of Dsz A_1 and Z with rapamycin and indirubin monoxime, respectively, included in the reference library. Both are well established and known to affect the kinases.

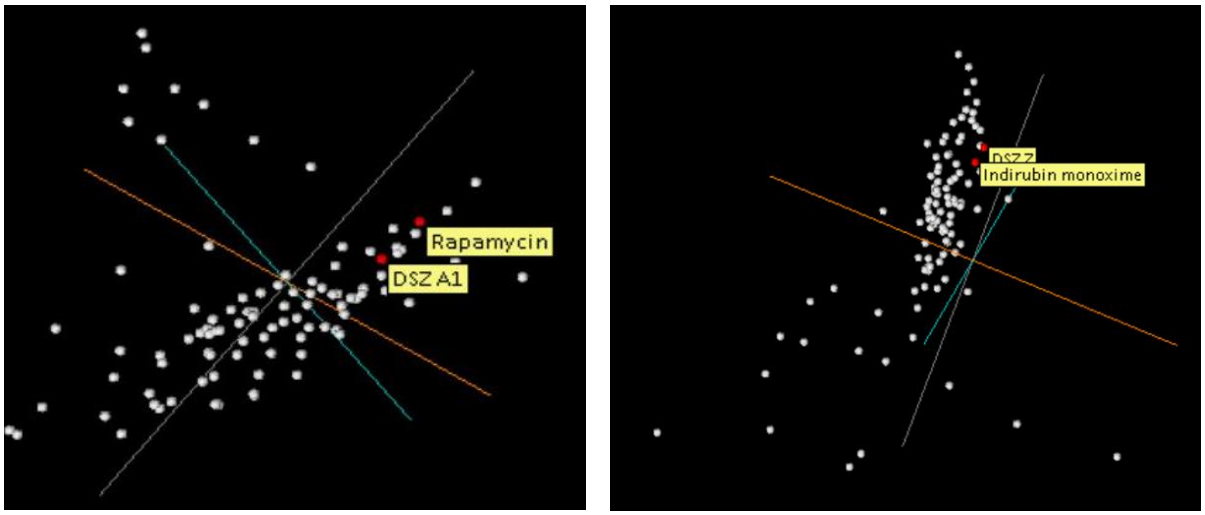

Figure 3.14: Principal Component Analysis (PCA) of Dsz A_1 and Z. Profiles were generated from images acquired by an automated microscope

KB-3-1 cells were incubated overnight. PCA analysis was applied on the transformed data obtained from automated microscope. 3 dimensional space shows the spread of all the compounds based on the level of similarity. Highlighted dots show closeness of Dsz A_1 and Z to kinase inhibitors.

3.6 Identification of the mode of action of disorazol A_1

Based on the hints provided by the high content analysis approaches, impedance monitoring with the xCELLigence and the image profiling using automated microscope, Dsz A_1 was further tested in various assays to ascertain its biological mechanism of action.

3.6.1 Nuclear localization of p53

To test the effect on the localisation of tumour suppressor protein p53 as seen earlier by (Elnakady et al., 2004). A-549 lung cancer cells were incubated with Dsz A_1 at 17.1 pM for 12-14 h at 37°C. Later the cells were fixed and permeabilised with formalin/Triton X-100 and immunostained for p53 and observed under a fluorescence microscope. Methanol treated cells were used as negative control. Figure 3.15 show that p53 is spread out all over the cytoplasmic region in case of control cells unlike Dsz A_1 treated cells where p53 is specifically localised in the nuclear region.

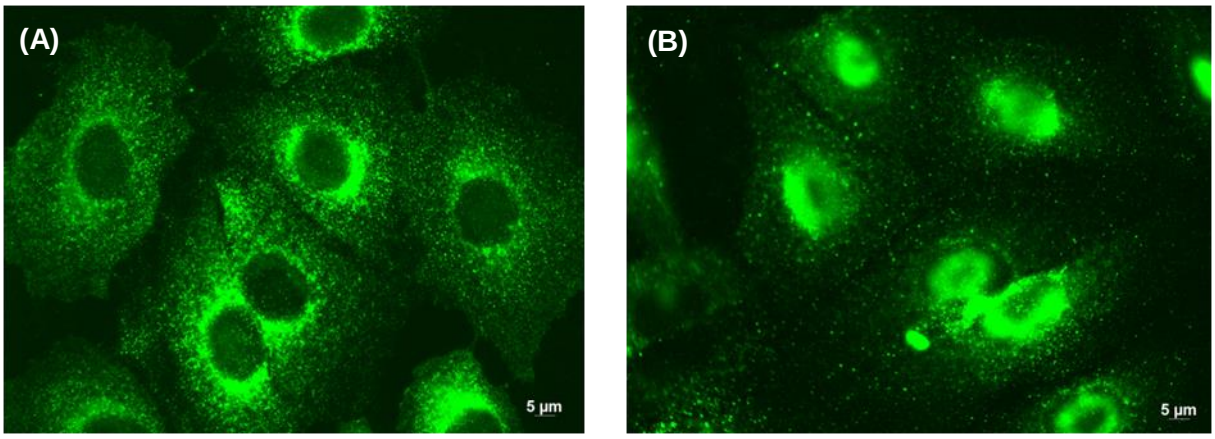

Figure 3.15: Nuclear localisation of p53

Immunofluroscent staining of A-549 cells treated with methanol (control, A) and Dsz A_1 (17.1 pM, B) for overnight shows that p53 (green) is confined to the cytoplasmic region in case of methanol whereas it is localised in the nucleus upon treatment of the cells with Dsz A_1.

3.6.2 Shuttling of Mdm2

A feedback loop runs between p53 and Mdm2 wherein Mdm2, an oncoprotein (Mayo and Donner, 2001) is phosphorylated by Akt and moves into the nucleus, where it interacts with p53 inhibiting its transcriptional activity and targets it for proteasomal degradation. To see the effect of Dsz A_1 on shuttling of phospho-Mdm2 within a cell, A-549 cells were incubated with Dsz A_1 at 17.1 pM for overnight. Methanol treated cells were taken as negative control. Cells were stained with a phospho-Mdm2 antibody from mouse and were made visible by using a secondary antibody anti-mouse Alexa® Fluor 488. Methanol treated cells showed phospho-Mdm2 localized in the nucleus compared to cytoplasmic location on treatment with Dsz A_1 (Figure 3.16).

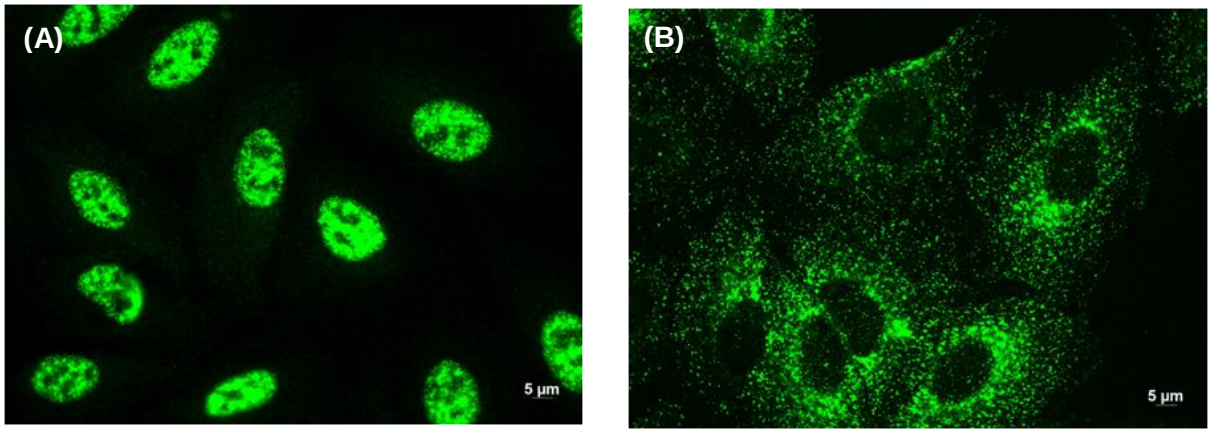

Figure 3.16: Shuttling of Mdm2

Immunofluroscent staining of A-549 cells with methanol (control, A) and Dsz A_1 (17.1 pM, B) for overnight shows that p-Mdm2 (green) is confined to nuclear region in case of methanol whereas phosphorylated mdm2 moves out of the nucleus upon treatment with Dsz A_1.

3.6.3 Effect of Dsz A_1 on phosphorylation state of p53

Earlier results showed the effect of Dsz A_1 on p53 localization. So to identify any changes on the phosphorylation state of p53, KB-3-1 cells were treated with various concentration of Dsz A_1 and methanol as negative control for overnight. The lysate was subjected to Western blot and probed for phosphorylated p53 and GAPDH. GAPDH served as loading control. As can be seen from Figure 3.17, cells treated with Dsz A_1 at pico molar range showed an increased level of phosphorylation in a concentration dependent manner when compared to the control.

Dsz A_1	0.01 pM	0.13 pM	1.3 pM	C

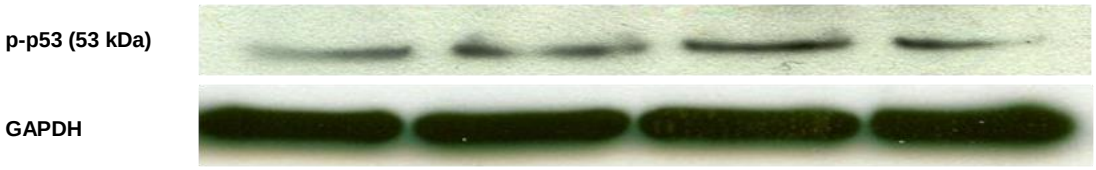

Figure 3.17: Dsz A_1 induces phosphorylation of p53

KB-3-1 cells treated with Dsz A_1 at various concentration for overnight showed an increase in phosphorylation of p53 compared to methanol (C) treated cells. GAPDH is taken as the loading control.

The change in the phosphorylation state of p53 based on Western blot is also depicted graphically in terms of their intensities in Figure 3.18.

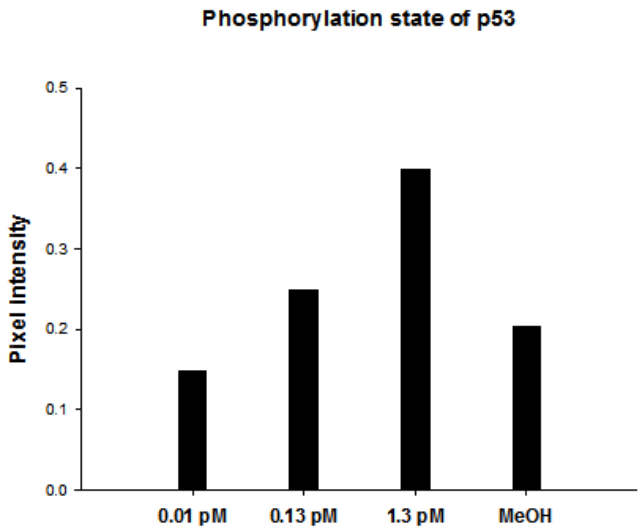

Figure 3.18: Induction of phosphorylation of p53 by Dsz A_1

Dsz A_1 induces a concentration dependent increase in the phosphorylation state of p53 in KB-3-1 cell lysate treated at various concentrations for overnight and later probed for phospho-p53 through Western blot.

3.6.4 Effect of Dsz A_1 on PI3K/Akt pathway

Based on the influence of Dsz A_1 on p53 and role of p53 in PI3 kinase pathway as described earlier, it was suspected that Dsz A_1 might have a target in this pathway which is often dysregulated in cancer cells. To investigate this hypothesis, a lysate was prepared from KB-3-1 cells treated with Dsz A_1 at various concentrations for overnight and probed for changes in various proteins involved in the pathway. In normal scenario a decrease in transcriptional activity of p53 causes decrease in stability of PTEN which thereby allows the PI3K/Akt pathway to carry on which involves an increase in phosphorylation of PDK1 and Akt, hence aiding in cell growth and proliferation. On the other hand cells treated with Dsz A_1 showed an increase in the phosphorylation state of p53 which might allow an increased stability of PTEN protein (Figure 3.19).

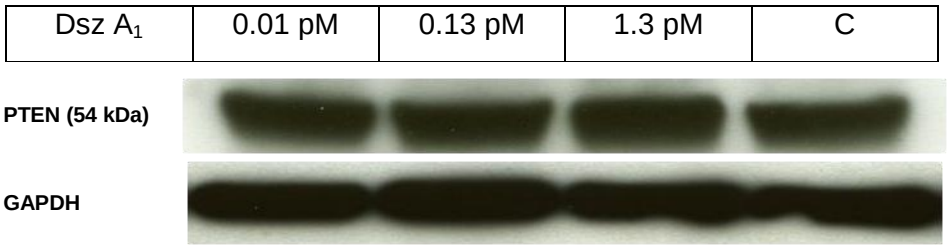

Figure 3.19: Dsz A_1 might induce PTEN stability

Lysate prepared from KB-3-1 cells treated with Dsz A_1 at various concentration showed slight increase in PTEN protein compared to methanol (C) treated cell lysate.

If PTEN attains stability, it would cause an inhibition of the PI3K/Akt pathway by decreasing the phosphorylation of various downstream proteins. Therefore, lysates from KB-3-1 cells treated with various concentrations of Dsz A_1 were subjected to Western blot and probed with an anti-phospho PDK1, anti-total PDK1, anti-phospho Akt and anti-total Akt. Figure 3.20 shows that Dsz A_1 inhibited the phosphorylation of both PDK1 and Akt i.e., Dsz A_1 induces an inhibition of the PI3K/Akt pathway.

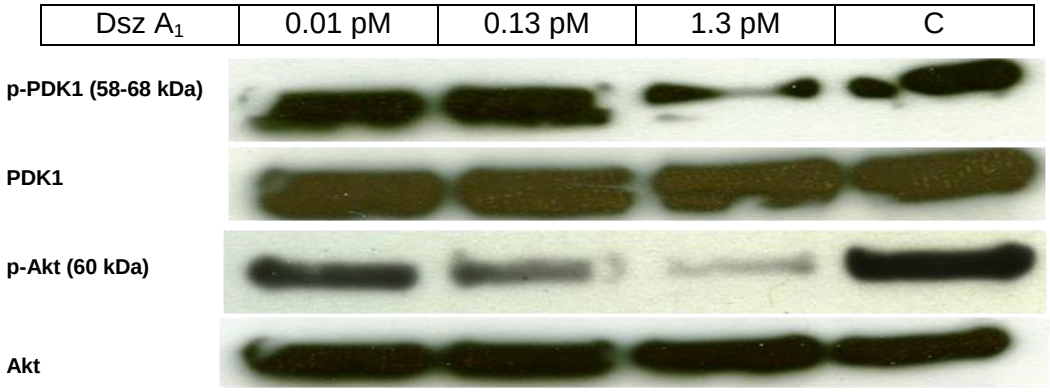

Figure 3.20: Dsz A_1 inhibits the PI3K/Akt pathway

Lysates prepared from KB-3-1 cells treated at various concentration of Dsz A_1 showed a concentration dependent inhibition of the phosphorylation of PDK1 and Akt as compared to methanol (C) treated cells, i.e., the .PI3K/Akt pathway was inhibited.

3.6.5 Verifying the target of Dsz A_1 with a DARTS approach

It was hypothesised that Dsz A_1 could be binding directly to PTEN, thus activating it and as a result antagonising the PI3K/Akt pathway. To investigate this point a drug affinity responsive target stability (DARTS) approach was used. This approach is based on the principle that a protein is less susceptible to protease digestion when bound to a ligand than when it is free due to stabilization of protein's folded state (Lomenick et al., 2009). Lysate from KB-3-1 cells were incubated with Dsz A_1 at various concentrations *i.e.*, 66 nM, 6 nM, 0.6 nM and 0.06 nM for two hours on ice. This was followed by Pronase® digestion for 30 min at 37°C. Methanol was taken as the negative control. A cell lysate treated with Dsz A_1 but not digested with Pronase® was taken as the positive control. Pronase® digestion was stopped by heating with SDS loading dye for 12 min at 96°C. The samples were separated by SDS-PAGE. A concentration dependent protection of a protein band around 50 kDa was noticed. PTEN protein has a molecular mass of 54 kDa. So this experiment was followed with Western blot wherein the protein bands after transferring it from the gel onto a nitrocellulose membrane were probed using an anti-PTEN antibody. The blot was later re-probed for GAPDH using an anti-GAPDH antibody which served as a loading control for the protein. As can be seen from Figure 3.21, the Dsz A_1 treated lysates showed a concentration dependent protection for PTEN.

Dsz A_1	66 nM	6.6 nM	0.6 nM	0.06 nM	-	66 nM
Pronase®	+	+	+	+	+	-

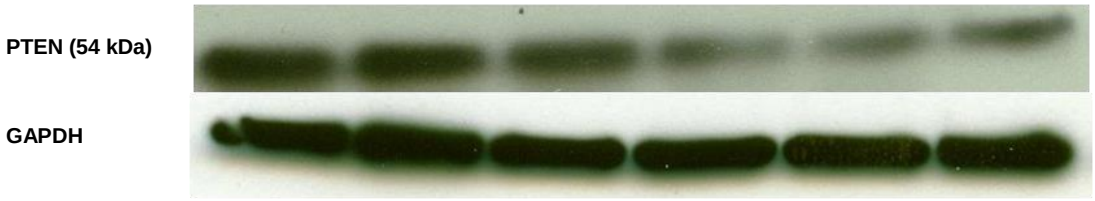

Figure 3.21: DARTS approach with Dsz A_1

Lysate prepared from KB-3-1 cells was incubated with Dsz A_1 at varying concentrations and later subjected to Pronase® digestion. A methanol treated lysate (-) which was also digested served as negative control whereas a Dsz A_1 treated but not digested lysate was taken as the positive control. Dsz A_1 showed a concentration dependent protection. GAPDH was used as loading control.

3.6.6 PTEN knockdown studies

To further verify that PTEN is the target for Dsz A_1 and it plays a role in the Akt pathway inhibition, PTEN in KB-3-1 cells was knocked down. The KB-3-1 cells were first transfected with siRNA PTEN for 48 h to knockdown PTEN. Negative control siRNA was used which is designed to have no known target in the cells. The transfected cells were later incubated with Dsz A_1 for overnight. Lysate from the knockdown cells were subjected to Western blot to check for the knocking down efficiency which is shown in Figure 3.22. Panel A shows the Western blot analysis with siRNA PTEN and negative control using scrambled siRNA.

GAPDH was used as a loading control Graphical representation of knockdown efficiency of siRNA PTEN is shown in panel B.

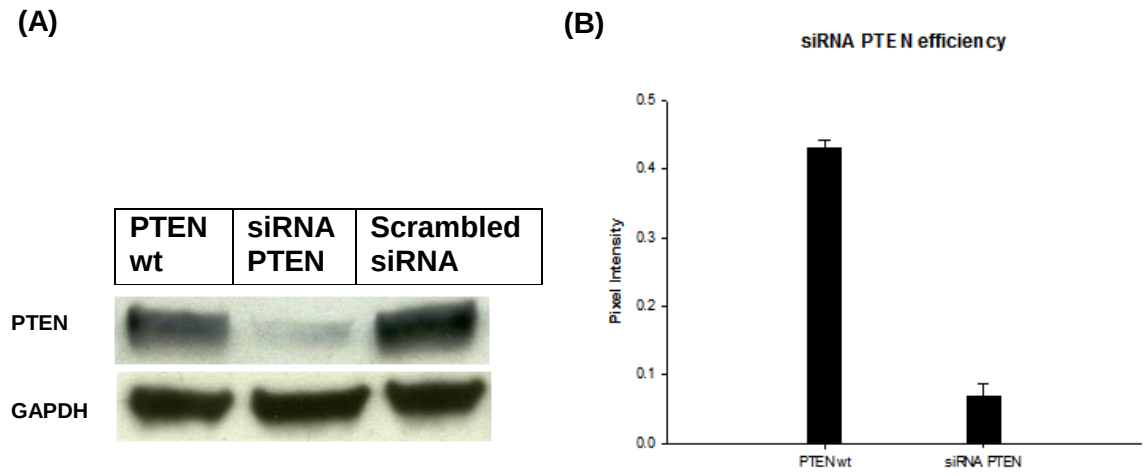

Figure 3.22: siRNA PTEN knockdown study for PTEN

Knockdown efficiency in KB-3-1 cell lysate is shown in panel A with Western blot probing using an anti-PTEN antibody. Scrambled siRNA is taken as the negative control which does not affect any known target in the cell. GAPDH was the loading control. A graphical representation of the respective protein band intensities are shown in panel B, where means and standard deviations from two experiments are given.

The lysate of knockdown cells treated with Dsz A_1 was used to check the effect on the phosphorylation state of Akt. The lysate was prepared after treating transfected KB-3-1 cells with 1.3 pM Dsz A_1, subjected to Western blot and probed with an anti-phospho-Akt. As shown in Figure 3.23A, there is a clear reduction in the phosphorylation state of Akt in the normal KB-3-1 cell lysate as compared to the knock down cell lysate which does not have PTEN anymore for it to decrease the phosphorylation of Akt. This proves that Dsz A_1 needs the presence of PTEN in cells for inhibiting cell growth and proliferation through inhibition of PI3K/Akt pathway. Figure 3.23B shows a graphical representation of the mean blot intensity with their standard deviation obtained from duplicate experiments.

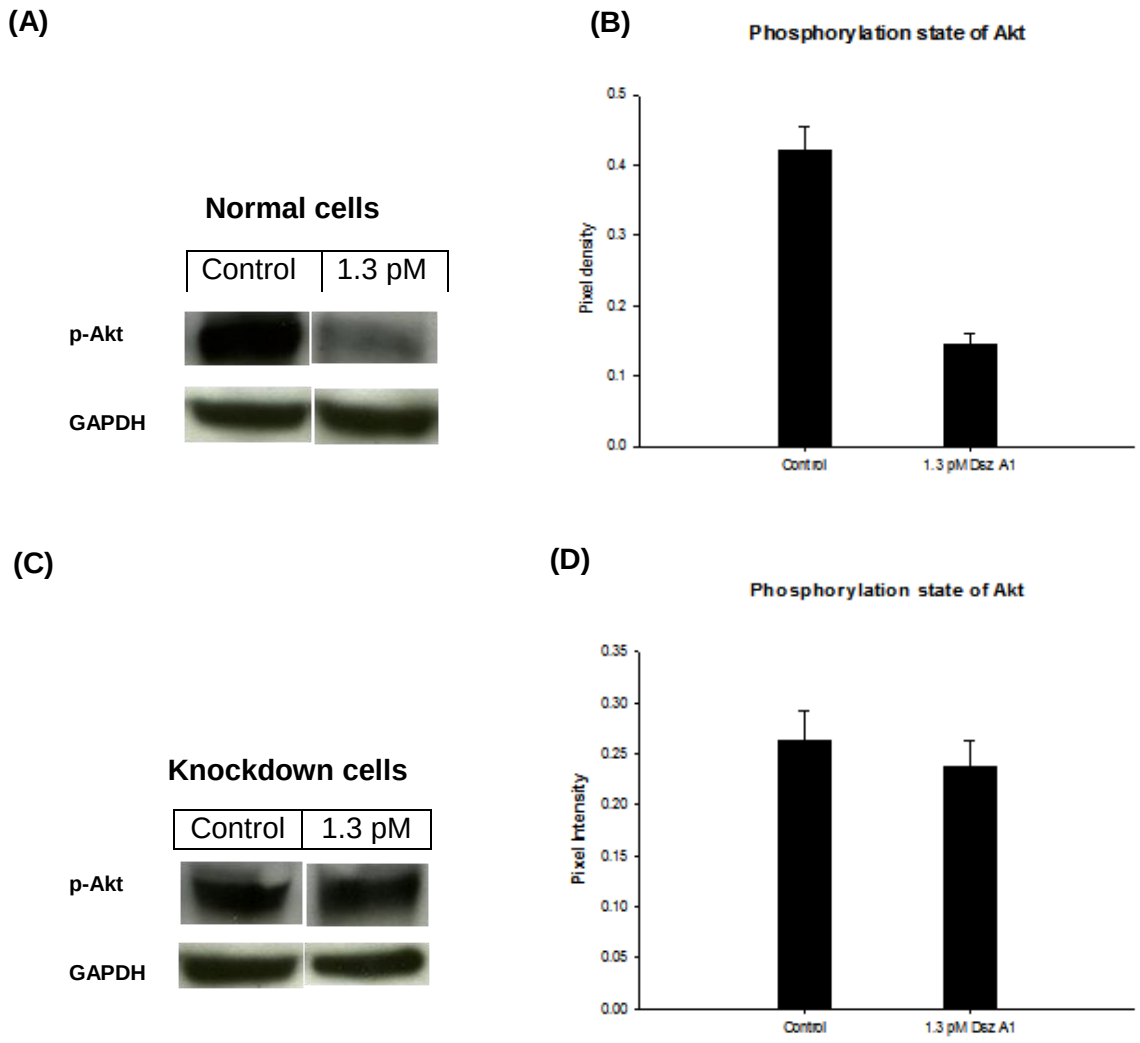

Figure 3.23: Effect of Dsz A_1 in PTEN knockdown KB-3-1 cells

Lysates were prepared after treating the knockdown cells with Dsz A_1 (1.3 pM) and probed for phospho-Akt by Western blotting. Panel A shows a clear reduction in the phosphorylation state of Akt in case of a normal cell lysate as compared to a non-reduced phosphorylation in a Dsz A_1 treated knockdown cell lysate (C). GAPDH was taken as the loading control for both normal and knockdown lysates. Panel B and D shows a graphical representation of the mean intensities with their respective standard deviation.

3.6.7 Influence of PTEN on apoptosis

Normal and knockdown cell lysates were used to check for the involvement of PTEN in apoptosis. The level of apoptosis was determined on the basis of mono- and oligonucleosomes in cell lysates produced in case of induced cell death. As can be seen from Figure 3.24 the level of apoptosis is greatly reduced in lysate prepared from PTEN knockdown cells as compared to the normal cells, both treated with Dsz A_1 at 1.3 pM.

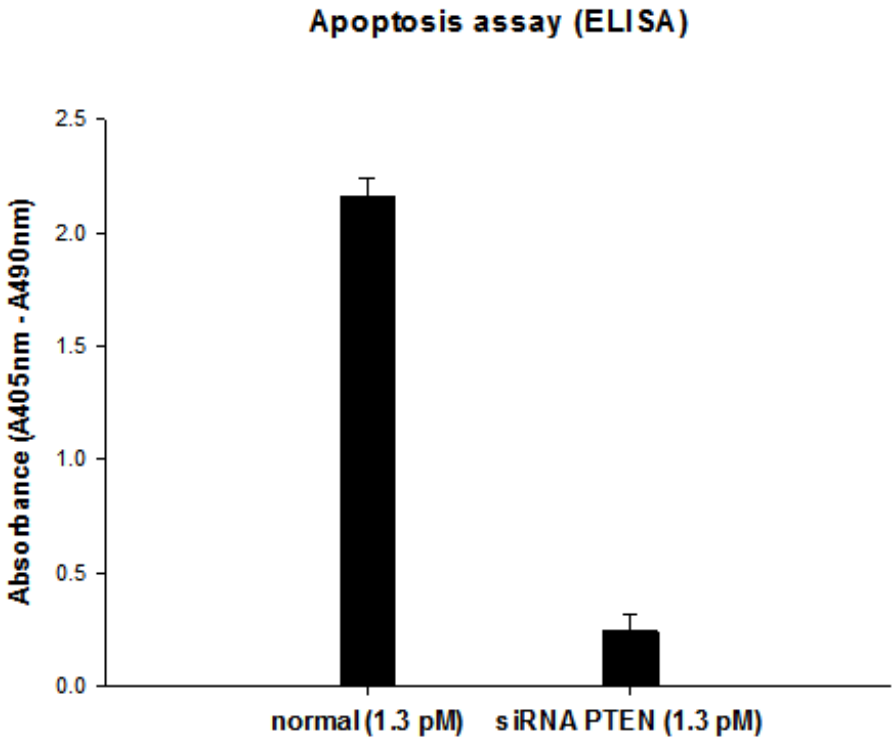

Figure 3.24: Level of apoptosis in normal and knockdown KB-3-1 cells treated with Dsz A_1

Normal cells and those that were knocked down with siRNA PTEN were treated with Dsz A_1 (1.3 pM). The level of apoptosis was determined by measuring induced mono and oligo-nucleosomes in the cells. There is drastic reduction of apoptosis in lysate from knockdown cells compared to the normal one despite their Dsz A_1 treatment.

3.6.8 Prediction of the binding domain of Dsz A_1 in PTEN

As all experiments pointed to PTEN being a direct target of Dsz A_1, docking studies with the known protein structure of PTEN were carried out to predict the binding domain of Dsz A_1 using the software Autodock (version 4). The crystal structure of PTEN was obtained from Protein Data Bank (accession number 1D5R (Lee et al., 1999)). It consists of a 179-residue N-terminal domain (phosphatase domain) and a 166-residue C-terminal domain. The signature motif HCXXGXXR is present as also in the active sites of protein tyrosine phosphatases (PTPs) and dual specificity protein phosphatases (DSPs). The structure of Dsz A_1 used for this study is shown in Figure 3.25.

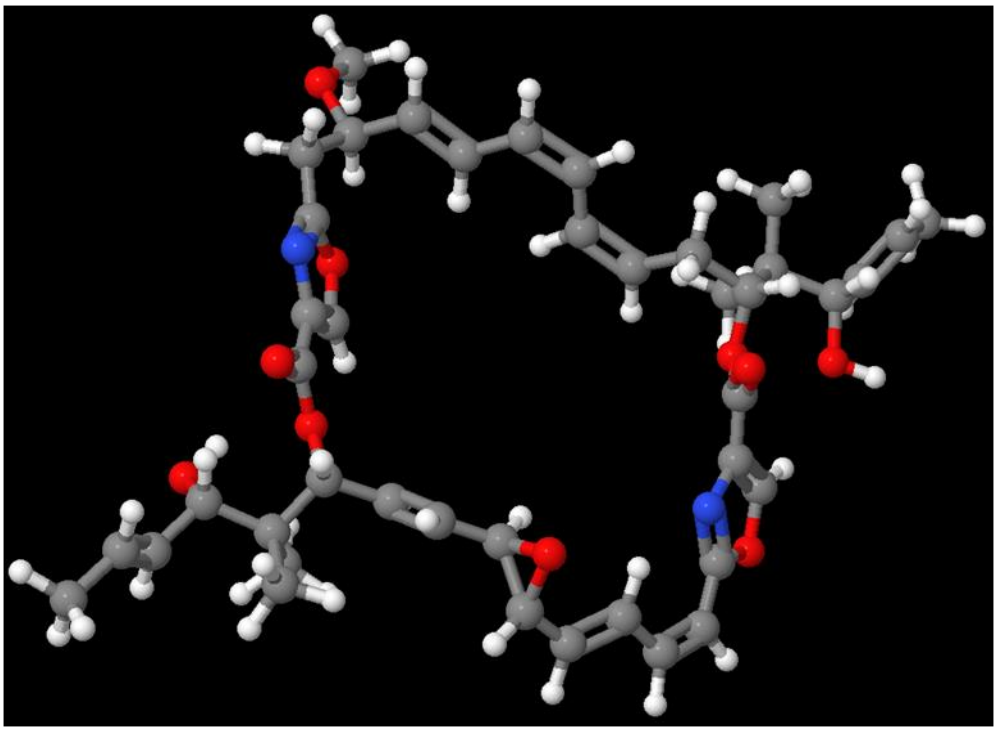

Figure 3.25: Structure of Dsz A_1 used for docking study

From docking studies, PTEN was found to bind primarily at thr^{319} and two arg$^{172, 173}$ with the epoxide ring of Dsz A_1 (Figure 3.26B). The binding energy of this interaction was found to be -10MeV. Interactions between whole PTEN protein and Dsz A_1 can be seen in Figure 3.26A.

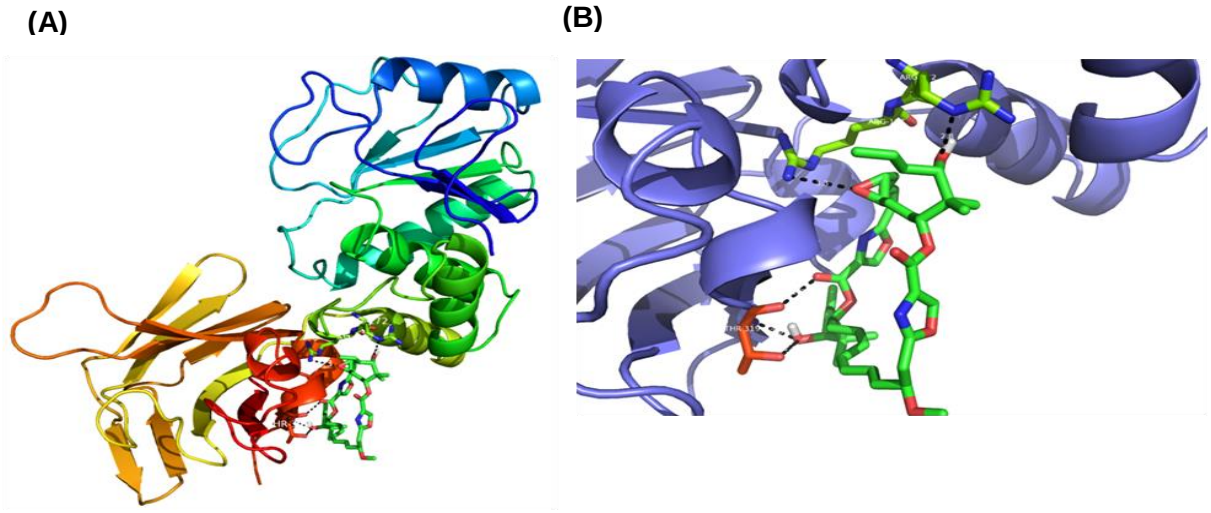

Figure 3.26: Docking site for Dsz A_1 on PTEN protein

Crystal structure of PTEN protein was obtained from Protein Data Bank (Id: 1D5R) and was docked with Dsz A_1 using Autodock (v4). Panel A showing the whole protein docking with Dsz A_1. Panel B shows the major interaction of the epoxide ring of Dsz A_1 with amino acids, threonine and two arginines at 319, 172 & 173 positions, respectively.

3.7 Identification of the mode of action of disorazol Z

As mentioned earlier in sections 3.5.1.2 and 3.5.2.1, Dsz Z seems to affect not only the microtubular structures of incubated cells but could also somehow affect kinase signalling pathway. Since belonging to the same chemical class, we wanted to investigate if the target or the pathway which Dsz A_1 affects would be similar for Dsz Z too First the effect of Dsz Z on cellular microtubules was investigated.

3.7.1 Influence of Dsz Z on tubulin structure

Based on the results of impedance measurements, Dsz Z clustered with microtubule affecting compounds. So to check this affect, PtK2 cells were cultured on sterile coverslips overnight and treated with Dsz Z at a concentration of 9.4 nM. Cells treated with methanol were taken as negative control. The cells were fixed and immunostained with an anti-α-tubulin antibody. As can be seen from Figure 3.27, Dsz Z induced multinucleated cells showing microtubular bundling.

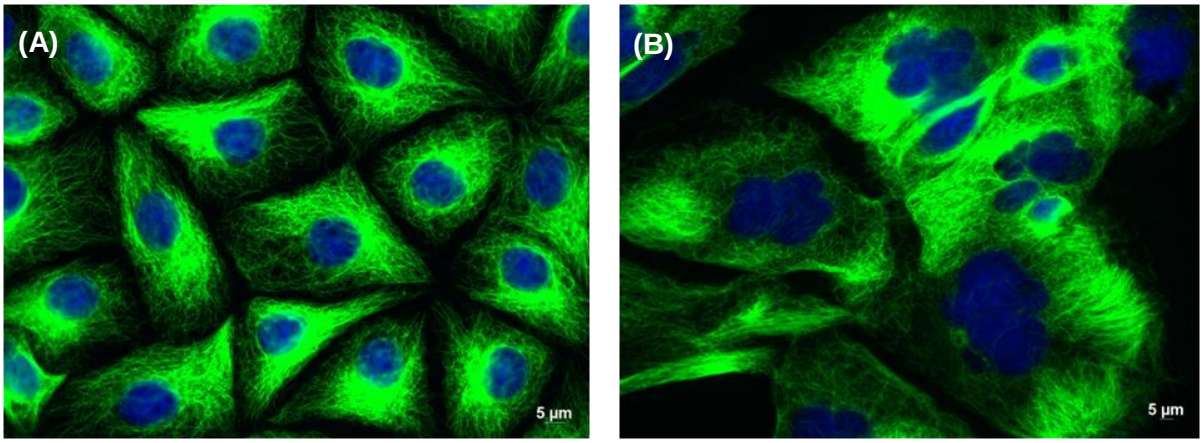

Figure 3.27: Dsz Z induces changes in microtubular structure

PtK2 cells were treated with Dsz Z (9.4 nM) (panel B) and methanol (panel A) for overnight. Cells were stained for α-tubulin (green) and nuclei (blue). Cells treated with Dsz Z showed microtubular bundling and multinucleated cells unlike methanol treated ones which have one nucleus each and normal microtubular network.

3.7.2 Effect of Dsz Z on p53 localization

To check the effect of Dsz Z on the localization of p53, A-549 cells were incubated with Dsz Z (67 pM) for overnight at 37°C and immunostained with an anti-p53 antibody. Methanol treated cells were taken as negative control. As can be seen from Figure 3.28 p53 is localised in the nucleus upon treatment with Dsz Z as compared to the cytoplasmic location of p53 in methanol treated cells. The effect closely resembles that of Dsz A_1.

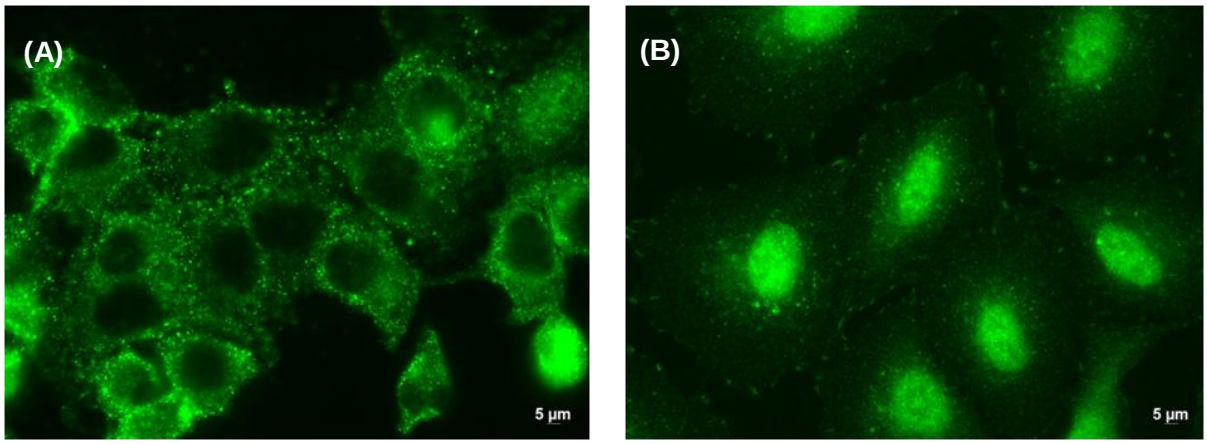

Figure 3.28: Effect of Dsz Z on p53 localization

A-549 cells were treated with Dsz Z at a concentration of 67 pM (panel B) and methanol (panel A) for overnight, fixed and stained with an anti-p53 antibody (green). Dsz Z treated cells show nuclear localization of p53 compared to cytoplasmic location in methanol treated cells.

3.7.3 Elucidating the target of Dsz Z with a DARTS approach

A DARTS approach was carried out with cell lysates prepared from KB-3-1 cells that have been treated at various concentrations of Dsz Z. A cell lysate treated with methanol was taken as negative control whereas a lysate treated with Dsz Z but not digested with Pronase® was considered positive control. Figure 3.29 depicts a Coomassie Blue staining after SDS-PAGE separation. It shows a protein band having molecular weight above 75 kDa that seemed to be protected in a concentration dependent manner.

Dsz Z (µM)	134	13.4	1.34	C	134
Pronase®	+	+	+	+	-

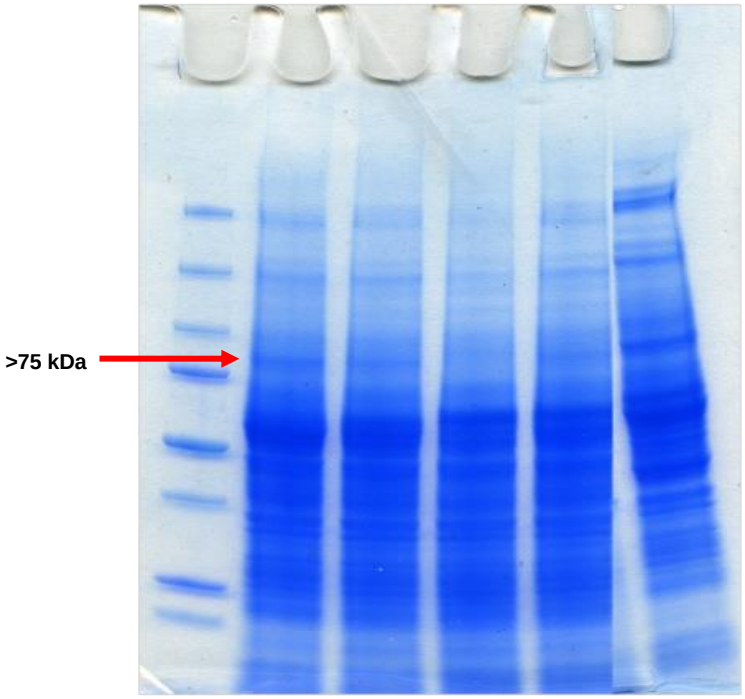

Figure 3.29: DARTS approach with Dsz Z

Cell lysate prepared from KB-3-1 cells were incubated with Dsz Z at various concentrations and subjected to a DARTS approach using Pronase® as the proteolytic enzyme. After SDS-PAGE the gel was stained with Coomassie Brilliant Blue. Methanol treated lysate (C) was the negative control and Dsz Z treated but not digested was taken as positive control. Dsz Z protected a protein band running above the 75 kDa mark.

Following the indication that Dsz A_1 is affecting the PI3K/Akt pathway, we tried to probe for the p85 regulatory unit of PI3 kinase as a potential target of Dsz Z. Hence the experiment was repeated with the same set of controls using an anti p85 antibody. This blot was re-probed for GAPDH which served as loading control. As can be seen from Figure 3.30, Dsz Z treated samples shows a concentration dependent protection for p85.

Dsz Z(µM)	134	13.4	1.34	0.13	C	134
Pronase®	+	+	+	+	+	-

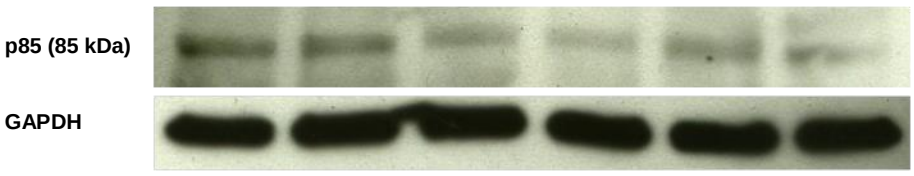

Figure 3.30: DARTS with Dsz Z followed by Western blot for p85

KB-3-1 cell lysate treated with varying concentration of Dsz Z were proteolytically digested with Pronase® and loaded onto SDS-PAGE. Methanol treated lysate (C) was taken as negative control and Dsz Z treated non-digested one was the positive control. The lysate was subjected to Western blotting and probed with an anti-p85 antibody. Dsz Z shows a concentration dependent protection for the regulatory subunit of PI3 kinase, p85. GAPDH was used as loading control.

3.7.4 Effect of Dsz Z on PI3 Kinase pathway

The DARTS result showed that the p85, regulatory subunit of PI3 kinase is being bound by Dsz Z. To verify if and how Dsz Z affects the phosphorylation state of p85, KB-3-1 cells were treated for overnight with Dsz Z at varying concentrations and subjected to Western blot analysis with an anti-phospho-p85 antibody. As can be seen from Figure 3.31, there is concentration dependent decrease in the phosphorylation state of p85. Methanol treated cells were taken as the negative control.

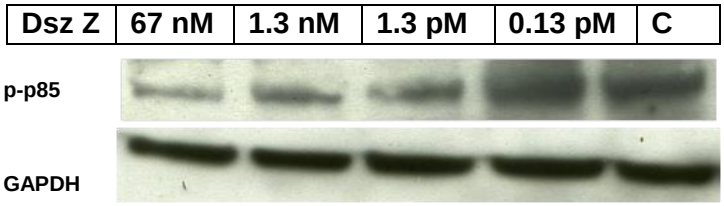

Figure 3.31: Effect of Dsz Z on phosphorylation state of p85

KB-3-1 cells were treated with Dsz Z at varying concentration for overnight before preparing the lysates. These were loaded onto SDS-PAGE and probed for p-p85 state using an anti-p-p85 antibody. A methanol treated lysate (C) was taken as negative control. GAPDH was taken as the loading control.

Like Dsz A_1 which affects the protein kinase B or Akt phosphorylation, Dsz Z was also tested for the same effects but the results were negative. Dsz Z does not affect Akt but another downstream protein of the PI3 kinase pathway called SGK1 which is structurally quite similar to Akt and also supports cell growth and proliferation upon phosphorylation by the PI3 kinase pathway. As can be seen from Figure 3.32, there is concentration dependent decrease in the phosphorylation state of proteins involved in PI3 Kinase/SGK pathway. In normal scenario when p85 regulatory subunit of PI3 kinase is phosphorylated, its inhibitory effect on the catalytic subunit p110 is released for p110 to carry out the downstream effect of phosphorylating PDK1 which in turn phosphorylates SGK1, thereby helping in cell growth. But when the cells are treated with Dsz Z, it inhibits the phosphorylation of p85, thereby stalling PI3K/SGK pathway.

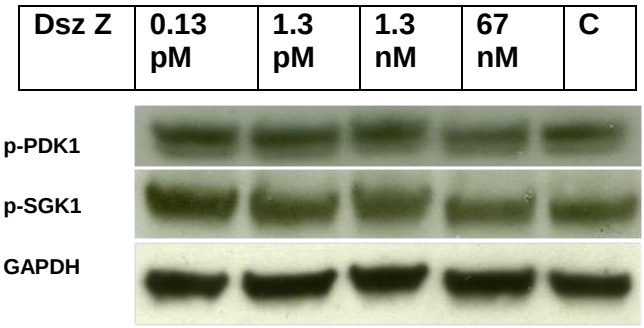

Figure 3.32: Effect of Dsz Z on PI3K/SGK pathway

KB-3-1 cells were treated with Dsz Z at various concentrations for overnight and lysates prepared from them were loaded onto SDS-PAGE. The blot was probed for p-PDK1 and p-SGK1 using an anti-p-PDK1 and anti-p-SGK1 antibodies respectively. Methanol treated lysate (C) and GAPDH were taken as negative and loading control respectively. There is gradual decrease in the phosphorylation state of both phospho proteins upon Dsz Z treatment.

3.7.5 p85 Knockdown studies

To further verify the target of Dsz Z, knockdown studies were carried out. Based on the DARTS results, p85 was chosen for knockdown. L-929 cells were transfected with siRNA p85α for 48 h for efficient knockdown. Scrambled siRNA was chosen as the negative control as it does not affect any known target in the cell. To check for the efficiency of p85α knockdown, a lysate was prepared from transfected L-929 cells and subjected to Western blotting. The level of p85α was probed using an anti-phospho p85α antibody as can be seen from Figure 3.33A. Panel B shows a graphical representation of the knockdown efficiency.

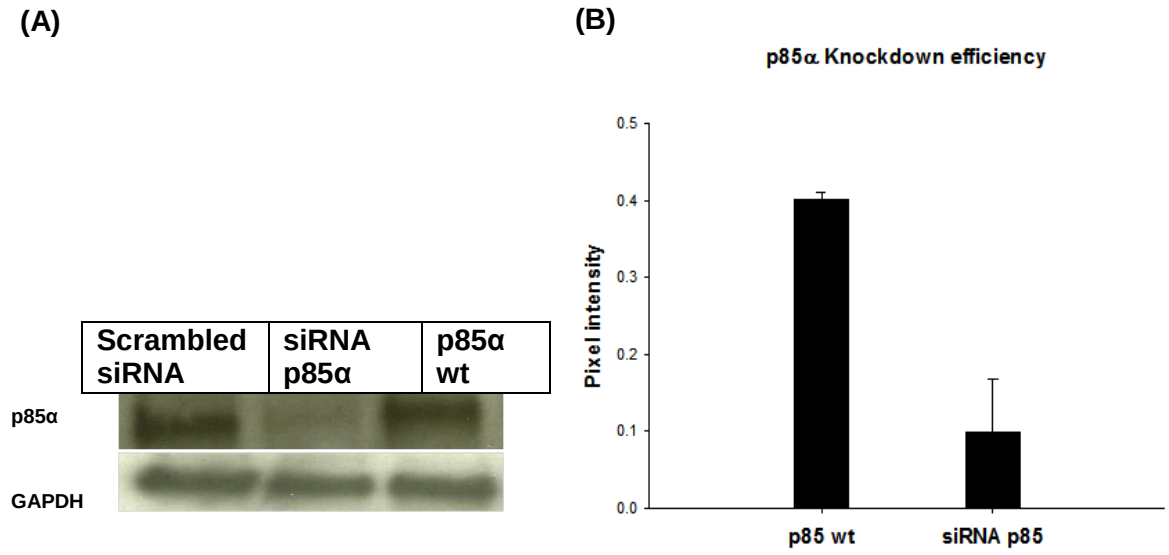

Figure 3.33: p85α knockdown efficiency

L-929 cells were transfected with p85α siRNA for 48 h before preparing the lysate for Western blot analysis. The blot was probed using an anti-phospho p85α antibody to check for the knockdown efficiency (panel A). Scrambled siRNA was used as negative control. Panel B shows the quantitative measurement based on the band intensity. Means and standard deviation from two experiments are given.

The same transfected L-929 cells were treated with 134 nM of Dsz Z for overnight before preparing the lysate. To verify the role played by p85α in the downstream process of SGK1 phosphorylation and thereby helping the cells to grow and proliferate, Dsz Z treated knockdown lysate was subjected to Western blotting and probed for any change in the phosphorylation of SGK1 using an anti-phospho SGK1. To compare the change, a lysate from normal cells was also used after treating the cells overnight with same concentration of Dsz Z. As shown in Figure 3.34, there is reduction in the inhibiting effect of Dsz Z on the phosphorylation state of SGK1 in the knockdown cells compared to normal cells. Graphical representation of the same is shown in Figure 3.34 B&D.

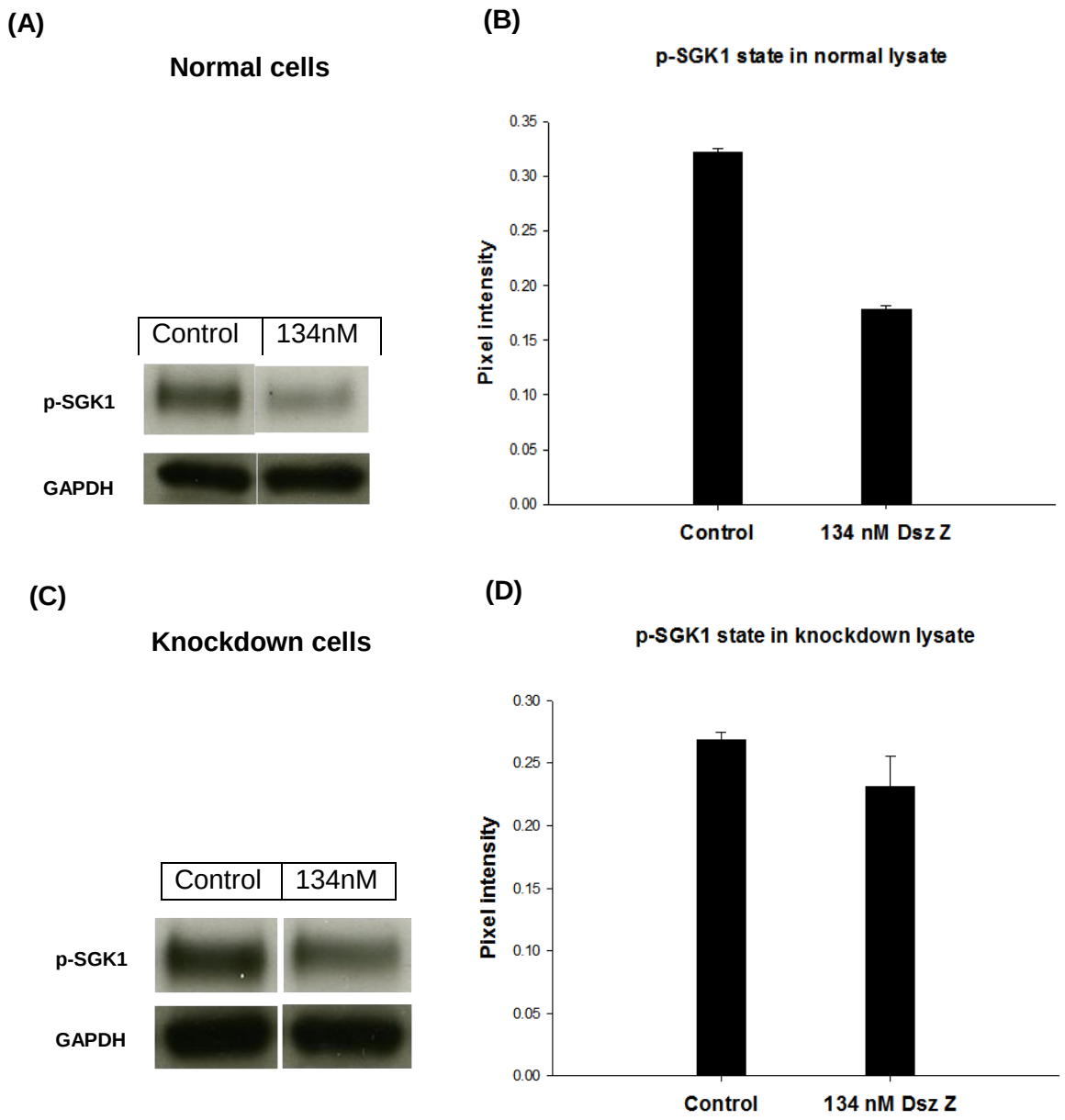

Figure 3.34: Effect of p85α knockdown on phosphorylation of SGK1

L-929 cells were transfected with p85α siRNA for 48 h and treated with Dsz Z (134 nM) for overnight. Both treated normal and knockdown cell lysates were subjected to Western blotting and probed using an anti-phospho-SGK1 and an anti GAPDH antibody. Panel A shows that the level of SGK1 phosphorylation is reduced on treatment with Dsz Z in normal lysate unlike in panel C the knockdown cells are no longer competent for the Dsz Z action. GAPDH is taken as loading control. Panel B and D shows the graphical representation of p-SGK1 with their means and standard deviation from two experiments.

3.7.6 Role of p85 in caspase 3/7 activity involved in apoptosis

To check for the role played by p85 in apoptosis, caspase 3/7 activity was measured for both normal and knockdown cell lysate treated with Dsz Z. Caspases are members of cysteine-aspartic acid specific proteases which play an effector role in apoptosis. Caspase 3/7 activity was measured using a Caspase 3/7 Glo® kit provided by Promega®. The luminescence signal provided is directly proportional to the level of caspase activity which in turn indicates

the level of apoptosis. As can be seen from Figure 3.35, the level of caspase activity in Dsz Z treated knockdown cells is reduced when compared to normal cells. This indicates that p85 is required for apoptosis to be carried out by Dsz Z.

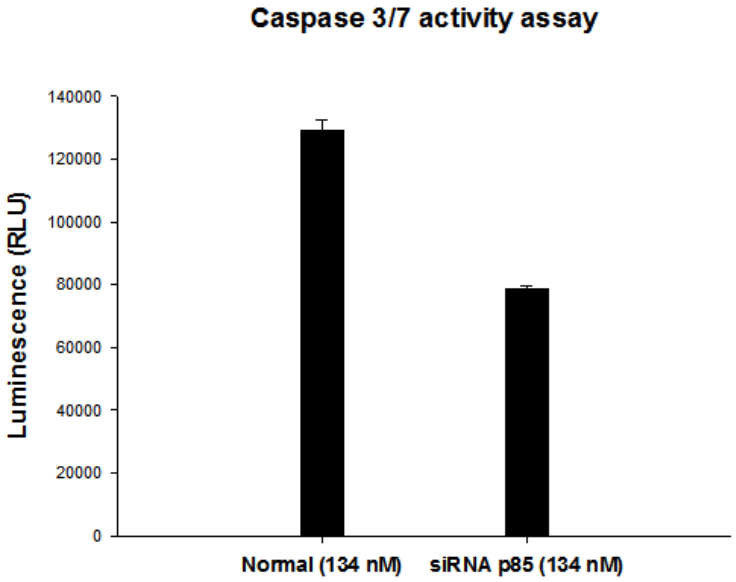

Figure 3.35: Role of p85 in apoptosis induced by Dsz Z

L-929 cells were transfected with p85α siRNA for 48 h and treated with 134 nM of Dsz Z for overnight before preparing the lysate. Dsz Z treated normal L-929 lysate and p85α knockdown lysate were measured for Caspase 3/7 activity. Caspase activity induced in knockdown cells is reduced when compared to normal cells.

4 Discussion

Natural products continue to provide a variety of “lead” structures which are used as templates for the development of new drugs. The majority of these leads are secondary metabolites from microbial system (Li and Vederas, 2009). Advances in various bioassays and in synthetic chemistry have combined to make natural products a cost effective source of leads (Borris, 1996). Many times nature not only provides us with bioactive compounds but those compounds also allow us to dwell on concept of evolutionary processes and their optimisation. One may think that isn’t it enough knowing that a compound is biologically active. Yes, but the need to know how these small molecules act within a cell (MoA) becomes important from past experiences of high attrition rate (Swinney and Anthony, 2011) observed for lead structures among pharmaceutical industries and it also helps to completely utilize its full potential by population-specific targeting.

The objective of this study was to make use of in-house established high content analysis approaches, *viz*., image analysis and impedance profiling to obtain hints of the MoA of small molecules of interest. An alkaloid jerantinine E and four polyketides namely paleo-soraphen A & B, disorazol A_1 and Z. were the compound of interest which were shown to have different mechanism of action and targets. High content analysis was used not only for identifying the MoA but was also compared to see if and how the indications provided by two approaches are different.

4.1 High content analysis (HCA)

High content analysis is a platform designed to define spatial and temporal activities of genes, proteins, and other cellular constituents in a living cells (Giuliano et al., 2003). Identification of small molecule modulators of protein function, and the process of transforming them into a “lead” are key activities in drug discovery (Bleicher et al., 2003). The study presented made use of HCA in two different cell-based assays, one being a cell invasive, labelling technique and the other being a label-free approach.

HCA by automated microscopy is a labelling technique wherein the cells are incubated with the compound of interest and later fluorescently tagged with a range of antibodies representing cellular proteins. Impedance monitoring is a label-free technique depending greatly on changing cell morphology.

4.1.1 Image analysis

Automated microscopy provides with a powerful tool for analysing the physiological state of the cell with high throughput and high information content when incubated with the compound of interest (Mitchison, 2005). It allows rapid visualization of a large group of cells and phenotypic analysis in a quantitative manner (Starkuviene and Pepperkok, 2007). In this study HCIA was first carried out for the reference compound who’s MoA are well-established. Cells when treated with these compounds in optimum concentration caused morphological and physiological changes. These changes were observed by fluorescently tagging the cells with appropriate antibodies and nuclear marker. Images were acquired using an automated microscope with some pre-defined application modules. Acquired

images were analysed and statistical analysis was carried out. Hierarchical clustering provided us with clusters of compounds having similar MoA, though all reference compounds did cluster with one another at various Euclidean distances forming a complete family of clusters. The reference library included 63 commercially available compounds (Table 2.3). Figure 3.1 shows profiles of all the reference compounds within their clusters. Many clusters showed compounds with the same MoA but on few occasions, compounds with dissimilar MoA clustered together. This could be due to some off-targets effects. For example, argyrin A clustered with microtubule affecting compounds, though it is known to be a proteasome inhibitor. p53 localizes to microtubules and in response to DNA damage, it is transported to the nucleus (Giannakakou et al., 2002) and hence being activated whereas for p53 to be degraded it requires proteasomes. So probably argyrin A stops proteasomal degradation of p53 and that made it to cluster with MT affecting compounds. Another cluster grouped MG132, a proteasome inhibitor, with kinase pathway affecting compounds. It has been shown that inhibition of cyclin-dependent kinase is regulated by proteasome (Pagano et al., 1995). Also it is not necessary that compounds in the same cluster are related to one another depending on their MoA but they could cluster together due to various reasons. If the test compound has a novel MoA that is not represented by the reference compounds, it is not possible to find a matching profile. Hence it clusters with the closest matching profile. With respect to the concentration used, sometimes compound always cluster in a one particular group irrespective of concentration but sometimes at lower concentrations compounds might interfere with p53 protein and at higher concentration the MT network is affected (Giannakakou et al., 2002). So clustering changes from a p53 affecting compound to MT effectors.

Transformed data can be analysed not only by using hierarchical cluster analysis providing us with heat maps as mentioned above but with the help of non-hierarchical cluster analysis compounds could be grouped. Self-organizing maps (SOMs) is a simple representation of similarity between the clusters. It does not necessarily provide us with hints about the compound's mechanism. All compounds are separated in a pre-determined number of clusters. 13 descriptors were taken into consideration and their average profiles are shown with the help of a graph line within each cluster of SOM. (Figure 3.2) Another method within non-hierarchical cluster analysis is principal component analysis (PCA) which places all the compounds within a 3D biological space. (Figure 3.3) This helps to identify outliers which could indicate a totally novel MoA.

Out of all the methods used in this study, heat maps generated by using hierarchical cluster analysis provided sound information about the MoA of the reference compounds.

4.1.2 Impedance profiling

The xCELLigence system is based on impedance measurement of the cells seeded on gold electrodes integrated in the well bottom of an E-plate. Incubation of cells with compounds causes morphological and physiological changes in the cell status which is reflected in change of impedance. These changes were measured over a period of few days. Acquired data were transformed to provide Z-scores which were later used in statistical analysis to generate a heat map. Euclidean distances were used to form a similarity matrix which grouped all the 63 reference compounds in different clusters based on different MoA. Figure 3.4 shows different clusters with few compounds highlighted. Most of the compounds

clustered in correct groups like box 3, 4, 5 and 6 but box 1 shows clustering of compounds inhibiting transcription via different ways along with cytochalasin D which is an actin inhibiting compound. A closer look to the dendrogram shows that though cytochalasin D is in the same cluster it has a big distance to other members. According to the dendrogram cytochalasin D seems to be closer to the compounds in box 2 containing latrunculin B and rhizopodin A which affects actin.

Thus, it becomes clear that as much as it is important for one to see the clusters at the right hand side of the heat map, it is also necessary to complement it with the Euclidean distance provided in the dendrogram to ensure the certainty of the hint.

Several strengths and weaknesses were observed for both the methods utilized in this study, *viz*., automated microscopy and xCELLigence. Automated microscopy as mentioned earlier is a cell invasive labelling method which forces one to obtain only an end-point result of the assay whereas xCELLigence on the other hand is a kinetic assay as it measures the change in impedance over a period of time in the presence of the compound. It could provide us with information about short as well as long-term effect response of the drug on cells. Despite of giving only end-point results, image profiling could be of advantage when analysis of phosphorylated proteins is decisive. It is not investigated as to how change in the phosphorylation state of the proteins affects the impedance reading but certainly this change will be detected by analysing their images which makes it one of the strength of automated microscopy. However, both approaches should be able to provide us with hints towards the MoA for test compound when included along with well-established reference compounds by comparing the test profile with that of the known MoA profiles.

Having said that, the presented study also pointed out that both the methods can only be used as a tool to get hints towards the MoA of a compound. One needs to remember that the clusterings are just indicators of possible targets and not sure shot protein/pathway target identifiers. They could also be indicating some secondary targets.

4.2 Mechanism of selected bioactive compounds

In terms of cytotoxicity, jerantinine E showed its activity in lower micromolar range (IC_{50} = 1.9 µM) whereas paleo-soraphen A & B, genetically inspired derivatives of soraphen A were found to be much less active in cancer lines On the other hand the two members of the disorazol family, disorazol A_1 and Z showed subnanomolar activity in a variety of cancer cell lines (IC_{50} = 0.0016 nM and 0.24 nM, respectively in KB-3-1 cells). Based on the results of high content analysis, the mechanisms of these compounds were elucidated.

4.2.1 Jerantinine E

Jerantinine E, one of the seven Aspidosperma indole alkaloids isolated from leaf extracts of the Malayan plant *Tabernaemontana corymbosa* showed a cytotoxicity against KB-3-1 cells which is rare among Aspidosperma alkaloids. The mechanism for this bioactivity was not known (Frei et al., 2013). Impedance profiling of jerantinine E (Jer E) with L-929 cells showed a profile (Figure 3.5) similar to those of microtubule affecting compounds like colchicine which directed our investigation towards tubulin based assays. Immunofluorescence staining of PtK2 cells treated overnight with Jer E showed (Figure 3.6)

multinucleated cells to nearly complete disruption of microtubules at 10 µg/mL as seen in case of cells treated with colchicine, an active alkaloid of *Colchicum* (Molad, 2002). These results made it very likely that Jer E is inhibiting tubulin polymerisation.

This assumption was assessed by (Frei et al., 2013). Jerantinine E inhibited tubulin polymerisation with an IC_{50} of 0.45 µM (Frei et al., 2013). In terms of % tubulin polymerisation inhibition Jer E showed 79 % compared to colchicine at 75 % (statistically significance with $p< 0.05$ [Student *t* test]).

The ability of tumour cells to infiltrate and disseminate widely is what makes them malignant (Nabeshima et al., 2002). Therefore, inhibition of cell migration by Jer E was also observed by (Frei et al., 2013) for four cancer cell lines (MCF-7, MDA-MB-231, A-549 and HT-178). These cell lines were exposed for 15 h at 2.5 µM and 15.6 µM. Migration inhibition was most pronounced for the breast cancer cell line, MCF-7 and MDA-MB-231 (Frei et al., 2013).

4.2.2 Paleo-soraphen A & B

For a large variety of polyketides at least one of the enzymatic steps seen within the PKS is non-functional. Paleo-soraphen A & B were synthesised chemically by following the structures predicted by an intact polyketide synthases modular assembly of soraphen A. Such genetic derivatives can help us to understand if and how the biological behaviour changes and give insights into the evolution of compounds.

Soraphen A, a potential antifungal and antitumor compound, inhibits the eukaryotic acetyl-coenzyme A carboxylase (ACC). Genetic analysis of the appropriate PKS identified two positions in the soraphen structure which differed from the genetically expected outcome (Schupp et al., 1995; Wenzel et al., 2006). The presence of double bond (Figure 1.14) between C9-C10 is proposed to be a consequence of postketide transformation whereas the absence of a double bond between C2-C3 in soraphen A is due to the inactivity of the dehydratase module in the domain (Schupp et al., 1995). Such structural variation may change its bioactivity. Impedance profiling showed that paleo-soraphen A has a similar profile to that of its parent compound, soraphen A, whereas paleo-soraphen B clustered with the topoisomerase I inhibitor, camptothecin (Figure 3.7).

Based on above results and previously known activity of soraphen A as antifungal, genetic derivatives were tested against fungi. Only paleo-soraphen A showed some activity against *Pythium debaryanum* (Lu et al., 2013).

With respect to paleo-soraphen B, its effect was compared to that of camptothecin by immunofluorescence staining of PtK2 cells. Topoisomerase I is shown to have a protein kinase activity that phosphorylates the splicing factor SC-35. These are found in speckles which occupy nuclear space. mRNA transcription and processing takes place in these speckles. Inhibition of mRNA transport from nucleus to cytoplasm causes rounding, enlargement of speckles and the accumulation of splicing factors within them. The activity of SC-35 is regulated by a phosphorylation-dephosphorylation system. Like camptothecin, paleo-soraphen B causes a rounding of speckles and equal distribution within the nucleus (Figure 3.8) unlike soraphen A and paleo-soraphen A. These speckles were quantified in terms of their average size. It was shown that both camptothecin and paleo-soraphen B

caused the average size of the speckles to be much smaller compared to controls (Figure 3.9).

The effect of paleo-soraphen A on eukaryotic ACC was found to be mild. It requires further investigation. But it supports the concept of evolutionary optimization (Lu et al., 2013). Genetic derivatives do require further investigations with respect to their mechanisms.

4.2.3 Disorazol A_1

Disorazol A_1 (Dsz A_1) was isolated from the culture broth of the myxobacterium *Sorangium cellulosum* So ce12. It is active against many filamentous fungi (MIC = 0.1 to 1 µg/mL) but not yeasts and bacteria. Dsz A_1 shows cytotoxicity in a subnanomolar range in mammalian cells (Table 3.1).

Earlier results with Dsz A_1 showed that it inhibits tubulin polymerisation in a concentration dependent manner but independent of microtubule-associated proteins (MAPs). At lower concentrations immunofluorescence staining also showed a nuclear accumulation of tumour suppressor protein p53 (Elnakady et al., 2004). To investigate this point and its role in increased cytotoxicity, a detailed study of mode of action was carried out.

When Dsz A_1 was applied to cells for their impedance profiling it clustered with compounds effecting microtubule (Figure 3.10). On the other hand in image profiling, it clustered with a totally different group of compounds i.e., kinase pathway effectors. These interesting findings could reflect the results obtained by the p53 investigations. As described earlier HCA methods can point towards different targets and in this case the image profiling seemed to be more sensitive for phosphorylated targets than the impedance profiling.

At picomolar levels of Dsz A_1, the “zip-code” (O’Brate and Giannakakou, 2003) of p53 protein changed from cytoplasm to nucleus (Figure 3.15) which could be explained by the observation that Dsz A_1 inhibits phosphorylation of Akt. In a normal scenario, when Akt is phosphorylated it activates or inhibits various downstream proteins, one of them being Mdm2 (Figure 1.9) which is activated by phosphorylation. Mdm2 (Mouse double minute 2) belongs to the family of E3 ubiquitin ligases. It shuttles between the nucleus and the cytoplasm as it contains nuclear localization and nuclear export signals within its structure, (Liang and Clarke, 2001; Vargas and Ronai, 2002) and helps to downregulate p53 activity (Pei et al., 2012). Phosphorylation of Mdm2 obligates its translocation from cytoplasm to nucleus where it interacts with p53, inhibit its transcriptional activity and target it for proteasomal degradation. In our study we observed an increase in the phosphorylation state of p53 (Figure 3.17) and a cytoplasmic translocation of Mdm2 (Figure 3.16) upon Dsz A_1 treatment.

Once p53 is being prevented from degradation, it induces an expression of a group of target genes which negatively regulate cell survival pathways like PI3K/Akt (Feng, 2010). These target genes involves the phosphatase enzyme PTEN which dephosphorylates PIP_3 to PIP_2 (Figure 1.10). The presented investigation gave hints that the picomolar levels of Dsz A_1 might enhance the stability of PTEN. PTEN protein “tail” (residues 354-403) is necessary for stability of PTEN but also acts to inhibit its function by phosphorylating the tail (Vazquez et al., 2000). One would need to further investigate as to how Dsz A_1 is stabilizing PTEN but at the same time being able to retain its activity.

Once PTEN stabilizes, it antagonizes the PI3K pathway. Once PIP_3 is converted to PIP_2, PH-domain containing proteins like PDK1 and Akt get de-recruited from the plasma membrane (Carracedo and Pandolfi, 2008) and there is reduced phosphorylation of PDK1 and Akt. (Figure 3.20) Activated Akt is a well-established survival factor (Di Cristofano and Pandolfi, 2000).

To confirm that Dsz A_1 shows the above described effects by binding directly to PTEN, a DARTS approach was carried out which clearly showed a concentration dependent protection of PTEN from proteolysis. (Figure 3.21) PTEN is a well-established tumour suppressor gene that induces apoptosis and controls cell growth by inhibiting the PI3K/Akt pathway (Ming and He, 2012).

Further confirming the role of PTEN, knockdown studies were done wherein PTEN was knockdown using siRNA PTEN in KB-3-1 cells. (Figure 3.22) Lysates prepared from these knockdown cells were probed for the level of phosphorylated Akt and compared with that of normal cells (Figure 3.23). These investigations confirmed that PTEN is the target protein of Dsz A_1. It's binding leads to a reduced phosphorylation of Akt and thereby inhibiting cell proliferation.

PTEN plays a critical role in DNA damage repair and DNA damage response thereby acting as guardian of genome integrity. (Ming and He, 2012; Shen et al., 2007). One of the DNA damage responses is apoptosis. The level of apoptosis was measured photometrically for lysates prepared from PTEN knockdown cells that were incubated with Dsz A_1. Comparison with normal lysates (Figure 3.24) showed that PTEN is required for Dsz A_1 induced apoptosis. PTEN might exert its tumour-suppressive effect through inhibition of cell-cycle progression or the induction of apoptosis as a consequence of blocking signalling pathways (Weng et al., 2001). Studies showed that Dsz A_1 blocks the PI3K\Akt pathway which could explain the event of apoptosis. But inhibition of cell cycle progression (G2\M blockage) (Elnakady et al., 2004) might not be contributed by PTEN as PTEN-mediated cell-cycle arrest takes place at G_1 (Eng, 2003) at least for MCF-7 cells. Therefore, probably cell cycle arrest and apoptosis are differentially regulated (Weng et al., 2001) in our case.

Once we had the confirmation of the role of PTEN which was induced by Dsz A_1, docking studies with PTEN protein (accession number: 1d5R) and Dsz A_1 were carried out. (Figure 3.26A) Major interactions were seen between Dsz A_1 and PTEN protein at the amino acids, threonine^{319} and two arginine's$^{172, 173}$. (Figure 3.26B) Interactions with the arginine are in the phosphatase domain (residues 7-185) of the PTEN protein which is responsible of binding with the phosphoinositide substrates (Lee et al., 1999). One of the interactions of arginine is with the epoxide ring of Dsz A_1 which is believed to contribute to an enhanced bioactivity. The interaction with thr^{319} belongs to the C2 domain (residues 186-351) of PTEN protein which binds to the phospholipid membrane.

4.2.4 Disorazol Z

Disorazol Z (Dsz Z) was produced by fermentation of the myxobacterium *Sorangium cellulosum* So ce1875. It was found to be effective against a range of tumour cells in nanomolar concentrations. (Table 3.1) It is as active in primary (HUVECs) as in tumour cells (e.g., KB-3-1). Conjugation of Dsz Z with the LHRH agonist peptide has shown to increase its activity in tumour cells with available LHRH receptors in breast, prostate and ovarian

cancers (Guenther et al., 2013). It was observed in the presented study that like Dsz A_1, Dsz Z also is cytostatic in nature and not cytotoxic as it did not reach the IC_{90} mark.

Impedance profiling of Dsz Z when treated at nanomolar levels showed that it clustered with colchicine, a microtubular effector and jerantinine E which was also found to be affecting microtubules (Figure 3.11).

Image profiling on the other hand showed a clustering with argyrin A, a proteasome inhibitor and a kinase inhibitor, indirubin monoxime (Figure 3.12). Dsz Z shows a similar profile to that of argyrin A probably due to the involvement of p53. Proteasome inhibitors stabilize and accumulate p53 which leads to apoptosis (Lopes et al., 1997). For p53 to be transcriptionally active, it needs to enter the nucleus. Cells when incubated with Dsz Z showed a translocation of p53 to the nucleus as seen in case of Dsz A_1 too (Figure 3.28).

Based on these results Dsz Z was also checked for its role in the PI3 kinase pathway.

The DARTS approach showed a protection of a protein band running above the 75 kDa marker. (Figure 3.29) Western blot analysis helped us to identify the protein being protected. The results were positive when the membrane was probed with an anti-p85 antibody. This showed that Dsz Z binds directly to the regulatory unit of PI3 kinase, p85.

Once the target was identified, their downstream proteins were analysed. As described earlier, p85 is involved in the regulation of the PI3K pathway by inhibiting the catalytic unit, p110 of the PI3 kinase. The site of p85 with which it binds and inhibits p110 thereby stalling PI3 kinase is also the site where p85 is phosphorylated. If this phosphorylation takes place, p110 is free and activated (Cuevas et al., 2001) but if p85 is prevented from being phosphorylated as is done by Dsz Z, p85 is free to go and bind with p110 and thus inactivating PI3K pathway. Dsz Z showed a concentration dependent decrease in phosphorylation of p85 (Figure 3.31).

Dsz Z was checked for its effect on the phosphorylation of Akt but results were negative, so the effect of Dsz Z was checked for other downstream proteins which might be involved in aiding cell growth. Literature talks about another cell survival signal involving a protein which is structurally similar to Akt (Brunet et al., 2001). This protein is independent of Akt but dependent on PI3 kinase for its activation and signalling.

Dsz Z inhibits phosphorylation of a kinase PDK1 which is responsible for phosphorylation and activation of SGK1 dependent cell growth. (Figure 3.32) These results show that Dsz Z affects the PI3K pathway but its downstream effector is different.

Knockdown studies of p85 showed that the presence of p85 (Figure 3.33) is required for further phosphorylation and activation of SGK1. As compared to the normal cells, knockdown cells were not able to prevent activation of SGK1. (Figure 3.34) Though the extent of phosphorylation of SGK1 in knockdown cells is higher than normal cells but there is no drastic reduction which can be explained by the fact that the regulatory unit isoform, p85α is encoded by PIK3R1 gene which also gives two shorter isoform, p55α and p50α through alternative-transcription sites and these individual isoforms show enhanced insulin sensitivity in absence of p85α and therefore activate PI3K signalling (Engelman et al., 2006; Okkenhaug and Vanhaesebroeck, 2001). A complete knockdown of the regulatory unit and

not just one isoforms could provide us with further details on the effect of Dsz Z on SGK1 inhibition.

Once the role of p85 was confirmed upon treatment with Dsz Z, its effect was assessed towards apoptosis. Caspase activity in lysates from knockdown cells incubated with Dsz Z was less compared to normal lysates indicating that p85 is required for a maximal induction of apoptosis by Dsz Z. p53 might also play a role in this effect as it stimulates the apoptotic pathway (Haupt et al., 2003).

5 Outlook

High content analysis has helped us to narrow down the downstream approach in elucidating the mode of action of bioactive compounds, but these methods are far from being perfect. Further investigations could help to enhance the correct prediction rate of the mode of action of new compounds, *e.g.*, by including more reference compounds and more descriptors, the latter being possible for image profiling. These will not only help to forgo the time spent on performing several experiments without knowing the possible target but most importantly reduce the attrition rate of drugs obtained from natural products.

A new approach could be established wherein the descriptors of both image and impedance profiling are combined. This could provide with better indications than what is now being provided individually. Though first steps were made towards such an approach during this study but it does require more investigations before such a method will be available.

All the selected bioactive compounds for this study showed different mechanisms of action. Jerantinine E was found to induce a depletion of microtubules in the cells and to inhibit tubulin polymerisation *in vitro. S*tudies on the binding sites could give more insights in the mode of action. HCA of paleo-soraphen A & B was just a stepping stone for further studies as in this study it was only shown that paleo-soraphen A had a similar profile to that of soraphen A whereas paleo-soraphen B might affect topoisomerase I. Directly measuring the inhibition of ACC and topoisomerase activity could provide some more evidence to support the findings. Such genetic derivatives can also help us to understand the modular assembly of PKS or NRPS multi-enzyme system in more detail. Members of the disorazol family namely Dsz A_1 and Z affected the same pathway (PI3K) but their downstream effector proteins and targets were different. Dsz A_1 on one hand targets the phosphatase PTEN which antagonized the PI3K pathway which leads to down regulation of Akt protein whereas on the other hand Dsz Z targets p85, the regulatory unit of PI3 kinase which also down regulates the PI3K pathways but does not affect Akt. It affects another kinase, SGK1 which is also involved in regulation of cell growth. Surface plasma resonance (SPR) technique and co-crystallization study of the target with that of the small molecule could provide further insights in the binding of these small molecules to their respective targets. The disorazols are potential antitumor drugs. The most successful approach could be tumour targeting with synthetic derivatives that specifically deliver the compounds to the tumour cells. The disorazol moiety is then used as a warhead to kill the malignant cells.

6 References

Abassi, Y.A., Xi, B., Zhang, W., Ye, P., Kirstein, S.L., Gaylord, M.R., Feinstein, S.C., Wang, X., and Xu, X. (2009). Kinetic cell-based morphological screening: prediction of mechanism of compound action and off-target effects. Chemistry & biology *16*, 712-723.

Atienza, J.M., Yu, N., Kirstein, S.L., Xi, B., Wang, X., Xu, X., and Abassi, Y.A. (2006). Dynamic and Label-Free Cell-Based Assays Using the Real-Time Cell Electronic Sensing System. Assay and drug development technologies *4*, 597-607.

Bickle, M. (2010). The beautiful cell: high-content screening in drug discovery. Analytical and bioanalytical chemistry *398*, 219-226.

Bleicher, K.H., Bohm, H.J., Muller, K., and Alanine, A.I. (2003). Hit and lead generation: beyond high-throughput screening. Nature reviews Drug discovery *2*, 369-378.

Bollag, D.M., McQueney, P.A., Zhu, J., Hensens, O., Koupal, L., Liesch, J., Goetz, M., Lazarides, E., and Woods, C.M. (1995). Epothilones, a new class of microtubule-stabilizing agents with a taxol-like mechanism of action. Cancer Res *55*, 2325-2333.

Borris, R.P. (1996). Natural products research prespectives from a major pharmaceutical company. Journal of Ethnopharmacology *51*, 29-38.

Bruhn, M.A., Pearson, R.B., Hannan, R.D., and Sheppard, K.E. (2013). AKT-independent PI3-K signaling in cancer - emerging role for SGK3. Cancer management and research *5*, 281-292.

Brunet, A., Park, J., Tran, H., Hu, L.S., Hemmings, B.A., and Greenberg, M.E. (2001). Protein kinase SGK mediates survival signals by phosphorylating the forkhead transcription factor FKHRL1 (FOXO3a). Molecular and cellular biology *21*, 952-965.

Campbell, R.B., Liu, F., and Ross, A.H. (2003). Allosteric activation of PTEN phosphatase by phosphatidylinositol 4,5-bisphosphate. The Journal of biological chemistry *278*, 33617-33620.

Cantley, L.C., and Neel, B.G. (1999). New insights into tumor suppression: PTEN suppresses tumor formation by restraining the phosphoinositide 3-kinase/AKT pathway. Proc Natl Acad Sci *96*, 4240–4245.

Carpenter, A.E. (2007). Image-based chemical screening. Nat Chem Biol *3*, 461-465.

Carracedo, A., and Pandolfi, P.P. (2008). The PTEN-PI3K pathway: of feedbacks and cross-talks. Oncogene *27*, 5527-5541.

Chalhoub, N., and Baker, S.J. (2009). PTEN and the PI3-kinase pathway in cancer. Annual review of pathology *4*, 127-150.

Chumakov, P.M. (2000). Function of the p53 Gene: Choice between Life and Death. Biochemistry (Moscow) *65*, 28-40.

Courtney, K.D., Corcoran, R.B., and Engelman, J.A. (2010). The PI3K pathway as drug target in human cancer. Journal of clinical oncology : official journal of the American Society of Clinical Oncology *28*, 1075-1083.

Cuevas, B.D., Lu, Y., Mao, M., Zhang, J., LaPushin, R., Siminovitch, K., and Mills, G.B. (2001). Tyrosine phosphorylation of p85 relieves its inhibitory activity on phosphatidylinositol 3-kinase. The Journal of biological chemistry *276*, 27455-27461.

Cully, M., You, H., Levine, A.J., and Mak, T.W. (2006). Beyond PTEN mutations: the PI3K pathway as an integrator of multiple inputs during tumorigenesis. Nature reviews Cancer *6*, 184-192.

Das, S., Dixon, J.E., and Cho, W. (2003). Membrane-binding and activation mechanism of PTEN. Proceedings of the National Academy of Sciences of the United States of America *100*, 7491-7496.

Denner, P., Schmalowsky, J., and Prechtl, S. (2008). High-Content Analysis in Preclinical Drug Discovery. Combinatorial Chemistry & High Throughput Screening *11*, 216-230.

Desai, S.D., Li, T.-K., Rodriguez-Bauman, A., Rubin, E.H., and Liu, L.F. (2001). Ubiquitin/26S Proteasome-mediated Degradation of Topoisomerase I As a Resistance Mechanism to Camptothecin in Tumor Cells. Cancer Res *61*, 5926-5932.

Di Cristofano, A., and Pandolfi, P.P. (2000). The Multiple Roles of PTEN in Tumor Suppression. Cell *100*, 387-390.

Editorial (2010). Mechanism matters. Nature medicine *16*, 347.

Elias, E., Lalun, N., Lorenzato, M., Blache, L., Chelidze, P., O'Donohue, M.F., Ploton, D., and Bobichon, H. (2003). Cell-cycle-dependent three-dimensional redistribution of nuclear proteins, P 120, pKi-67, and SC 35 splicing factor, in the presence of the topoisomerase I inhibitor camptothecin. Experimental cell research *291*, 176-188.

Elnakady, Y.A., Sasse, F., Lünsdorf, H., and Reichenbach, H. (2004). Disorazol A1, a highly effective antimitotic agent acting on tubulin polymerization and inducing apoptosis in mammalian cells. Biochemical Pharmacology *67*, 927-935.

Eng, C. (2003). PTEN: one gene, many syndromes. Human mutation *22*, 183-198.

Engelman, J.A., Luo, J., and Cantley, L.C. (2006). The evolution of phosphatidylinositol 3-kinases as regulators of growth and metabolism. Nature reviews Genetics *7*, 606-619.

Feng, Z. (2010). p53 regulation of the IGF-1/AKT/mTOR pathways and the endosomal compartment. Cold Spring Harbor perspectives in biology *2*, a001057.

Firestone, G.L., Giampaolo, J.R., and O'Keeffe, B.A. (2003). Stimulus-Dependent Regulation of Serum and Glucocorticoid Inducible Protein Kinase (SGK) Transcription, Subcellular Localization and Enzymatic Activity. Cellular physiology and biochemistry : international journal of experimental cellular physiology, biochemistry, and pharmacology *2003*, 001-012.

Freeman, D.J., Li, A.G., Wei, G., Li, H.-H., Kertesz, N., Lesche, R., Whale, A.D., Diaz, H.M., Rozengurt, N., Cardiff, R.D*., et al.* (2003). PTEN tumor suppressor regulates p53 protein levels and activity through phosphatase-dependent and -independent mechanisms. Cancer cell *3*, 117-130.

Frei, R., Staedler, D., Raja, A., Franke, R., Sasse, F., Gerber-Lemaire, S., and Waser, J. (2013). Total synthesis and biological evaluation of jerantinine E. Angewandte Chemie *52*, 13373-13376.

Furumai, R., Komatsu, Y., Nishino, N., Khochbin, S., Yoshida, M., and Horinouchi, S. (2001). Potent histone deacetylase inhibitors built from trichostatin A and cyclic tetrapeptide antibiotics including trapoxin. Proceedings of the National Academy of Sciences of the United States of America *98*, 87-92.

Gerth, K., Bedorf, N., Irschik, H., Hofle, G., and Reichenbach, H. (1994). The soraphens: a family of novel antifungal compounds from Sorangium cellulosum (Myxobacteria). I. Soraphen A1 alpha: fermentation, isolation, biological properties. J Antibiot (Tokyo) *47*, 23-31.

Gerth, K., Pradella, S., Perlova, O., Beyer, S., and Müller, R. (2003). Myxobacteria: proficient producers of novel natural products with various biological activities—past and future biotechnological aspects with the focus on the genus Sorangium. Journal of Biotechnology *106*, 233-253.

Giannakakou, P., Nakano, M., Nicolaou, K.C., O'Brate, A., Yu, J., Blagosklonny, M.V., Greber, U.F., and Fojo, T. (2002). Enhanced microtubule-dependent trafficking and p53 nuclear accumulation by suppression of microtubule dynamics. Proceedings of the National Academy of Sciences of the United States of America *99*, 10855-10860.

Giuliano, K.A. (1997). High-Content Screening: A New Approach to Easing Key Bottlenecks in the Drug Discovery Process. Journal of Biomolecular Screening *2*, 249-259.

Giuliano, K.A., Haskins, J.R., and Taylor, D.L. (2003). Advances in high content screening for drug discovery. Assay and drug development technologies *1*, 565-577.

Guenther, E., Schaefer, O., Teifel, M., and Paulini, K. (2013). Conjugates of disorazoles and their derivatives with cell-binding molecules, novel disorazole derivatives, processes of manufacturing and uses thereof. US Patent *8*, 1-17.

Hafsi, S., Pezzino, F.M., Candido, S., Ligresti, G., Spandidos, D.A., Soua, Z., McCubrey, J.A., Travali, S., and Libra, M. (2012). Gene alterations in the PI3K/PTEN/AKT pathway as a mechanism of drug-resistance (review). International journal of oncology *40*, 639-644.

Harvey, A.L. (2008). Natural products in drug discovery. Drug discovery today *13*, 894-901.

Haupt, S., Berger, M., Goldberg, Z., and Haupt, Y. (2003). Apoptosis - the p53 network. Journal of cell science *116*, 4077-4085.

Hopkins, C.D., and Wipf, P. (2009). Isolation, biology and chemistry of the disorazoles: new anti-cancer macrodiolides. Natural product reports *26*, 585-601.

Horwitz, S.B. (1994). Taxol (paclitaxel): mechanisms of action. Annals of oncology : official journal of the European Society for Medical Oncology / ESMO *5 Suppl 6*, S3-6.

Huss, M., Sasse, F., Kunze, B., Jansen, R., Steinmetz, H., Ingenhorst, G., Zeeck, A., and Wieczorek, H. (2005). Archazolid and apicularen: novel specific V-ATPase inhibitors. BMC biochemistry *6*, 13.

Irschik, H., Jansen, R., Gerth, K., Höfle, G., and Reichenbach, H. (1995). Disorazol A, an efficient inhibitor of eukaryotic organisms isolated from myxobacteria. THE JOURNAL OF ANTIBIOTICS *48*, 31-35.

Irschik, H., Trowitzsch-Kienast, W., Gerth, K., Hofle, G., and Reichenbach, H. (1988). Saframycin Mx1, a new natural saframycin isolated from a myxobacterium. J Antibiot (Tokyo) *41*, 993-998.

Jiang, B.H., and Liu, L.Z. (2009). PI3K/PTEN Signaling in Angiogenesis and Tumorigenesis. Adv Cancer Res *102*, 19-65.

Kim, Y.B., Lee, K.H., Sugita, K., Yoshida, M., and Horinouchi, S. (1999). Oxamflatin is a novel antitumor compound that inhibits mammalian histone deacetylase. Oncogene *18*, 2461-2470.

Kobayashi, T., and Cohen, P. (1999). Activation of serum- and glucocorticoid-regulated protein kinase by agonists that activate phosphatidylinositide 3-kinase is mediated by 3-phosphoinositide-dependent protein kinase-1 (PDK1) and PDK2. Biochem J *339*, 319±328.

Kobayashi, T., Deak, M., Morrice, N., and Cohen, P. (1999). Characterization of the structure and regulation of two novel isoforms of serum- and glucocorticoid-induced protein kinase. Biochem J *344*, 189-197.

Koehn, F.E., and Carter, G.T. (2005). The evolving role of natural products in drug discovery. Nature reviews Drug discovery *4*, 206-220.

Lang, F., Artunc, F., and Vallon, V. (2009). The physiological impact of the serum and glucocorticoid-inducible kinase SGK1. Current opinion in nephrology and hypertension *18*, 439-448.

Lang, F., Bohmer, C., Palmada, M., Seebohm, G., Strutz-Seebohm, N., and Vallon, V. (2006). (Patho)physiological significance of the serum- and glucocorticoid-inducible kinase isoforms. Physiological reviews *86*, 1151-1178.

Lang, F., and Cohen, P. (2001). Regulation and physiological roles of serum- and glucocorticoid-induced protein kinase isoforms. Science's STKE : signal transduction knowledge environment *2001*, re17.

Lang, F., Perrotti, N., and Stournaras, C. (2010). Colorectal carcinoma cells—Regulation of survival and growth by SGK1. The International Journal of Biochemistry & Cell Biology *42*, 1571–1575.

Lee, J.-O., Yang, H., Georgescu, M.-M., Cristofano, A.D., Maehama, T., Shi, Y., Dixon, J.E., Pandolfi, P., and Pavletich, N.P. (1999). Crystal Structure of the PTEN Tumor Suppressor: Implications for Its Phosphoinositide Phosphatase Activity and Membrane Association. Cell *99*, 323–334.

Leslie, N.R., and Downes, C.P. (2002). PTEN: The down side of PI 3-kinase signalling. Cellular Signalling *14*, 285–295.

Leslie, N.R., and Downes, C.P. (2004). PTEN function: how normal cells control it and tumour cells lose it. Biochem J *382*, 1-11.

Li, J.W.H., and Vederas, J.C. (2009). Drug Discovery and Natural Products: End of an Era or an Endless Frontier? Science *325*, 161-165.

Liang, J., and Slingerland, J.M. (2003). Multiple roles of the PI3K/PKB (Akt) pathway in cell cycle progression. Cell cycle *2*, 339-345.

Liang, S.-H., and Clarke, M.F. (2001). Regulation of p53 localization. Eur J Biochem *268*, 2779-2783.

Lim, K.H., Hiraku, O., Komiyama, K., and Kam, T.S. (2008). Jerantinines A-G, cytotoxic Aspidosperma alkaloids from Tabernaemontana corymbosa. Journal of natural products *71*, 1591-1594.

Lomenick, B., Hao, R., Jonai, N., Chin, R.M., Aghajan, M., Warburton, S., Wang, J., Wu, R.P., Gomez, F., Loo, J.A.*, et al.* (2009). Target identification using drug affinity responsive target stability (DARTS). Proceedings of the National Academy of Sciences of the United States of America *106*, 21984-21989.

Lopes, U.G., Erhardt, P., Yao, R., and Cooper, G.M. (1997). p53-dependent induction of apoptosis by proteasome inhibitors. The Journal of biological chemistry *272*, 12893-12896.

Lu, H.H., Raja, A., Franke, R., Landsberg, D., Sasse, F., and Kalesse, M. (2013). Synthesis and biological evaluation of paleo-soraphens. Angewandte Chemie *52*, 13549-13552.

MacLean-Fletcher, S., and Pollard, T.D. (1980). Mechanism of action of cytochalasin B on actin. Cell *20*, 329-341.

Mayo, L.D., and Donner, D.B. (2001). A phosphatidylinositol 3-kinase/Akt pathway promotes translocation of Mdm2 from the cytoplasm to the nucleus. Proceedings of the National Academy of Sciences of the United States of America *98*, 11598-11603.

Mayo, L.D., and Donner, D.B. (2002). The PTEN, Mdm2, p53 tumor suppressor-oncoprotein network. Trends in biochemical sciences *27*, 462-467.

McKeehan, W., and Hardesty, B. (1969). The mechanism of cycloheximide inhibition of protein synthesis in rabbit reticulocytes. Biochemical and biophysical research communications *36*, 625-630.

Mellor, P., Furber, L.A., Nyarko, J.N., and Anderson, D.H. (2012). Multiple roles for the p85alpha isoform in the regulation and function of PI3K signalling and receptor trafficking. The Biochemical journal *441*, 23-37.

Ming, M., and He, Y.Y. (2012). PTEN in DNA damage repair. Cancer letters *319*, 125-129.

Mitchison, T. (2005). Small-molecule screening and profiling by using automated microscopy. Chembiochem : a European journal of chemical biology *6*, 33-39.

Molad, Y. (2002). Update on colchicine and its mechanism of action. Current rheumatology reports *4*, 252-256.

Muthukumar, Y., Roy, M., Raja, A., Taylor, R.E., and Sasse, F. (2013). The marine polyketide myriaporone 3/4 stalls translation by targeting the elongation phase. Chembiochem : a European journal of chemical biology *14*, 260-264.

Nabeshima, K., Inoue, T., Shimao, Y., and Sameshima, T. (2002). Matrix metalloproteinases in tumor invasion: role for cell migration. Pathology international *52*, 255-264.

Newman, D.J., Cragg, G.M., and Snader, K.M. (2000). The influence of natural products upon drug discovery (Antiquity to late 1999). Natural product reports *17*, 215-234.

O'Brate, A., and Giannakakou, P. (2003). The importance of p53 location: nuclear or cytoplasmic zip code? Drug Resistance Updates *6*, 313-322.

Okkenhaug, K., and Vanhaesebroeck, B. (2001). New Responsibilities for the PI3K Regulatory Subunit p85 Science Signaling *2001*, pe1-pe1.

Pagano, M., Tam, S.W., Theodoras, A.M., Beer-Romero, P., Del Sal, G., Chau, V., Yew, P.R., Draetta, G.F., and Rolfe, M. (1995). Role of the ubiquitin-proteasome pathway in regulating abundance of the cyclin-dependent kinase inhibitor p27. Science *269*, 682-685.

Park, J., Leong, M.L.L., Buse, P., Maiyar, A.C., Firestone, G.L., and Hemmings, B.A. (1999). Serum and glucocorticoid-inducible kinase (SGK) is a target of the PI 3-kinase-stimulated signaling pathway. EMBO J *18*, 3024-3033.

Pei, D., Zhang, Y., and Zheng, J. (2012). Regulation of p53: a collaboration between Mdm2 and MdmX. Oncotarget *3*, 228-235.

Perlman, Z.E., Slack, M.D., Feng, Y., Mitchison, T.J., Wu, L.F., and Altschuler, S.J. (2004). Multidimensional drug profiling by automated microscopy. Science *306*, 1194-1198.

Rabinovsky, R., Pochanard, P., McNear, C., Brachmann, S.M., Duke-Cohan, J.S., Garraway, L.A., and Sellers, W.R. (2009). p85 Associates with unphosphorylated PTEN and the PTEN-associated complex. Molecular and cellular biology *29*, 5377-5388.

Sakoda, H., Gotoh, Y., Katagiri, H., Kurokawa, M., Ono, H., Onishi, Y., Anai, M., Ogihara, T., Fujishiro, M., Fukushima, Y.*, et al.* (2003). Differing roles of Akt and serum- and glucocorticoid-regulated kinase in glucose metabolism, DNA synthesis, and oncogenic activity. The Journal of biological chemistry *278*, 25802-25807.

Sansal, I., and Sellers, W.R. (2004). The biology and clinical relevance of the PTEN tumor suppressor pathway. Journal of clinical oncology : official journal of the American Society of Clinical Oncology *22*, 2954-2963.

Schenone, M., Dancik, V., Wagner, B.K., and Clemons, P.A. (2013). Target identification and mechanism of action in chemical biology and drug discovery. Nature chemical biology *9*, 232-240.

Schneiker, S., Perlova, O., Kaiser, O., Gerth, K., Alici, A., Altmeyer, M.O., Bartels, D., Bekel, T., Beyer, S., Bode, E.*, et al.* (2007). Complete genome sequence of the myxobacterium Sorangium cellulosum. Nature biotechnology *25*, 1281-1289.

Schupp, T., Toupet, C., Cluzel, B., Neff, S., Hill, S., Beck, J.J., and Ligon, J.M. (1995). A Sorangium cellulosum (myxobacterium) gene cluster for the biosynthesis of the macrolide antibiotic soraphen A: cloning, characterization, and homology to polyketide synthase genes from actinomycetes. Journal of bacteriology *177*, 3673-3679.

Shariff, A., Kangas, J., Coelho, L.P., Quinn, S., and Murphy, R.F. (2010). Automated image analysis for high-content screening and analysis. J Biomol Screen *15*, 726-734.

Shen, W.H., Balajee, A.S., Wang, J., Wu, H., Eng, C., Pandolfi, P.P., and Yin, Y. (2007). Essential role for nuclear PTEN in maintaining chromosomal integrity. Cell *128*, 157-170.

Solly, K., Wang, X., Xu, X., Strulovici, B., and Zheng, W. (2004). Application of real-time cell electronic sensing (RT-CES) technology to cell-based assays. Assay and drug development technologies *2*, 363-372.

Stambolic, V., MacPherson, D., Sas, D., Lin, Y., Snow, B., Jang, Y., Benchimol, S., and Mak, T.W. (2001). Regulation of PTEN transcription by p53. Molecular cell *8*, 317-325.

Starkuviene, V., and Pepperkok, R. (2007). The potential of high-content high-throughput microscopy in drug discovery. British journal of pharmacology *152*, 62-71.

Strobel, G., Daisy, B., Castillo, U., and Harper, J. (2004). Natural products from endophytic microorganisms. J Nat Prod *67*, 257-268.

Su, G.H., Sohn, T.A., Ryu, B., and Kern, S.E. (2000). A novel histone deacetylase inhibitor identified by high-throughput transcriptional screening of a compound library. Cancer Res *60*, 3137-3142.

Sulis, M. (2003). PTEN: from pathology to biology. Trends in cell biology *13*, 478-483.

Swinney, D.C., and Anthony, J. (2011). How were new medicines discovered? Nature reviews Drug discovery *10*, 507-519.

Tamguney, T., and Stokoe, D. (2007). New insights into PTEN. Journal of cell science *120*, 4071-4079.

van Maanen, J.M., Retel, J., de Vries, J., and Pinedo, H.M. (1988). Mechanism of action of antitumor drug etoposide: a review. Journal of the National Cancer Institute *80*, 1526-1533.

Vargas, D.-A., and Ronai, Z. (2002). p53–Mdm2—the affair that never ends. Carcinogenesis *23*, 541-547.

Vazquez, F., Ramaswamy, S., Nakamura, N., and Sellers, W.R. (2000). Phosphorylation of the PTEN tail regulates protein stability and function. Molecular and cellular biology *20*, 5010-5018.

Vivanco, I., and Sawyers, C.L. (2002). The phosphatidylinositol 3-Kinase AKT pathway in human cancer. Nature reviews Cancer *2*, 489-501.

Weissman, K.J., and Muller, R. (2009). A brief tour of myxobacterial secondary metabolism. Bioorganic & medicinal chemistry *17*, 2121-2136.

Weissman, K.J., and Muller, R. (2010). Myxobacterial secondary metabolites: bioactivities and modes-of-action. Natural product reports *27*, 1276-1295.

Weng, L.-P., Brown, J.L., and Eng, C. (2001). PTEN induces apoptosis and cell cycle arrest through phosphoinositol-3-kinase/Akt-dependent and -independent pathways. Hum Mol Genet *10*, 237-242.

Wenzel, S.C., and Muller, R. (2007). Myxobacterial natural product assembly lines: fascinating examples of curious biochemistry. Natural product reports *24*, 1211-1224.

Wenzel, S.C., and Muller, R. (2009). Myxobacteria—'microbial factories' for the production of bioactive secondary metabolites. Mol BioSyst *5*, 567–574.

Wenzel, S.C., Williamson, R.M., Grünanger, C., Xu, J., Gerth, K., Martinez, R.A., Moss, S.J., Carroll, B.J., Grond, S., Unkefer, C.J., *et al.* (2006). On the Biosynthetic Origin of Methoxymalonyl-Acyl Carrier Protein, the Substrate for Incorporation of "Glycolate" Units into Ansamitocin and Soraphen A. J Am Chem Soc *128*, 14325–14336.

Zhao, Q., Zeino, M., Eichhorn, T., Herrmann, J., Müller, R., and Efferth, T. (2013). Molecular docking studies of myxobacterial disorazoles and tubulysins to tubulin. J Biosci Med *3*, 37-44.

List of Figures

List of Tables